On the Potential Use of Small Scale Fire Tests for Screening Steiner Tunnel Results for Spray Foam Insulation

by

Matthew J. DiDomizio

A thesis
presented to the University of Waterloo
in fulfilment of the
thesis requirement for the degree of
Master of Applied Science
in
Mechanical Engineering

Waterloo, Ontario, Canada, 2013

I hereby declare that I am the sole author of this thesis. This is a true copy of the thesis, including any required final revisions, as accepted by my examiners.

I understand that my thesis may be made electronically available to the public.

Abstract

The goal of this study is to assess the potential of using bench-scale fire testing to screen materials for the Steiner tunnel fire test. It is hypothesized that the chemical and physical changes made to a material to improve its fire performance in small scale fire tests will have a predictable response in the Steiner tunnel. This hypothesis is based on the observation that fire test results can, in some cases, provide insight on a material's relative fire hazard, and the assumption that the relative hazard should be consistent across scale.

The ASTM E84 Steiner tunnel test provides a relative ranking of material hazard in two categories. The horizontal Flame Spread Index (FSI) is used to rank the flame hazard of a material, and the Smoke Developed Index (SDI) is used to rank the smoke hazard of a material. Two fire tests are proposed to independently assess each hazard at the bench-scale. The ASTM E1354 cone calorimeter test measures a material's open-flaming heat release rate; it is proposed that the cone calorimeter test can be used to assess a material's relative flame hazard. The ISO 5659-2 smoke density chamber test measures a material's closed-environment smoke development; it is proposed that the smoke density chamber test can be used to assess a material's relative smoke hazard.

The material selected for this study is fire-retarded sprayed polyurethane foam (FRSPF) insulation. Specific details of the foam chemistry, fire retardants, and the manufacturer are confidential. Generally, the foam can be described as medium-density (approximately 2 lbs/ft^3), closed-celled, and semi-rigid. The fire retardant additives are comprised of differing ratios and concentrations of phosphorous- and halogen-containing compounds.

A series of 30 Steiner tunnel tests is conducted on 20 different formulations. Repeated testing is conducted on several formulations in order to assess variability in the Steiner tunnel test results. Cone calorimeter and smoke density chamber tests are conducted on a subset of those formulations, in sets of 3–5 tests per formulation.

Key performance indicators are identified from each fire test, relationships between those indicators are examined, and correlations are presented where strong relationships are apparent. Empirical prediction models are proposed for FSI and SDI based on the success rate of prediction, and minimization of error between experimental (measured) and modelled (predicted) results. It is concluded that for the materials tested in this study, there is sufficient evidence of consistency in relative performance to recommend bench-scale screening tests as a cost-effective alternative to repeated Steiner tunnel testing.

Acknowledgements

First and foremost, I would like to thank my supervisor, Prof. Elizabeth Weckman, for all that she has contributed not only to this body of work, but also to my education in the field of fire safety engineering and training in fire research methods. Under Beth's guidance we have been able to derive meaningful conclusions from this research, and I hope that we may expand on these findings in the future. I would also like to thank Prof. Al Strong for his continued encouragement of my research, as well as Prof. David Torvi and Prof. Michael Worswick for their contributions in the review process.

I would like to thank Mr. Gord Hitchman for his ongoing support in this research, from technical collaboration in fire testing and design of experiment to creative discussions and interpretations of fire test results. In particular, I would like to acknowledge his contributions to the normalization models, and the idea to approximate burned volumes based on flame spread. I would like to thank Mr. Andy Barber for his technical expertise in troubleshooting electronics in the smoke density chamber, without which we never would have brought the test rig to life.

I would like to acknowledge the contributions of Dr. Gregor Lawson, Mrs. Connie Stowell, Dr. Nick Xie, and Mr. Larry Genyn, without whom the mixture design, preparation, and large-scale fire testing of the materials in this study would not have been possible. Also, the financial contributions of the Natural Sciences and Engineering Research Council of Canada in supporting my research under the FedDev Applied Research and Commercialization program are acknowledged.

Finally, I would like to thank my colleagues in the University of Waterloo fire research group, for their friendship, ongoing support, and especially for their humour in times of stress. And I would like to acknowledge the contributions of two students in particular, for their assistance in the digitization and analysis of test results: Mr. Ibrahim Anwar, and Mr. Kaushik Jamadagni.

Table of Contents

List of Figures

List of Tables

Nomenclature

Abbreviations

FSI	Flame spread index (Steiner tunnel).
FSI_M	Predicted value of flame spread index from a model (Steiner tunnel).
FSI_S	Screened range of flame spread index from a model (Steiner tunnel).
SDI	Smoke developed index (Steiner tunnel).
SDI_M	Predicted value of smoke developed index from a model (Steiner tunnel).
SDI_S	Screened range of smoke developed index from a model (Steiner tunnel).
TSO	Total smoke obscuration (Steiner tunnel).
TSO_R	Reference smoke obscuration (Steiner tunnel).

Greek Symbols

α	Volumetric expansion factor (cone calorimeter).
β	Depth burning rate (Steiner tunnel).
ϕ	Oxygen consumption factor (cone calorimeter).
τ	Time elapsed from the start of the test (Steiner tunnel).
τ_1	Time to peak flame spread (Steiner tunnel).
τ_2	End-of-test time (Steiner tunnel).

Roman Symbols

$\dot{m}_e$	Mass flow rate of gases through the stack (cone calorimeter).
$A_b\,(x)$	Burned section area along the length of a specimen (Steiner tunnel).
A_s	Exposed specimen surface area (cone calorimeter, smoke density chamber).

C	Orifice plate coefficient (cone calorimeter).
C_f	Range extension filter correction factor (smoke density chamber).
$D_b(x, y)$	Burned depth along the length and width of a specimen (Steiner tunnel).
$D_{b,max}$	Maximum burned depth along the centreline of a specimen (Steiner tunnel).
d_{filter}	Range of the photomultiplier control unit (smoke density chamber).
$DS(t)$	Specific optical density at time t (smoke density chamber).
DS_1	Peak specific optical density (smoke density chamber).
$E(\tau)$	Photoelectric voltage at time τ (Steiner tunnel).
E_{max}	Photoelectric voltage at 100% light transmission (Steiner tunnel).
E_{O_2}	Heat release per mass of oxygen consumed (cone calorimeter).
$f(\tau)$	Flame spread at time τ (Steiner tunnel).
f	Position of the range-extension filter (smoke density chamber).
F_1	Flame spread area; area under the $f(\tau)$ curve (Steiner tunnel).
f_1	Peak flame spread (Steiner tunnel).
F_2	Maximum flame spread area; area under the $f_{max}(\tau)$ curve (Steiner tunnel).
f_2	Final flame spread (Steiner tunnel).
F_T	Total flame spread area (Steiner tunnel).
$f_{max}(\tau)$	Maximum flame spread at time τ (Steiner tunnel).
L	Total length of a specimen (Steiner tunnel).
L_p	Length of the light path (smoke density chamber).
$m_s(t)$	Specimen mass at time t (cone calorimeter, smoke density chamber).
M_{air}	Molecular weight of dry air (cone calorimeter).
M°_{air}	Molecular weight of ambient air (cone calorimeter).
M_{H_2O}	Molecular weight of water vapour (cone calorimeter).
M_{O_2}	Molecular weight of oxygen (cone calorimeter).
$ML(t)$	Specimen mass loss at time t (cone calorimeter, smoke density chamber).
ML_b	Specimen mass loss over the burning period (cone calorimeter).
p°_{air}	Barometric pressure of ambient air (cone calorimeter).
$p_{s,air}$	Saturation pressure of water vapour in ambient air (cone calorimeter).
$q(t)$	Rate of heat release at time t (cone calorimeter).

$q''(t)$	Rate of heat release per exposed specimen area at time t (cone calorimeter).
RH°_{air}	Relative humidity of ambient air (cone calorimeter).
$SO(\tau)$	Smoke obscuration at time τ (Steiner tunnel).
t	Time elapsed from the start of a test (cone calorimeter, smoke density chamber).
t_1	Time to minimum optical transmission (smoke density chamber).
$t_b(x)$	Time of exposure to flames along the length of a specimen (Steiner tunnel).
T_e	Temperature of gases in the stack (cone calorimeter).
$TO(t)$	Optical obscuration at time t (smoke density chamber).
TO_1	Peak optical obscuration (smoke density chamber).
$TR(t)$	Optical transmission at time t (smoke density chamber).
TR_1	Minimum optical transmission (smoke density chamber).
V_b	Burned volume of a specimen (Steiner tunnel).
V_c	Internal volume of the chamber (smoke density chamber).
$W_b(x)$	Burned width along the length of a specimen (Steiner tunnel).
x	Position along the length of a specimen (Steiner tunnel).
X_{CO_2}	Volume fraction of carbon dioxide in the sample gas (cone calorimeter).
$X^{\circ}_{CO_2}$	Volume fraction of carbon dioxide in ambient air (cone calorimeter).
X_{CO}	Volume fraction of carbon monoxide in the sample gas (cone calorimeter).
X°_{CO}	Volume fraction of carbon monoxide in ambient air (cone calorimeter).
$X^{\circ}_{H_2O}$	Volume fraction of water vapour in ambient air (cone calorimeter).
X_{O_2}	Volume fraction of oxygen in the sample gas (cone calorimeter).
$X^{\circ}_{O_2}$	Volume fraction of oxygen in ambient air (cone calorimeter).
y	Position along the width of a specimen (Steiner tunnel).
Δp	Pressure differential across the stack orifice plate (cone calorimeter).
Δx	Incremental distance along the length of a specimen (Steiner tunnel).

Chapter 1

Introduction

Polymeric insulation has an assortment of desirable properties in comparison to the traditional fibre insulation used in some buildings, including excellent thermal efficiency, vapour permeability, structural support, and flexibility in terms of installation. Sprayed polyurethane foams (SPFs) are a subgroup of these materials, and are known for their versatility in a wide variety of applications with different installation requirements. Even with desirable insulation properties, the comparatively poor fire performance of SPFs and high potential for SPFs to contribute to fire growth necessitates strict regulations on their use in building construction. The need to adhere to legislated requirements for safety necessitates the use of fireproofing, or fire-retarding, of these materials when they are used in structures.

A Canadian manufacturer of SPFs, hereafter referred to as "the manufacturer", has entered into a research relationship with the University of Waterloo with the objectives of improving the fire performance of their current commercial product line, as well as understanding how they might improve the fire performance of future products. Materials must satisfy the flammability criteria outlined in the National Building Code of Canada: Class A characterization in flame spread and smoke development in the Steiner tunnel test must be achieved in order to designate an insulation product as "fire-rated".

It is not currently possible to predict the direct consequence on the fire performance of a material from the addition of particular fire retardants (FRs) to a base material due to the complexity of the chemical interactions of FRs with a burning material during combustion. Common industry practice is to combine past experiences with trial-and-error testing until a particular combination of FRs in sufficient concentration yields a passing result in a particular fire test. A significant problem with this practice is cost, not only in terms of testing costs, but also because it greatly prolongs the R&D phase of materials development, adding development costs and delaying introduction of the product to the market.

Small-scale fire performance testing is available to manufacturers at a fraction of the cost of large-scale tests, and small-scale tests may be conducted in rapid succession compared to the turn-around time for a large-scale test. Furthermore, the material costs for small-scale testing are significantly less. It is not clear whether small-scale tests are directly scalable to large-scale tests, however, it has been suggested that relative material rankings across scales may be similar [1].

Even if the chemical interactions of FRs with the combustion reaction cannot be predicted fundamentally, it is possible that the net effect of a particular combination of FRs could have a similar relative response across scales. If this is the case, the chemical and physical changes made to a material to improve its fire performance in small scale fire tests will have a predictable response in the Steiner tunnel. This is the basis of a process known as "screening", where a manufacturer will determine the best performing material at the small-scale, and will then recommend that material be selected for testing at the large-scale.

The problem with "blind screening", or screening without a comprehensive understanding of the scalability of selected performance parameters, is that it may not produce a reliable indication as to a material's expected performance. Therefore, a screening tool is needed which can evaluate material response at the small-scale, and predict the expected large-scale response within reasonable limitations.

The Steiner tunnel fire test evaluates the fire performance of a material in two categories: flame spread and smoke development. Therefore, in this work two separate small scale tests are selected as potential screening tests through which to evaluate the performance of a material on the basis of each of these – flame and smoke.

The cone calorimeter test is a small-scale fire test that determines the heat release rate of a material as it burns in a well controlled environment. Heat release rate is a measure of the energy potential of a fire, and is used to describe the size of a fire. A material found to have a greater heat release rate in the cone calorimeter might be expected to contribute more to a growing fire than a material with low heat release rate. Since heat release rate relates to a material's potential to contribute to fire growth, it can be used to assess a material's relative fire hazard. Therefore, of primary interest in the present work is the determination of a relationship between the relative flame hazard as evaluated in the cone calorimeter test, and the flame spread index in the Steiner tunnel test.

The smoke density chamber test is a small-scale fire test that determines the specific optical density of smoke from a burning material in a well controlled environment. Specific optical density is a measure of the amount of smoke generated from a fixed size sample of material in a fixed volume. A material which produces more smoke when it is burned in the same environment as another material will have a greater specific optical density, so

this parameter describes a material's potential to develop smoke and, as such, can be used to assess the relative smoke hazard from one material to another. Therefore, it is desired in this work to develop a relationship between the relative smoke hazard as evaluated in the smoke density chamber test, and the smoke developed index in the Steiner tunnel test.

The primary objective of this study is to develop a screening tool which will assist an engineer or R&D scientist in recommending the probability of a given material passing the Steiner tunnel test based on its performance in the two small-scale tests described above. Such a tool will allow the manufacturer to screen the majority of R&D materials at the small-scale and, based on the predicted large-scale response, make a recommendation as to the best materials to test at the large-scale. This will result in decreased R&D cycles for flammability criteria as well as reduced R&D costs, allowing the manufacturer to bring products to market in less time, and potentially gain market advantage.

The proposed screening tool will be developed based on empirical correlations between identified performance indicators for flame spread and smoke development at the large- and small-scales. Empirical models for prediction of flame spread and smoke developed indices will be developed based on cross-test correlations. A stated goal of the manufacturer is for the empirical model to be able to predict Steiner tunnel results to within 20% difference from their actual results for the tests conducted.

The scope of this study is limited to development of a screening tool by which to assess the fire performance of fire-retarded sprayed polyurethane foam materials in the Steiner tunnel test, and in the potential for scaling small-scale results for these materials to the large-scale. Any findings on the scalability of fire test results are limited to this specific sub-group of materials. The findings are of particular relevance to the manufacturer as they develop multiple product lines from a single base material. Furthermore, findings are of value to the fire safety engineering community for use in the development of future performance-based empirical scaling models for fire tests.

Chapter 2

Background

This study involves the evaluation of the fire performance of materials at different scales. Fire performance is evaluated using a wide variety of fire test methods, which are standardized by various organizations. Several organizations responsible for regulation of test standards in Canada and the United States include: the American Society for Testing and Materials (ASTM), the International Organization for Standardization (ISO), the Underwriters Laboratories (UL), the Underwriters Laboratories of Canada (ULC), and the National Fire Protection Association (NFPA).

Fire testing is conducted at various scales and in various burning environments, depending on the objective of the fire test. Throughout the years, there has been a continuing desire to develop models by which to scale results between different tests, either to predict material behaviour or to develop inputs for numerical fire models. Several examples are discussed in this chapter; those fire parameters which are found to be relevant to scaling models are identified.

Furthermore, background is provided on the material of interest in this study: fire-retarded sprayed polyurethane foam insulation. The behaviour of such materials in the Steiner tunnel with respect to traditional construction materials is discussed.

Finally, the three fire tests of interest to this study are outlined: the Steiner tunnel test, the cone calorimeter test, and the smoke density chamber test.

2.1 Fire Testing of Building Materials

Building materials and assemblies are subjected to fire testing in order to achieve requisite performance ratings in the jurisdiction in which they are to be used. Fire testing is useful

in that it allows for different materials to be tested under a standard set of conditions in order to rank the response of a material to a given fire scenario. Fire testing may be conducted at various scales, from "as-installed" configurations of wall or ceiling sections in the ASTM E119 fire test for building construction and materials [2], to small finger-sized sections of insulation in the ASTM D2863 fire test for measuring a material's oxygen index [3]. Through one or a combination of such tests, materials are evaluated and assigned a performance rating, which then dictates where and how that material may be used in building construction.

The fire testing of building materials has historically been divided into two broad categories: reaction-to-fire tests, and fire resistance tests. Reaction-to-fire tests attempt to quantify a material's response to fire in several categories, including ignitability, flame spread, heat release, and smoke and toxic gas production; while fire resistance tests attempt to quantify the ability of a material or construction assembly to resist the spread of fire, or to contain heat and fire gases in the event of a fire. Three reaction-to-fire tests are discussed in the context of this project: the Steiner tunnel, cone calorimeter, and smoke density chamber fire tests. The tests are briefly introduced here and explained in detail in Sections 2.3, 2.4, and 2.5 respectively.

The ASTM E84 Steiner tunnel test is a large-scale fire test which measures horizontal flame spread and total smoke generation from a specimen subjected to an active gas flame in a ventilated enclosure [4]. The test is used as the primary means for evaluation of building materials with a lining end-use application, such as ceilings, walls, and floors. Furthermore, it has been adopted for use in many other applications including the evaluation of polymeric insulation materials of interest in this work.

The ASTM E1354 cone calorimeter test is a small-scale fire test which measures the rate of heat release and mass loss from a horizontally- or vertically-mounted specimen subjected to radiant heat exposure and an active ignition source in a well-ventilated environment [5]. The cone calorimeter fire test measures several relevant fire properties, the most important of which is heat release rate, from hazard classification and fire modelling perspectives [6].

The ISO 5659-2 smoke density chamber test is a small-scale fire test which measures specific optical density of smoke generated and mass loss during the combustion of a horizontally-mounted specimen subjected to radiant heat exposure and an active ignition source in a sealed under-ventilated enclosure [7].

In the Canadian building industry, it is common practice to determine the fire rating of a construction material or assembly via large-scale fire testing, often through measurements of fire resistance and flame spread, for example. The significant economic, time, and environmental investments associated with large-scale fire testing tend to discourage R&D, which might require the testing of multiple configurations and repeated testing

for validation. In comparison, small scale fire testing can often provide a manufacturer with precise and repeatable results in less time, at less cost, and with less environmental impact than large scale testing.

A concern has been raised with respect to using small-scale testing to assign fire ratings for building construction materials based on the dependence of such results on configuration and methodology. For example, in determining the relevance of small-scale test results in the context of a large-scale fire scenarios, Flisi [8] notes that the significance of small-scale tests must be questioned, on the grounds that there is doubt in using any small-scale result in ascertaining the risk in a real fire situation. Flisi demonstrates for a collection of standard building materials tested across several countries according to the test methodologies of the respective countries, that their ranked performance is greatly dependent on the country in which the test is conducted. For example, expanded polystyrene is found to be extremely combustible according to the test methodologies of several countries, while only moderately combustible according to the test methodologies of others. The poor correlation Flisi observed in results between small-scale tests indicates doubt in their utility for scaling to larger fire scenarios.

In other work, Schartel and Hull [9] note that one of the major challenges in scaling fire tests is the outstanding role that length scale plays in determining fire behaviour. The length scale of a fire has a significant influence on fuel-air mixing, and thus the combustion reactions as well as the resulting temperatures. For example, a large compartment fire is expected to have greater heat release rates, generate more buoyant vapours, have greater compartment temperatures, and be less susceptible to environmental changes than a bench-scale material fire. It has traditionally been difficult to recreate the key physical interactions which occur in a larger length scale fire using small-scale tests; however, over the past few decades, the development of advanced predictive models, some of which incorporate data from smaller scale tests, are leading toward more reliable predictions of fire behaviour. There is a need in the fire and materials community to develop a means by which to confidently relate the performance of building materials in large-scale fire scenarios to the performance of those materials in small-scale tests.

Research into relationships between large-scale and small-scale fire performance can generally be divided into two categories: predictive models, and empirical correlations. These will be discussed in the following two sections.

2.1.1 Empirical Correlations for Scaled Fire Performance

A strictly empirical model describes a phenomenon by approximating the general shape of the relationship between measured or observed parameters without theoretical significance

necessarily being attached to the parameters of the model. This is in direct contrast with mechanistic models, in which the correlation is a means by which to quantify the relationship between the processes that govern the phenomenon of interest [10].

Over the years, a number of empirical correlations have been developed for the purpose of relating small-scale fire test results to large-scale fire performance for specific products [11]. Such a correlation may lead to the development of an empirical predictive model which, if supported by sufficient testing, could prove an invaluable tool to product manufacturers. The resulting tool could be used to anticipate the expected response of a material at the large-scale based on its measured response at the small-scale within a defined margin of error. Such an empirical predictive model may be termed an "engineering tool" or "screening tool".

Consider the experiments performed by Wu and Bill [12] regarding the scaling of wet bench fire hazard testing for clean room facilities in the semiconductor industry. It was observed that the full-scale wet bench fire testing results were consistent in terms of chemical heat release rate, fire propagation, and smoke generation with the results of the standardized small-scale tests. In this instance, it was observed that the standardized small-scale fire test was a viable screening test by which to predict the results of the more expensive full-scale fire test.

Empirical relationships between heat release rate in the cone calorimeter and fire performance in various large scale tests have been the focus of much research over the years. One example is Babrauskas' [13] work in predicting large-scale heat release rates and burning times for upholstered furniture and wall linings. A correlation was developed between the peak heat release rate in the large-scale furniture calorimeter and the predicted peak heat release rate based on small-scale cone calorimeter results. Furthermore, it was demonstrated that the ratio of ignition time to peak rate of heat release in the cone calorimeter showed promise in the empirical prediction of time to flashover in the ISO 9705 room corner test. This ratio remains a relevant factor in successive studies on the prediction of flashover phenomena, as demonstrated by Wickström and Göransson [14, 15], Östman and Tsantaridis [16, 17], Hansen and Hovde [18], and Petrella [19].

Petrella [19] concedes that while the ratio of ignition time to peak rate of heat release in the cone calorimeter is useful for predicting flashover potential, it is an incomplete parameter for prediction of full-scale fire behaviour. Even so, empirical relationships between ignition time and heat release rate in the cone calorimeter and flashover properties in the room corner test continue to be developed. Recently, Wang et al. [20] produced such a model utilizing a two-step method. In the first step, a material is classified using a technique known as linear discriminant analysis; the scope of the study covers 52 different materials including wood linings, polystyrene foam, polyurethane foam, and a variety of

fire-retardant materials. In the second step, a flashover time prediction is developed based on the input of the material classification step, as well as cone calorimeter results. In comparison to the models developed by Östman and Tsantaridis [16, 17], and Hansen and Hovde [18], the method showed improved empirical predictive capabilities for a wide range of materials.

Several studies have attempted to correlate smoke generation between the ISO 9705 room corner test and the cone calorimeter. One example is Heskestad and Hovde [21], who compared the ratio of smoke generation to heat generation between the two tests. Multiple regressions on empirical models found that the bench-scale parameters could be used to predict full-scale performance for some of the materials tested. Wood materials tended to demonstrate fairly proportional scaling; however, plastic products tended to generate significantly more smoke at the small-scale, while only slightly more at the large-scale. Within the sub-category of plastic products, deviations were observed (polyethylene foam compared to polystyrene and polyurethane foams, for example). Further to this point, Dietenberger and Grexa [22] found a good correlation between smoke extinction area in the room corner test and peak smoke extinction area in the cone calorimeter test for a variety of different wood wall lining materials. These studies exemplify the difficulty in applying "generalized" empirical fire models to polymer materials, which may demonstrate significantly different cross-scale behaviour in comparison to wood materials.

2.1.2 Predictive Models for Scaled Fire Performance

The motivation for the development of predictive models is to overcome the limitations of empirical models, namely that they are only applicable to specific materials or to the types of products investigated during their development. A predictive model can, in theory, predict the behaviour of a material in a large-scale fire scenario based on thermo-physical properties of the material and measured fire performance parameters. Oftentimes these parameters are determined experimentally using small-scale fire tests.

Cleary [23] identifies three aspects of flammability that control the fire hazards related to the size of the fire: ignitability, flame spread, and heat release rate. He suggests that the lateral ignition and flame spread (LIFT) test and the cone calorimeter test together are capable of providing the data needed to characterize a material's flammability (smoke and toxicity are excluded from the scope of this study). He identifies a number of measured fire performance parameters that can be used to adequately characterize ignitability, flame spread, and heat release rate. These are:

- the minimum heat flux required for ignition;
- the ignition temperature;

– the effective thermal inertia ($k\rho c$);

– the flame spread parameter (from the LIFT test); and

– the minimum temperature required for flame spread.

Cleary also identifies peak heat release rate and burning time measured in the cone calorimeter to be important results, although he does not go so far as to recommend using them as input parameters in a model for fire performance at larger scales.

In 2006, almost 14 years later, Quintiere [24] proposed that the fire performance of a material may be scaled by extrapolation from four key measured properties:

– the critical heat flux below which piloted ignition cannot occur;

– the thermal response parameter (derived from critical heat flux and ignition time);

– the ratio of effective heat of combustion to heat of gasification; and

– the available energy per unit area.

It is suggested that these four properties govern the processes which dictate a material's flammability, including: ignition, burning rate per unit area, energy release rate, and flame spread. To this end, Quintiere and Lian [25] have developed a method to predict the potential for and time to flashover in the ISO 9705 room corner test, finding good correlation with actual results.

Grayson et al. [26] suggest a more comprehensive list of measured fire performance parameters which show promise in predictive models for fire behaviour. Notably, the list includes parameters identified both in Cleary's [23] and Quintiere's [24] work:

– the critical heat flux below which piloted ignition cannot occur;

– the ignition temperature;

– the surface temperature at which lateral flame spread ceases;

– the thermal inertia;

– the flame spread parameter;

– the effective heat of combustion;

– the effective heat of gasification; and

– the available energy per unit area.

It is notable that the parameters identified by Grayson et al. [26] are based on the definition of material flammability in terms of energy release, not toxicity or smoke development. Babrauskas [6] states that even though fire deaths and injuries are primarily caused by hot smoke and toxic gases, the relative toxicity of fire gases tends to be insignificant in the modelling of fire scenarios compared to the heat release rate. It is for this reason that the cone calorimeter, primarily a heat release rate test, is often used to generate input parameters for fire models.

As important as the cone calorimeter results may be, it must be emphasized that their interpretation requires more than a simple evaluation of the data, but also consideration of the area of application. Complications arise when attempting to correlate the measured heat release rate of a small-scale test to a large-scale situation. Babrauskas [6] notes that even when the same phenomena are observed in large-scale fires and in bench-scale tests, there may not necessarily be a simple, direct relationship between the heat release rates of the two. Schartel and Hull [9] advise that a consensus is needed within the fire science community on the interpretation of cone calorimeter results in order for the results to be accurately related to full-scale tests. This is of particular importance as the fire science community's need to screen new fire-retardant materials increases, and the cone calorimeter test emerges as an economical and flexible choice.

Some tests, such as the Steiner tunnel test, report an indexed value of fire performance relative to some standard materials (red oak and cement board, in the case of the Steiner tunnel [4]). While useful in comparing the response of various materials to a baseline, indices determined using these tests tend to be less useful in fire modelling than in experimental measurements of specific fire parameters.

Janssens [11] proposes a model by which to predict the total flame length and smoke production rate at a given time in the Steiner tunnel from the ignition temperature and heat release rate measured in the cone calorimeter. The model has a physical basis, and its predictive capability is evaluated for twelve different construction materials. The model demonstrates good predictive capabilities for the traditional interior finish materials for which the Steiner tunnel test was originally designed (plywood, gypsum, wall coverings, and wood planks), but produces drastically different results for newer materials such as polymeric insulation and oriented strand board.

Janssens' model predicted a flame spread index in excess of 600 greater than the measured flame spread index (approximately 50) for the polyisocyanurate foam [11]. The discrepancy is attributed to the foam having a very short ignition time in the cone calorimeter, and consequently very high predicted rate of flame spread in the Steiner tunnel. The behaviour of exposed polymer foam materials in the Steiner tunnel test is described as "anomalous" in comparison to traditional Steiner tunnel materials [11]. In practice, polymer foam materials tend to follow a distinct flame propagation trend of progression, peak, and regression, as will be demonstrated in Section 2.3. This behaviour is certainly contrary to the progressive flame-front propagation typical of traditional Steiner tunnel materials; however, this fact alone should not discourage future models from attempting to generalize the prediction of flame spread. Perhaps inclusion of a material classification step, as in the case of Wang et al.'s [20] flashover model, would lend credence to a generalized model.

Work toward accurate and generalized predictive models continues, but currently there is no model capable of accurately and consistently predicting large-scale test results based on measured fire parameters across a range of material performance data input into the model. Welch [27] posits that, in the context of developing a general fire model capable of estimating large-scale fire performance of building materials, at the present time, models which are entirely theoretically-based must be excluded on the basis of practicality. In short, theoretical models either lack supporting knowledge or technology required for true prediction of fire behaviour, or implement assumptions which limit the scope, and thus usefulness for broad applications. He points out that "recourse must be made to some degree of empiricism" [27], arguing for a balance between empiricism and fundamentals in predictive models. In materials R&D, compromise must be made to bring a product to market within the allocated budget and time frame. Indeed, maintaining a balance between practicality and theoretical justification of a model is crucial from an engineer's perspective. Development of empirical models can be a powerful method for evaluating the fire performance of materials, but the fundamentals upon which a model is based must always be considered in its use. Furthermore, as computational resources increase and progress continues in fire research, the industry can expect the balance to continue to shift toward increasing accommodation of fundamentals, particularly in the most universal models.

2.2 Sprayed Polyurethane Foam Insulation

Polyurethane insulation refers to a broad category of urethane-based materials used for insulation in buildings. Urethanes are formed by the reaction of an organic isocyanate compound with a polyol (an alcohol compound with hydroxyl groups available for organic reactions). Common isocyanates selected for polyurethane insulation include toluene diisocyanates (TDI), methylene diphenyl diisocyanates (MDI), and various aromatic diisocyanates. A sprayed polyurethane foam is formed by mixing the liquid-phase urethane base with catalysts, surfactants, blowing agents and other chemicals to form a mixture which is suitable for spray application. For insulation, the sprayed mixture must adhere well, set rapidly, and the final product must provide suitable insulative, structural, physical, and flammability properties.

Sprayed polyurethane foams are manufactured in multi-component liquid form, for which the components are mixed as the liquids are sprayed into wall and ceiling cavities for their end-use application. Foams are formulated to be flexible or rigid, or anywhere between. The materials are generally classified by their cellular structure and density. SPFs may be open-celled, in which case the cellular microstructure is not completely closed, or

closed-celled, in which case the cellular microstructure is smaller and more dense. Within each cellular category are density brackets, where high density SPFs tend to provide greater structural support and increased resistance to air and water vapour permeation.

Polyurethane foam insulations have excellent thermal resistance and installation flexibility compared to other common insulation types, and are therefore desirable for building thermal efficiency [28]. They are also highly combustible and can release dense, toxic smoke when burning. While the ignition temperature of polyurethane foam insulation tends to be comparable with that of traditional wood construction materials [29], once ignited it tends to burn rapidly having the potential to contribute significantly to fire growth.

The combustible nature of certain insulations has led the National Building Code of Canada to require the use of a thermal barrier protection which prevents the surface of the material from reaching a critical temperature for a minimum time when exposed to the standard ASTM E119 fire test [30]. The exact temperature and time requirements have changed throughout revisions of the code, and also depend on the size of a building and whether the building is equipped with sprinklers [31]. Any polymer insulation used in buildings must be covered by a thermal barrier (typically gypsum board) in order to adhere to the building code. Depending on the end-use, the insulation material itself may also contain fire retardant additives in order to achieve the desired flammability criteria. As attested by Hirschler [32], it has been shown throughout the years that the addition of fire retardants to polyurethane foams can delay ignition, reduce the heat release rate of the burning material, and shorten the burning time.

In the case of sprayed polyurethane foams, fire retardant additives may be injected into the base foam as liquids or fine powders, becoming dispersed throughout the material's cell structure as it is sprayed and allowed to set. Jurs [33] outlines the subgroups of flame retardant additives commonly found in polymers. These additives inhibit burning via one or multiple mechanisms, as described below.

1. Charring – In a polymer's condensed phase, charring adds a protective layer of incombustible solid between a flame front and the polymer fuel, interrupting the supply of vapours to the flame and slowing flame propagation.

2. Dilution – The presence of filler components in a solid polymer matrix can help to dilute the flame and absorb heat, thus lowering the net polymer temperature and discouraging ignition, flame spread, and fire growth.

3. Reaction Chemistry – In a polymer's vapour phase, the combustion reaction can be chemically "choked" with the addition of halogens or other chemicals that scavenge high energy free radicals from combustion zones, thus reducing reaction pathways and slowing the combustion reaction.

Even with fire barrier protection, many applications of SPF specifically require that the material be "fire rated", generally referring to a "Class A" characterization in flame spread and smoke development as determined in the ASTM E84 Steiner tunnel fire test (refer to Table 2.1 for the requirements for different levels of performance classification). The Steiner tunnel fire test measures flame propagation along a horizontal specimen exposed at one end to a gas flame in a ventilation controlled chamber, and the smoke developed by the burning material over the duration of the test. In order to achieve the required classification, a material must both resist the spread of flame and limit the production of smoke as it burns. This test apparatus forms the subject matter of Section 2.3.

There are many commercial applications for which it is important that a material achieve a Class A flame spread and smoke rating in the ASTM E84 Steiner tunnel fire test. In these cases, it is often found that adding increasing amounts of different combinations of fire retardants will improve a material's flame performance in the Steiner tunnel test accordingly; however, this improvement is often observed to come at the cost of degraded smoke performance. A balance must be achieved between the ratios and total concentrations of fire retardants (FRs) used in order to obtain improved flame performance without sacrificing smoke performance. This balance can often be determined, but usually only after a great deal of Steiner tunnel testing.

As alluded to in the example above, the process of SPF mixture design with respect to fire performance is largely empirical. The mixture design process will generally include a "fire retardant optimization" phase, during which FR concentrations and ratios of different FRs are adjusted, and intermediate mixtures are tested at scale until a sufficient performance classification is achieved. While there are a great many fire retardants available commercially, there is no general guideline on the use of these products pertaining to meeting performance standards. In the absence of such guidelines, a manufacturer's R&D team may start with a particular FR mixture from past experience or word-of-mouth, and adjust levels as necessary until the desired performance level is met.

The main concern with the FR optimization phase of mixture design is the amount of time, not to mention cost, that is inherent in repeated large-scale fire testing. Even in the absence of a physical model for FR interaction in a fire test, the FR optimization phase of mixture design would be much improved if scaled-down fire tests could be conducted on intermediate mixtures. Herein lies the motivation for this study: if SPF materials can be screened using small-scale fire tests, then the FR optimization phase of mixture design can be expedited and the overall R&D cost of mixture design consequentially reduced. It is the objective of this research to determine whether such a relationship does exist, and whether it is quantifiable, repeatable, and sufficiently accurate so as to determine the expected relative performance of materials in the large-scale Steiner tunnel test.

The Steiner tunnel test method and candidate small scale test methods – cone calorimeter and smoke density chamber – are discussed in the following three sections.

2.3 Overview of the ASTM E84 Steiner Tunnel Test

The Steiner tunnel test is a large-scale flame spread test that is used to evaluate the flammability and smoke hazard of interior finish materials. The apparatus and test method were originally developed in the mid-1900's, and have since undergone numerous revisions and additions [34, 35]. In addition to interior finish materials, the test is also used to evaluate polymeric insulation products, such as sprayed polyurethane foam.

A Steiner tunnel test reports two results: the flame spread index, FSI, and the smoke developed index, SDI. These two results are used to describe the performance of a specimen relative to the reference material, red oak, which has a flame spread index of approximately 90* and a smoke developed index of 100†. Additionally, the smoke developed index of fibre cement board has been established to be 0 [4]. The methodologies for calculation of flame spread and smoke developed indices are outlined in Sections 2.3.1 and 2.3.2.

In the current US building code, interior finish materials are classified in the Steiner tunnel test according to their FSI and SDI. There are three classifications for lining materials [36], as outlined in Table 2.1. These same classifications are used in Canadian tests.

Table 2.1: Classifications for interior finish materials in the Steiner tunnel test.

Class	Flame Spread Index	Smoke Developed Index
Class A	0–25	0–450
Class B	26–75	0–450
Class C	76–200	0–450
Plenum Materials	0–25	0–50

*ASTM E84 stipulates that a standard configuration of red oak exposed to the prescribed time-temperature curve in the tunnel will result in a flame that propagates to the end of the specimen (19.5 feet) in a time no less than 5 min 15 s and no more than 5 min 45 s. Assuming linear rate of flame spread, this stipulation results in a flame spread index for red oak of approximately 90.

†Calculation of the smoke developed index for a given specimen involves normalization of the measured obscuration by the obscuration measured for red oak during calibration. By definition, therefore, the smoke developed index of red oak in any Steiner tunnel is exactly 100.

The Steiner tunnel test is conducted in the US and Canada according to one of four test standards: ASTM E84 [4], UL 723 [37], CAN/ULC S102 [38], and CAN/ULC S102.2 [39]. The methodology in ASTM E84, UL 723, and CAN/ULC S102 stipulates the mounting of specimens in the "ceiling position", with the exposed surface of the foam facing down. The three test methods are fairly similar, although the calculation methodologies differ slightly in the CAN/ULC S102 method [4, 37, 38]. Furthermore, CAN/ULC S102 requires that the CAN/ULC S127 test also be conducted; if the flame spread rating for a given material is greater in CAN/ULC S127, then the result takes precedence over the CAN/ULC S102 result [40]. CAN/ULC S102.2 is intended to test materials and assemblies used in flooring; it differs from the other Steiner tunnel test methods in that it mounts samples with the exposed surface of the specimen facing up [39]. Flame spread and smoke developed classifications in the S102.2 test are not assumed to be comparable to flame spread and smoke developed indices in the other three methods due to the effects of sample orientation on combustion [41].

The ASTM E84 standard has been selected for this study, since this is the standard to which the manufacturer of the FRSPF tests their materials. Flame spread index and smoke developed index are calculated according to the standard [4].

The Steiner tunnel apparatus consists of a 24-foot long insulated fire test chamber with an open end for air intake, and an exhaust end for extraction of air and fire gases. A dual-port 3/4 inch diameter methane gas burner is located on the intake end of the test chamber, which is accordingly designated the "fire end". The "exhaust end" of the tunnel is fitted with a gradual rectangular-to-round transition piece, to which a cylindrical exhaust duct is connected. A photometer system, consisting of a lamp and photoelectric cell, is mounted within the exhaust duct to measure optical obscuration of the fire gases. Figure 2.1 shows a schematic of the exterior of the Steiner tunnel along its side, while Figure 2.2 shows a section through the burner outlets looking down the length of the tunnel.

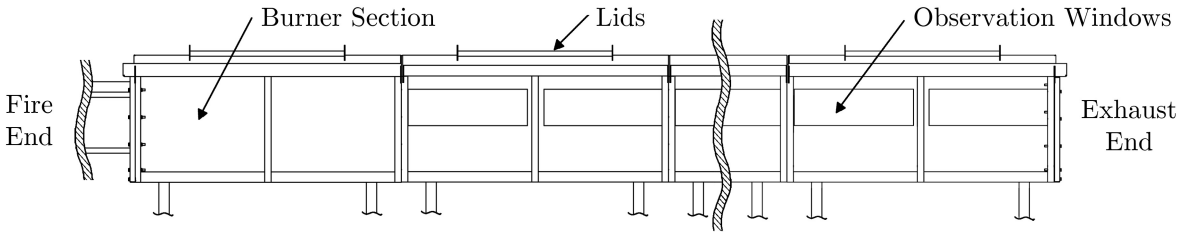

Figure 2.1: Side profile of the observation side of a representative Steiner tunnel.

Figure 2.1 shows that side of the test chamber is outfitted with insulated windows along its length, which allow for observation of flame propagation by the test operator. The top of the test chamber is a removable lid, which is insulated and water-sealed to limit heat and

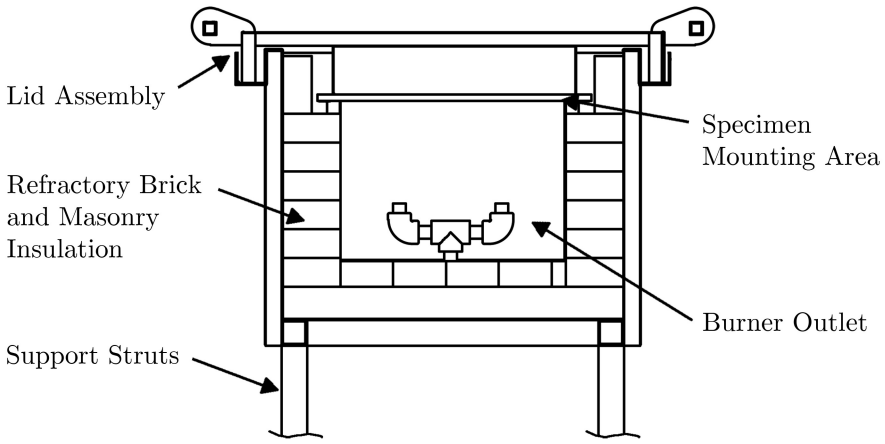

Figure 2.2: Section profile through the burner outlet of a representative Steiner tunnel.

gas leakage. A specimen is placed on the test chamber ledges with the exposed side facing down (in the ASTM E84 configuration), at a distance of approximately 7.5 inches (19 cm) above the burner ports, and the lid is positioned over the back side of the specimen. With the specimen in place, the tunnel is sealed and the draft is adjusted to achieve the desired flow rate within the tunnel.

The test commences with ignition of the gas burner. The test operator observes and records the distance and corresponding time of flame front propagation along the specimen length in intervals of 15 seconds. Output from the photoelectric cell is recorded at intervals of 1 second. The test is terminated after 10 minutes of exposure of the specimen to the gas burner, upon which the gas burner is deactivated. Flame spread distance and photoelectric cell voltage are plotted against time for the test duration and are used to determine flame spread and smoke developed indices. The calculation methodologies for flame spread and smoke developed indices are presented in Sections 2.3.1 and 2.3.2 respectively.

2.3.1 Flame Spread Index

Flame propagation along the length of the specimen is observed by the test operator through the observation windows on the side of the tunnel, as shown in Figure 2.1. The observed position of the flame front at a given time increment, $f(\tau)$, is recorded by the test operator every 15 seconds from the start of the test. Flame spread area, F_1, is calculated using trapezoidal integration [42] with spacing of 15 seconds (N = 40 for a 10 minute test), as in Equation 2.1. Since the spacing matches the sampling frequency of the test, there is

no error from numerical approximation.

$$F_1 = \sum_{i=0}^{N-1} \left[\frac{(\tau_{i+1} - \tau_i)(f_{i+1} + f_i)}{2} \right] = \frac{15}{2} \cdot \sum_{i=0}^{N-1} (f_{i+1} + f_i) \tag{2.1}$$

Maximum flame propagation, $f_{max}(\tau)$, is the maximum recorded flame position up to a given time increment. $f(\tau)$ and $f_{max}(\tau)$ are only distinct when the flame front undergoes a period of regression, as exemplified in Figure 2.3. In the figure, the red trace (with light grey area) corresponds to the flame propagation curve, which first increases with time until $\tau = 3$ min, and then decreases with time until the end of the test. The blue trace (with dark grey area) in Figure 2.3 corresponds to the maximum flame propagation curve, which identically increases with time during the forward propagation period, and then remains at that peak when the flame front regresses.

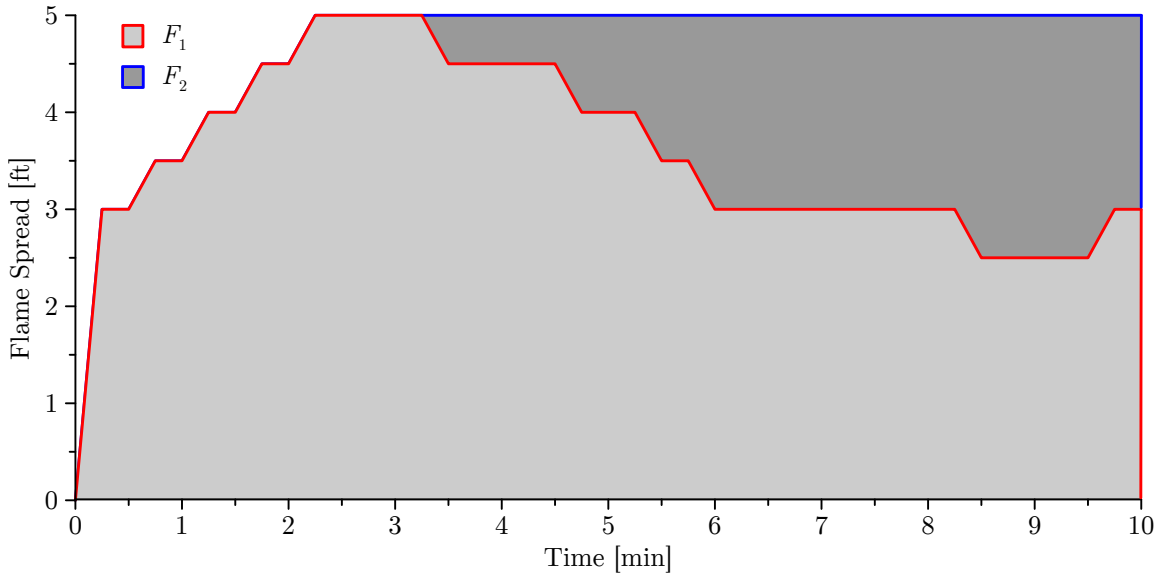

Figure 2.3: Illustrative flame spread curve for a FRSPF specimen.

Total flame spread area, F_T, may be calculated as the summation of flame spread area, F_1, and maximum flame spread area, F_2. The two areas are distinguished in Figure 2.3. Total flame spread area is calculated numerically by integrating the maximum flame spread curve, as in Equation 2.2.

$$F_T = \sum_{i=0}^{N-1} \left[\frac{(\tau_{i+1} - \tau_i)(f_{max,i+1} + f_{max,i})}{2} \right] = \frac{15}{2} \cdot \sum_{i=0}^{N-1} (f_{max,i+1} + f_{max,i}) \tag{2.2}$$

Maximum flame spread area is calculated by subtracting flame spread area from total flame spread area, as in Equation 2.3. F_2 is not used directly in the calculation of the

flame spread index, but the methodology is included for reference.

$$F_2 = F_T - F_1 = \frac{15}{2} \cdot \sum_{i=0}^{N-1} \left(f_{max,i+1} + f_{max,i} - f_{i+1} - f_i \right) \tag{2.3}$$

Flame spread index is computed from total flame spread area according to Equation 2.4.

$$FSI = \begin{cases} \dfrac{4900}{195 - F_T} & F_T > 97.5 \text{ ft} \cdot \text{min} \\ 0.515 \cdot F_T & F_T \leq 97.5 \text{ ft} \cdot \text{min} \end{cases} \tag{2.4}$$

Flame spread areas are reported in units of ft·min for tests conducted according to ASTM E84. In this study, all variables are converted to their metric equivalents, so flame spread area is calculated in units of m·s. Furthermore, ASTM E84 dictates that the reported FSI is rounded to the nearest 5. All calculations in this study are based on the actual FSI, derived from Equations 2.1 through 2.4.

In traditional building materials such as wood, flame propagation tends to occur predictably, and in a single direction. In contrast, fire-retarded sprayed polyurethane foam tends to burn in a multi-stage manner: an initial period of flame propagation, followed by a period of flame regression, and sometimes followed by successive periods of flame propagation or steady burning. This behaviour is exemplified in Figure 2.4, which shows the flame spread of the same FRSPF material as in Figure 2.3 plotted along with the flame spread of a red oak reference specimen. Note that the red oak calibration curve is provided with each test result from the Steiner tunnel testing facility.

2.3.2 Smoke Developed Index

The Steiner tunnel apparatus is equipped with a photoelectric cell to measure changes in the attenuation of incident light by the passing smoke, particulate, and other effluent. The output of the cell is a voltage which is directly proportional to the amount of light received from the light source [4]. The smoke obscuration curve, $SO(\tau)$, is determined from the output of the photoelectric cell as in Equation 2.5. The output voltage is divided by the calibrated maximum transmission voltage (in the case of the apparatus in this study, this is 10 Volts), and subtracted from 100% to give a percentage obscuration.

$$SO(\tau) = 100\% - \frac{E(\tau)}{E_{max}} = 1 - \frac{E(\tau)}{10} \tag{2.5}$$

Total smoke obscuration, TSO, is interpreted as the average smoke obscuration over the test duration. Total smoke obscuration is calculated by integrating smoke obscuration

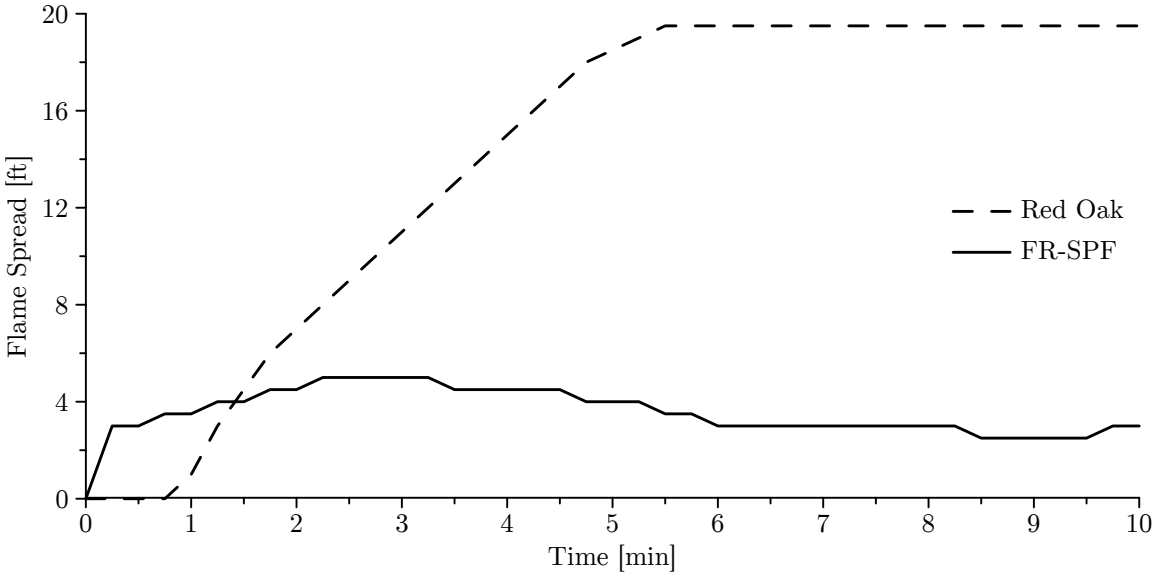

Figure 2.4: Comparison of flame spread curves for an FRSPF and red oak.

with respect to time over the duration of the test, and dividing by the total test duration, τ_2. Trapezoidal integration [42] with spacing of 1 second is used to compute the integral, as in Equation 2.6. Since the polling frequency of the data acquisition system matches the spacing in the computation algorithm, error from numerical approximation is considered to be insignificant.

$$TSO = \frac{1}{\tau_2}\int_0^{\tau_2} SO\left(\tau\right)\cdot \mathrm{d}\tau = \frac{1}{\tau_2}\cdot\sum_{i=0}^{N-1}\left[\frac{\left(\tau_{i+1}-\tau_i\right)\left(SO_{i+1}+SO_i\right)}{2}\right] \tag{2.6}$$

Since the test duration is constant at 600 seconds, and the sampling interval is constant at 1 second, Equation 2.6 simplifies to Equation 2.7.

$$TSO = \frac{1}{1200}\cdot\sum_{i=0}^{N-1}\left(SO_{i+1}+SO_i\right) \tag{2.7}$$

Reference smoke obscuration, TSO_R, is calculated using Equation 2.7 for a red oak reference specimen. Reference smoke obscuration is determined by the testing laboratory on a monthly basis according to the ASTM E84 standard. The testing facility has reported the reference smoke obscuration to be 16.20% consistently for all 30 tests in this study.

Smoke developed index is calculated by dividing the total smoke obscuration by the reference smoke obscuration, as in Equation 2.8.

$$SDI = 100\cdot\frac{TSO}{TSO_R} = 617.3\cdot TSO \tag{2.8}$$

ASTM E84 dictates that the reported SDI is rounded to the nearest 5 when SDI is less than 200, and rounded to the nearest 50 when SDI is greater than or equal to 200. All calculations in this study are based on the actual SDI, derived from Equations 2.5 through 2.8.

Smoke development tends to be related to the intensity of burning and amount of material burning at a given time. Typical behaviour consists of an initial period of comparatively high obscuration, followed by a period of declining obscuration. For fire-retarded sprayed polyurethane foams in this study, the period of declining obscuration has been observed to follow the period of flame regression. Figure 2.5 shows the smoke obscuration curves corresponding to the same specimens for which flame spread results were plotted in Figure 2.4.

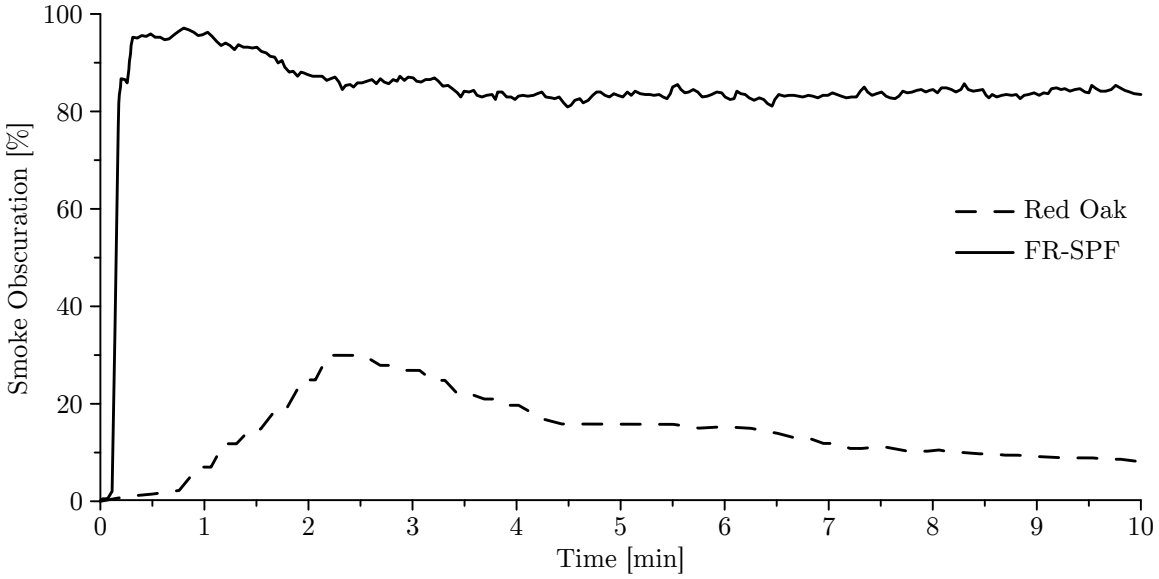

Figure 2.5: Comparison of smoke developed curves for an FRSPF and red oak.

Even without prior knowledge of the calculation methodologies for the flame spread index and smoke developed index, it is apparent from Figures 2.4 and 2.5 that the FRSPF materials demonstrate significantly less flame spread and significantly more smoke obscuration than standard wood construction materials.

2.4 Overview of the Cone Calorimeter Test

The cone calorimeter test is a bench-scale heat release rate test that is used to evaluate a range of material fire properties, the most important of which, from the perspective of fire

modelling at least, is the experimentally determined heat release rate [6]. The principle of oxygen consumption calorimetry is used to determine experimentally the heat release rate for materials exposed to uniform radiant heating and active ignition. The test may be used to develop conclusions on the basis of ignitability, average heat release rate, burning mass loss, char yield, effective heat of combustion, combustion efficiency, and visible smoke development for a range of different materials [5].

The test was originally developed in 1982 at the National Institute of Standards and Technology (NIST), then the National Bureau of Standards (NBS) [43]. The basic principle of operation has not changed since the 1982 NBS calorimeter, although revisions have led to significant improvements in operation and test method [44].

The cone calorimeter test may be conducted according to several standards, of which the most prevalent in the US and Canada include:

- ASTM E1354, first published in 1990 [5, 44];
- ISO 5660, first published in 1993 [45, 44];
- NFPA 264, first published in 1992 [46]; and
- ULC S135, first published in 2004 [47], and formerly listed as CAN/ULC S135, first published in 1992 [48].

Test methods and calculations are fairly similar between the standards, with the primary difference being the manner in which results are reported. The ASTM E1354 standard is followed in this study, at the request of the manufacturer.

The modern apparatus used in this study is manufactured by Fire Testing Technology (FTT), a UK-based company that specializes in the development of fire testing instrumentation. The apparatus is located at the University of Waterloo Live Fire Research facility (UWLFR), and is in regular operation by technical staff in the fire research group. The apparatus is shown in Figures 2.6 and 2.7, and further described below.

A sample measuring nominally 100 mm by 100 mm in area and 25 mm thick is mounted in a steel sample holder, covered by a steel edge frame, and loaded onto the specimen platform (Figure 2.6). A conical radiant heat source is positioned above the specimen platform, and the surface of the specimen is exposed to a prescribed level of heat flux. The radiant heat source is initially covered by insulated shutters; the start of the test coincides with activation of the shutters, and exposure of the specimen to the radiant heat. Additionally, an electric spark igniter is located approximately 10 mm above the surface of the specimen.

Specimens are prepared and conditioned 24 hours in advance of testing. Figure 2.8a shows a prepared specimen of sprayed polyurethane foam, while Figure 2.8b shows the specimen mounted in the sample holder and edge frame.

Figure 2.6: Detail of the specimen platform on the UWLFR cone calorimeter.

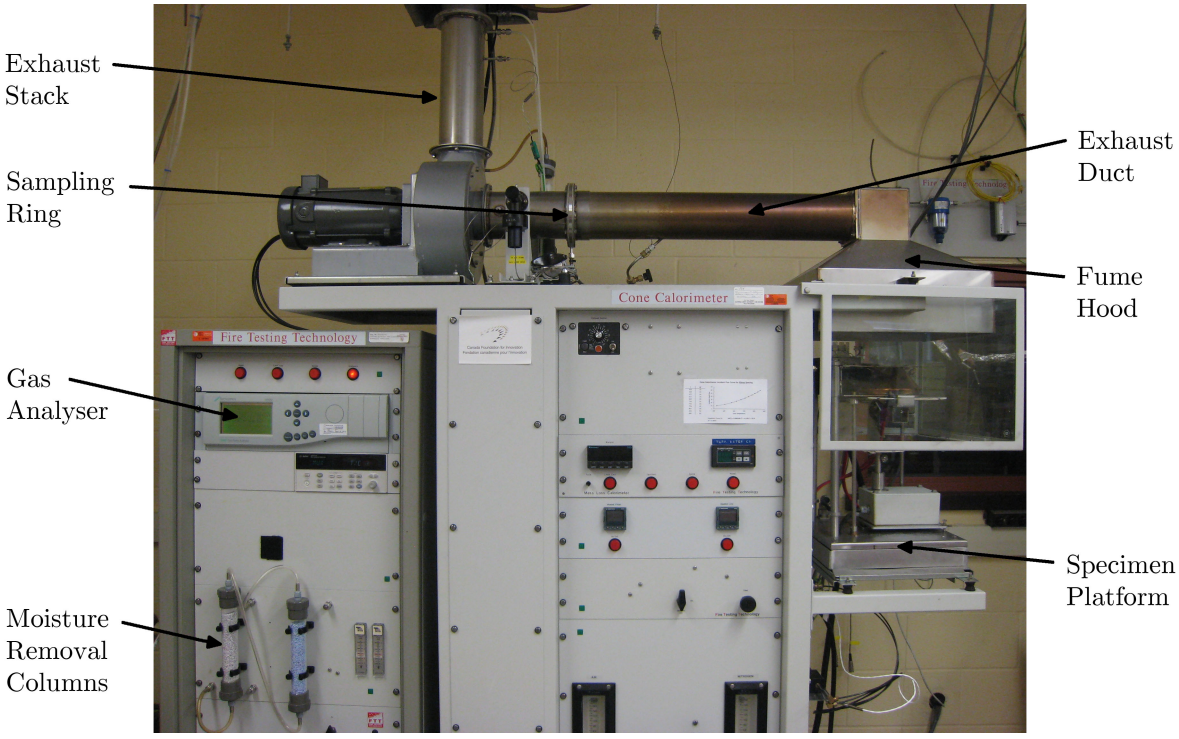

Figure 2.7: The UWLFR cone calorimeter, with relevant sections identified.

(a) A prepared and conditioned specimen.

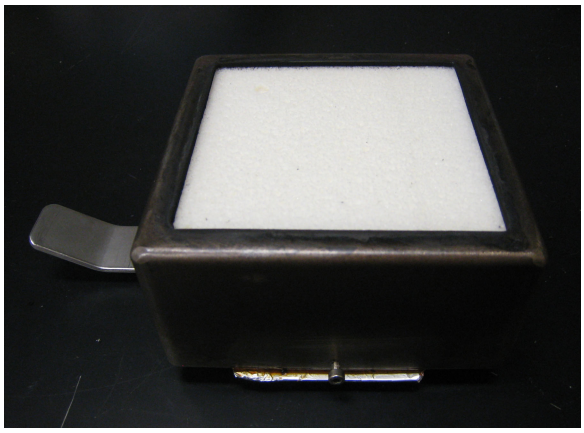

(b) Sample holder and edge frame.

Figure 2.8: A prepared specimen mounted in the sample holder and edge frame.

As the sample is exposed to incident flux, it heats and begins to vapourize. Depending on the interaction of the vapourized specimen with ambient air, radiant heat from the cone heater, and the electric energy from the spark igniter, the specimen may ignite. Observation of specimen ignition corresponds to the start of the "burning period," as it is referred to in this work. Figure 2.9 shows a burning specimen.

Figure 2.9: A burning specimen in the cone calorimeter test.

As the sample burns, a load cell measures the decaying mass of the sample while combustion gases are collected in the fume hood, pass through the exhaust duct, and are

extracted through the exhaust stack (Figure 2.7). In the exhaust duct, a sampling ring draws combustion gases into the gas sampling system. The gas sampling system includes soot filtration, moisture removal by means of a sorbent drying agent, and a gas analyser which measures the volume fractions of oxygen, carbon dioxide, and carbon monoxide in the sample gas. Temperature and pressure differential across an orifice plate are measured in the exhaust stack, and are used to approximate the volume flow rate of gases in the stack.

As the specimen burns, flames will eventually extinguish, indicating the end of the burning period. Burning behaviour may undergo a transition to small, barely visible flames with very little heat release. ASTM E1354 is notably unspecific on the definition of flame extinction, defining sustained flaming as "existence of flame on or over most of the specimen surface for periods of at least 4 seconds" [5]. In this work, the end of the burning period is marked by the extinction of visible flames or the transition to barely visible flames with measured heat release rate less than 5 kW/m^2.

FTT's software, Conecalc [49], runs on a computer connected via serial cable to the cone calorimeter. During a test, the software records a number of data channels; six of these channels are used in the calculation of heat release rate, burning mass loss, and derived results:

- volume fraction of oxygen in the sample gases, X_{O_2};
- volume fraction of carbon dioxide in the sample gases, X_{CO_2};
- volume fraction of carbon monoxide in the sample gases, X_{CO};
- pressure drop in the exhaust stack, Δp;
- temperature in the exhaust stack, t_e; and
- specimen mass, m_s.

The FRSPF used in this study is observed to vapourize and ignite quickly. Following ignition, a period of rapid fire growth is observed, concluding with a peak rate of heat release. Next, a period of decaying fire growth ending with flame extinction are observed. Finally, non-flaming combustion (smoldering) occurs until test conclusion. According to the ASTM E1354 standard, the test is concluded 60 seconds following extinction of visible flames, although data collection may continue if the smoldering heat release rate or mass loss rate is significant.

The calculation methodologies for heat release rate, burning mass loss, and derived parameters are presented in Section 2.4.1.

2.4.1 Heat Release Rate

Heat release rate per exposed specimen area, $q''(t)$, is calculated using a process known as oxygen consumption calorimetry. It has been shown that for a large number of organic substances, a constant net heat is released per unit of oxygen consumed. For organic solids, this value is taken to be 13.1 MJ/kg, which was calculated as an average value for a variety of solid materials and is considered to be accurate, with very few exceptions, to within ±5% [50]. The principle behind oxygen consumption calorimetry is to approximate a burning specimen's heat release rate by measuring the change in the mass percentage of oxygen in the combustion gases. Carbon monoxide and carbon dioxide levels are also incorporated into the calculation, to account for incomplete combustion.

Heat release rate per unit exposed surface area of a burning sample is calculated by Equation 2.9. Note that the oxygen consumption factor and mass flow rate of gases are time indexed, and the "(t)" term is excluded for simplicity. Refer to the Nomenclature section for additional explanation of the terms used in the oxygen consumption calorimetry procedure.

$$q''(t) = \frac{E_{O_2}}{A_s}\left(\frac{\phi}{1+\phi(\alpha-1)}\right)\dot{m}_e\frac{M_{O_2}}{M^{\circ}_{air}}\left(1-X^{\circ}_{H_2O}-X^{\circ}_{CO_2}\right)X^{\circ}_{O_2} \tag{2.9}$$

The volumetric expansion factor, α, depends on the composition and burning behaviour of the fuel. For example, $\alpha = 1$ for the complete combustion of carbon in dry air, while $\alpha = 1.21$ for pure hydrogen fuel. Since the composition of R&D materials is rarely, if ever, known, the recommended average value of 1.105 is deemed appropriate for the majority of cone calorimeter testing [51].

The oxygen consumption factor, ϕ, is calculated by Equation 2.10.

$$\phi = \frac{X^{\circ}_{O_2}(1-X_{CO_2}-X_{CO}) - X_{O_2}\left(1-X^{\circ}_{CO_2}\right)}{\left(1-X_{O_2}-X_{CO_2}\cdot X_{CO}\right)X^{\circ}_{O_2}} \tag{2.10}$$

Mass flow rate of gases through the stack, $\dot{m}_e$, is approximated from the known dimensions of the stack (diameter of 114 millimetres), gas temperature within the stack (stack thermocouple), and the pressure pressure drop in the stack (stack orifice plate). The orifice plate coefficient, C, is calibrated for a standard volume flow rate of 24 L/s [51]. Mass flow rate of gases through the stack is calculated by Equation 2.11.

$$\dot{m}_e = C\sqrt{\frac{\Delta p}{T_e}} \tag{2.11}$$

Ambient temperature, pressure and relative humidity are measured prior to the test. The mole fraction of water vapour in the incoming air is calculated by Equation 2.12.

$$X^{\circ}_{H_2O} = RH^{\circ}_{air} \left(\frac{p_{s,air}}{p^{\circ}_{air}} \right) \tag{2.12}$$

The molecular weight of the incoming air, which is required in Equation 2.9, is calculated by Equation 2.13.

$$M^{\circ}_{air} = M_{air} \left(1 - X^{\circ}_{H_2O}\right) + M_{H_2O} \cdot X^{\circ}_{H_2O} \tag{2.13}$$

Conecalc calculates heat release rate per exposed specimen area in units of kW/m^2, according to Equation 2.9. Exposed specimen area is measured by the user prior to the test. When the standard edge frame is used, the exposed specimen area is fixed at 88.4 cm^2. Heat release rate can be calculated for all tests in which the edge frame is used by Equation 2.14. It is useful to reduce the result to its base energy rate unit for developing unit-based correlations. Note that the heat release rate calculated by Equation 2.14 is in units of Watts (Joules per second), and $q''(t)$ is entered in units of kW/m^2.

$$q(t) = 8.84 \cdot q''(t) \tag{2.14}$$

Peak heat release rate, q_p, is the maximum heat release rate achieved in a test. This parameter is useful in characterizing relative performance, where a lesser peak heat release rate is desirable from a fire safety perspective.

Total heat release from the start of the test is calculated as in Equation 2.15.

$$Q(t) = \int_0^t q(t) \cdot \mathrm{d}t \tag{2.15}$$

Trapezoidal integration [42] with spacing of 1 second is used to compute the integral, as in Equation 2.16.

$$Q(t) = \frac{q(t)}{2} + \sum_{i=1}^{t-1} q(i) \tag{2.16}$$

Total heat release during a specified time interval is calculated as in Equation 2.17.

$$Q(t_1, t_2) = \int_{t_1}^{t_2} q(t) \cdot \mathrm{d}t \tag{2.17}$$

Trapezoidal integration [42] with spacing of 1 second is used to compute the integral, as in Equation 2.18.

$$Q(t_1, t_2) = \frac{q(t_1) + q(t_2)}{2} + \sum_{i=1}^{t_2 - t_1 - 1} q(t_1 + i) \tag{2.18}$$

Average heat release (alternatively, burning heat release) is defined as the total heat release during the burning period, and is calculated by Equation 2.19. Note that the burning period, t_b, is defined as the difference between the time to flame extinction, t_{fo}, and the time to ignition, t_{ign}.

$$Q_b = \frac{q\left(t_{ign}\right) + q\left(t_{fo}\right)}{2} + \sum_{i=1}^{t_b - 1} q\left(t_{ign} + i\right) \tag{2.19}$$

Average heat release rate (alternatively, burning heat release rate) is defined as the average heat release rate during the burning period, and is calculated by Equation 2.20.

$$q_b = \frac{Q_b}{t_b} = \frac{q\left(t_{ign}\right) + q\left(t_{fo}\right)}{2 \cdot t_b} + \frac{1}{t_b} \sum_{i=1}^{t_b - 1} q\left(t_{ign} + i\right) \tag{2.20}$$

The calculation and interpretation of burning heat release rate are visualized in Figure 2.10, where t_{sot} indicates the start of test time, and t_{eot} indicates the end of test time.

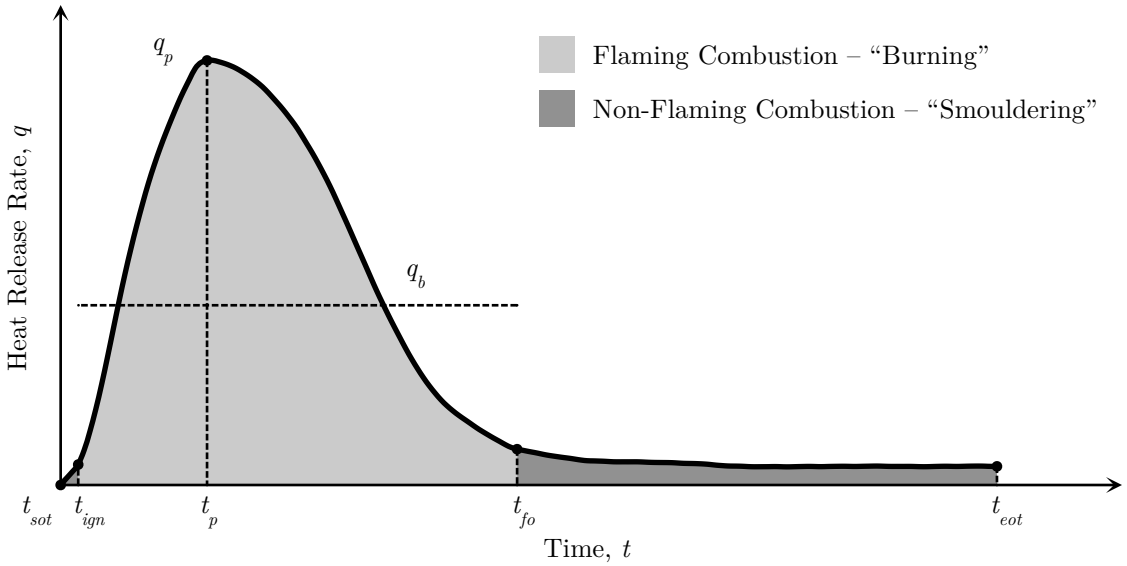

Figure 2.10: Flaming and non-flaming combustion regions in a cone calorimeter test.

Total mass loss from the start of the test is calculated as in Equation 2.21, where $m_{s,o}$ is the initial mass of the specimen.

$$ML\left(t\right) = m_{s,o} - m_s\left(t\right) \tag{2.21}$$

Mass loss during a specified time interval is calculated as in Equation 2.22.

$$ML\left(t_1, t_2\right) = m_s\left(t_1\right) - m_s\left(t_2\right) \tag{2.22}$$

Burning mass loss, defined as the total mass lost during the burning interval, is calculated by Equation 2.23.

$$ML_b = m_s\left(t_{ign}\right) - m_s\left(t_{fo}\right) \tag{2.23}$$

2.5 Overview of the Smoke Density Chamber Test

The smoke density chamber fire test is used to measure the amount of smoke generated from a burning specimen, and the specific optical density of the smoke that is generated. The apparatus is essentially a closed system of fixed volume, in which a plane specimen is exposed to a radiant heat source. Although the test results are not assumed to have a direct relationship to large-scale fire hazards, the test is useful for characterizing and evaluating the smoke performance of materials in a controlled fire scenario. The test can accommodate a range of material types from various fields, including building materials.

Development of the smoke density chamber test can be traced back to 1967 at NIST, formerly NBS [52]. In the late 1960's, there existed a general interest in the building materials and aircraft industries in the problem of smoke generation of materials; this interest led to the development of the NBS proposed test method and apparatus in 1969 [52]. Since its development, NIST has continued to study the results of the test and their application to fire safety science. One such study was conducted by Lee at NBS, who correlated test results from 22 participating laboratories across the United States [53]. The study showed that reproducible results were attainable for a variety of materials tested under flaming and non-flaming exposure conditions in the smoke density chamber apparatus. Construction of an improved and standardized apparatus was recommended.

Over the years, the NBS apparatus has evolved to accommodate a range of configurations, and to include modern computer controls. Figure 2.11 shows a modern smoke density chamber manufactured by FTT. This particular apparatus, the one used in this research, is located at the UWLFR facility, and is in regular operation by technical staff in the fire research group.

The first version of the test standard for the smoke density chamber was an appendix to Lee's NBS report, titled "Test Method for Measuring the Smoke Generation Characteristics of Solid Materials" [53]. This NBS test method served as a foundation for the development of test methods by other standardizing bodies. Three primary standards regulate the smoke density chamber fire test in Canada and the United States.

ASTM E662 was first published in 1979, and was developed directly from the original NBS test method. As with the original NBS apparatus, the ASTM E662 apparatus includes

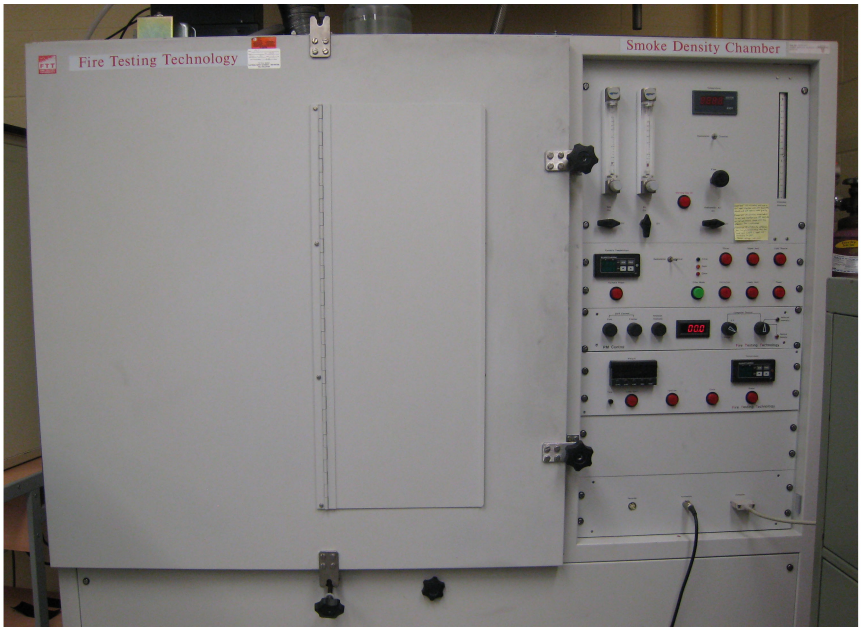

Figure 2.11: The UWLFR smoke density chamber.

a vertically-oriented radiant heater with a 3 inch diameter circular opening. The specimen is also mounted vertically, parallel to the radiant heater [54].

ISO 5659-2 was first published in 1994, and incorporates a variety of changes to the apparatus test methodology. The most significant change is replacement of the NBS-style radiant heater with a horizontally-oriented cone heater, similar to that used in the cone calorimeter. The horizontal orientation allows the specimen holder to include a load cell, identical to that used in the cone calorimeter, in the case of the FTT model [7].

ASTM E1995 was first published in 1998, and incorporates many of the changes introduced by the ISO method, including the cone heater. The standard does not, however, supersede ASTM E662, and both apparatus configurations remain viable options [55].

The differences in sample orientation, radiant heating source, and load cell are illustrated for the UWLFR apparatus in Figure 2.12.

All three standards stipulate identical specifications for chamber size, photometric system, and collection of optical transmission data. The ISO 5659-2 standard is followed in this study, at the request of the manufacturer.

The main test chamber is an airtight compartment of porcelain-enamelled metal construction, with internal dimensions of 914 mm wide, 914 mm tall, and 610 mm deep. The front-mounted door has an observation window placed such that the burning specimen may be observed, but laboratory light will not interfere with the photometric system. The

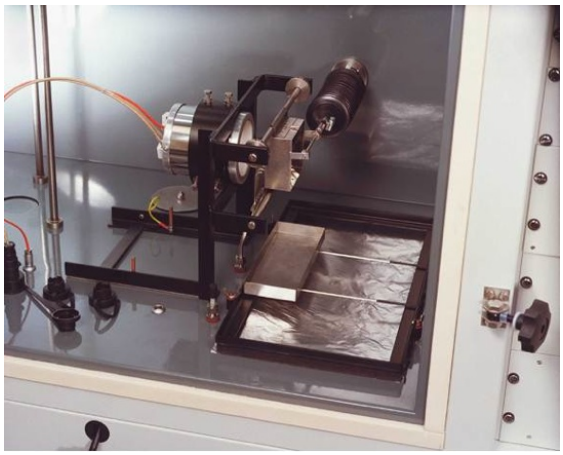

(a) Vertical orientation, ASTM E662.

(b) Horizontal orientation, ISO 5659-2.

Figure 2.12: Differences in orientation between ASTM E662 and ISO 5659-2.

entire chamber is covered on the back-side with electric hot wires to warm the chamber walls during a test. Glass windows of 51 mm diameter are located on the top and bottom of the chamber, for the photometric system and light source respectively.

The light source is a 6.5 Volt 2.75 Amp tungsten filament lamp housed in a light-tight box under the bottom of the chamber. Light is directed through a 51 mm diameter lens and through the lower optical window into the chamber. The lower optical window is heated to minimize condensation of water vapour and other combustion products on the glass.

The photometric system can be divided into two parts: the optical system housing on the top of the chamber, and the photomultiplier control unit. The optical system housing is positioned on the top of the chamber, directly over the upper optical window. A lens is used to focus the light beam to a small point at a circular aperture, which can be rotated between three positions: dark (zero transmission), clear (full transmission), and filtered (filtered transmission). The range extension filter extends the range of the photomultiplier tube to allow it to remain accurate both at very high and very low transmission values. The photomultiplier tube is located in the upper part of the housing. It sends a signal to the photomultiplier control unit proportional to the intensity of the light beam. In addition to the range extension filter, the photomultiplier tube can apply a range adjustment of 0.1, 1, 10, or 100 to the incoming signal. This allows the photometric system to smoothly transition between large changes in the optical transmission.

The cone heater, load cell, and specimen platform are located to the side of the light path, as illustrated in Figure 2.13. As with the cone calorimeter, a specimen is placed in a

steel sample holder, covered by a steel edge frame, and placed on the load cell attachment. The specimen size is slightly smaller in the smoke density chamber test than in the cone calorimeter test, measuring 75 mm by 75 mm in area, and up to 25 mm thick. As in the cone calorimeter test, specimens are prepared and conditioned 24 hours in advance of testing.

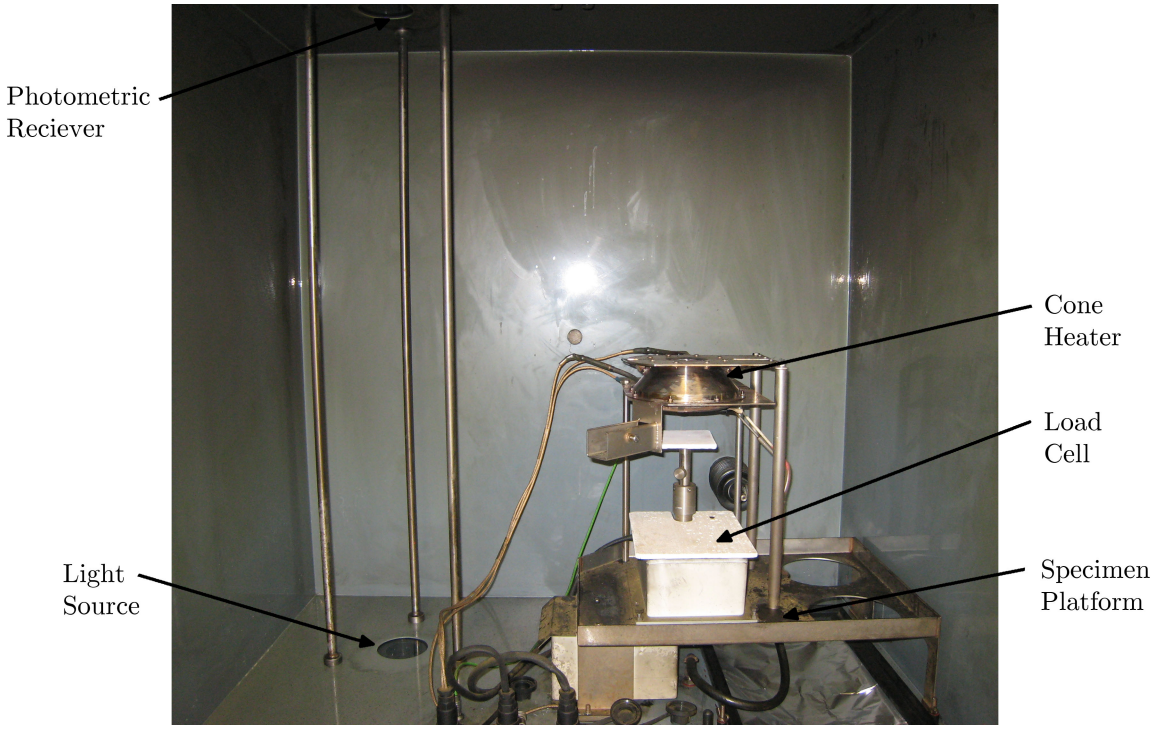

Figure 2.13: Detail of the interior of the UWLFR smoke density chamber.

A spark igniter is also present in the smoke density chamber, with a primary function of igniting a propane burner. The burner consists of a single tube attached to the spark igniter. Propane and air are pre-mixed and enter the chamber at a very low flow rate. The burner flame is calibrated by adjusting the flow rates of propane and air supplies to obtain a flame which is approximately 3 cm in length and primarily blue in colour, with an orange tip.

As the sample is exposed to incident flux, it begins to vapourize and, depending on the influence of the fire-retardant additives, may ignite. As the sample burns, a load cell measures the decaying mass of the sample. Combustion gases build up within the chamber, and the photometric system measures the reduction in transmission along the light path from bottom to top of the chamber.

FTT's software, Smokebox [56], runs on a computer connected via serial cable to the

smoke density chamber. Unlike the cone calorimeter test, only two data channels are recorded by Smokebox:

- specimen mass, $m_s(t)$; and
- optical transmission, $T_R(t)$.

The FRSPF used in this study tends to vapourize and ignite rapidly upon exposure to radiant heat. The chamber is observed to rapidly fill with dark smoke, eventually building up to a minimum transmission value. Burning time tends to be short, since the decreasing amount of oxidant remaining in the ambient environment tends to be insufficient to sustain flaming combustion. The chamber is sealed during the test, and it becomes increasingly pressurized as the sample burns. As combustion gases expand, controlled leakage occurs. Eventually, the rate of smoke production from the burning sample becomes slower than the rate of leakage from the apparatus, and the transmission begins to slowly increase. According to the ISO standard, the test is concluded 60 seconds following minimum transmission.

The calculation methodologies for optical obscuration and specific optical density are presented in Section 2.5.1.

2.5.1 Specific Optical Density

Optical obscuration is calculated from the recorded optical transmission, as in Equation 2.24.

$$TO(t) = 100\% - TR(t) \tag{2.24}$$

Specific optical density is calculated from the recorded optical transmission, as in Equation 2.25. The calculation is dependent on the recorded position of the range-extension filter, f, and the range setting on the photomultiplier control unit, d_{filter}.

$$DS(t) = \frac{V_c}{A_s \cdot L_p}\left[\log\left(\frac{100}{TR(t)}\right) + f \cdot d_{filter}\right] \tag{2.25}$$

Exposed specimen area is measured by the user prior to the test. When the standard edge frame is used, the exposed specimen area is fixed at 42.4 cm^2. Equation 2.25 can be simplified by evaluating the constant parameter $V_c/(A_s \cdot L_p) = 132$. The equation can be further simplified by eliminating d_{filter} using the range extension filter correction factor, C_f, which is a calibrated value. When the range extension filter is not in the light path ($f = 0$), the specific optical density is calculated by Equation 2.26; otherwise, the specific optical density is calculated by Equation 2.27.

$$DS(t) = 132 \cdot \log\left(\frac{100}{TR(t)}\right) \tag{2.26}$$

$$DS\left(t\right) = 132\left[\log\left(\frac{100}{TR\left(t\right)}\right) + 2\right] + C_f \tag{2.27}$$

Total mass loss from the start of the test is calculated as in Equation 2.28, where $m_{s,o}$ is the initial mass of the specimen.

$$ML\left(t\right) = m_{s,o} - m_s\left(t\right) \tag{2.28}$$

Time to minimum optical transmission, t_1, stands out as a particularly important time index. Minimum transmission is reached when rate of particulate smoke generation fails to exceed the rate of pressure loss within the chamber, which is controlled by the internal pressure relief system. t_1 effectively signals the time at which accumulation of smoke is at a maximum for a given sample.

Data indexed at t_1 represents "peak" values for the particular test. TO_1 represents a material's peak optical obscuration, DS_1 represents a material's peak specific optical density, and ML_1 represents a material's total mass loss at the time of peak optical obscuration. Since the smoke density chamber test is considered to be a cumulative measurement of smoke generation, the label "total" is used interchangeably with "peak" for TO_1, DS_1, and ML_1.

With critical results from the cone calorimeter and smoke density chamber tests identified, comparisons will be made for flame spread and smoke development from the Steiner tunnel across a series of polyurethane foam formulations. In the following chapter, details of the experimental methods used for all three fire tests are provided, leading up to results and development of models for flame spread and smoke development in Chapters 4 and 5 respectively.

Chapter 3

Experimental Method

The experiments undertaken in this research involve characterization of the fire performance of sprayed polyurethane foam materials using the Steiner tunnel test, the cone calorimeter and the smoke density chamber. Based on the data and results, the potential for scaling small-scale test results for these materials to the larger Steiner tunnel test is investigated. This chapter outlines the experimental method employed for each test, as well as the calculation methods used for quantification of error in the results.

3.1 Steiner Tunnel Tests

As outlined in Section 2.3, Steiner tunnel testing is conducted according to the ASTM E84 standard per the requirements of the manufacturer. This portion of the experimental testing is conducted at Exova Laboratories in Mississauga, ON, since the facilities to conduct these tests are not currently available in the University of Waterloo Fire Labs. For each test conducted, a complete report was supplied to the manufacturer. A sample of a test report, with confidential information removed, may be found in Appendix B. In addition to the reporting, the author was permitted to stand witness for a number of the tests, at the discretion of the testing laboratory.

The potential variability of Steiner tunnel test results was identified as an issue to be taken into consideration in this study, however it is also important to have a sufficient spread in foam formulations to allow development of correlations with some confidence. To this end, twenty foam formulations were selected and used in the main study. The overall test budget then allowed between two and four repeat tests on several formulations. Table 3.1 summarizes the five formulations selected for repeatability testing, and the number of tests conducted on each.

Table 3.1: Formulations selected for repeated Steiner tunnel testing.

Formulation	Number of Tests
F6	4
F7	3
F8	3
F9	2
F11	3

The test reports provided by Exova do not provide the actual flame spread and smoke developed indices, but rather rounded values which are the official "reported" test results. From a scientific perspective, using rounded values in the development of correlations is not appropriate, as it would add error and hence greater uncertainty to the results. Therefore, flame spread and smoke developed indices are re-calculated using the raw test data that is contained in the "Flame Spread" and "% Light Absorption" plots in the report. The recalculation method is described below.

First, the plots of raw test results are scanned into high resolution digital image files (600 dpi, 16-bit grayscale). Flame spread and percent light absorption plots are then cropped from the original scans, and digitized using Engauge Digitizer [57], a graph digitization program. Engauge Digitizer reconstructs data points from the scanned plots, and outputs the results in plain text comma separated value format, UTF8 encoding. Three plots are required for calculation of flame spread and smoke developed indices: flame spread versus time, percent light absorption of the sample versus time, and percent light absorption of the red oak reference versus time.

From the flame spread versus time plot, the value of flame spread is taken at each specific increment of 15 seconds from $\tau = 0$ s to $\tau = 600$ s, and filtered into a table of 40 increments. From this table, total flame spread area is calculated according to Equation 2.2, and flame spread index is calculated according to Equation 2.4.

From the percent light absorption versus time plots for both the sample and red oak, total smoke obscuration and reference smoke obscuration are calculated using Equation 2.7. Total smoke obscuration and reference smoke obscuration are then input into Equation 2.8 to compute the smoke developed index.

The ASTM E84 rounding algorithm is applied to all computed results in order to validate them with the values supplied on each individual test report. In all cases, cross-checked values of flame spread and smoke developed index are found to be identical.

Finally, the burned centreline depth is measured at the burned end of the specimen

following completion of the test. As outlined in Section 3.1.1, burned centreline depth is used to approximate the volume of each sample that actually burned during each test. Burned volume is hypothesized to be a contributing factor in smoke development, as discussed in Section 3.1.1.

3.1.1 Burned Volume Approximation

While witnessing Steiner tunnel tests during the preliminary stages of this research, it was observed that specimens which performed poorly in terms of smoke developed during testing showed evidence that the flame front had actually burned deeper into the specimens, compared to specimens that performed better in terms of smoke generation. Based on this observation, it was postulated that smoke performance should be related not only to the type of foam being burned, but also to the amount of material burned. Since the Steiner tunnel test does not require a report of mass loss rate and cannot easily accommodate determination of specimen mass loss results, and it was of interest to further understand the observation made, it was necessary to develop a method by which to approximate the burned volume of the specimen. This information combined with the measured values of percent light absorption should provide further insight into the generation of smoke from different samples during Steiner tunnel tests.

Practical considerations, background on the observed burning profile of a typical Steiner tunnel test specimen, a proposed model for approximation of burned specimen volume, and evaluation of the model are presented below.

Background and Practical Considerations

The Steiner tunnel apparatus does not accommodate a means by which to monitor specimen mass as a function of time during a test. This is because it is very difficult to make such measurements due to the physical configuration of the tunnel. Test specimens are supported directly on the frame of the apparatus, so it is not possible to include a load cell under the specimen as is common in other fire test methods. While it might be possible to measure the mass of the entire apparatus and specimen by placing load cells under each support, and creating an algorithm to determine the net mass loss of the specimen, this is impractical to implement due to the size and weight of the tunnel test apparatus itself. Finally, the before-test and after-test masses of each specimen section might be measured in order to calculate a net mass lost; however, this is again impractical and would be subject to significant inaccuracy due to differences in post-test temperature decay, amongst other factors.

In the first instance, Exova, the testing laboratory who undertook the Steiner tunnel tests for this work, did not have load cells that could accommodate the panels under test in the apparatus. This rendered determination of before-test and after-test masses of the samples impractical. Further, at the conclusion of a test, the flame source is shut off and the specimen is allowed to safely cool in the ventilated environment of the tunnel. Following this, the apparatus lid is removed, and the specimen sections are removed. In order to determine a post test mass for each specimen, the mass of each section would ideally be measured immediately following the end of the test in order to minimize further decay of mass during cooling. However, cooling rate depends on the temperature reached during the test and the heat absorbed by the apparatus, so it is not possible to impose the same cooling rate on all test specimens. Since cooling rate cannot be controlled, a post-test mass measurement will result in an inherent and, as yet, unquantifiable error in the final mass loss data.

As an alternative to measuring mass loss, it was decided that the volume of the specimen burned could be approximated based on the flame propagation and burned depth, and would provide a reasonable estimation of the amount of material burned for a common family of cellular polymers and density range. To this end, complete profiles of the burned depth were developed for two specimens: F10 and F11-1. Depth measurements were taken using a thin rod depth gauge at two-foot intervals along the length of each specimen, with three measurements made across the width of the sample at each measurement location. The results are tabulated in Appendix A, and shown in Figure 3.1. Note that length and width positions along the specimen are measured using the IP unit system to correspond with the ASTM E84 test standard. Depth measurements are taken using the SI unit system, and the model developed in this section is based in SI units.

Figure 3.1 shows that burned depth tends to be parabolic close to the burned end of the specimen, flattening out approaching the unburned end. Maximum burned depth always occurs at the width centreline. This is confirmed upon visual inspection of the specimen remains. The burned depth was observed to be at a maximum in the first 4 feet of the specimen, which is the section of specimen that is continually exposed to flame. Based on the measurements, then, a model is proposed to approximate the burned section depth along the length of a specimen, from which the total burned volume may be calculated.

Discretized Burned Volume

The first step in approximating the burned specimen volume is to generate an integral expression for burned volume, and then to discretize it into an expression that might be evaluated using experimental data.

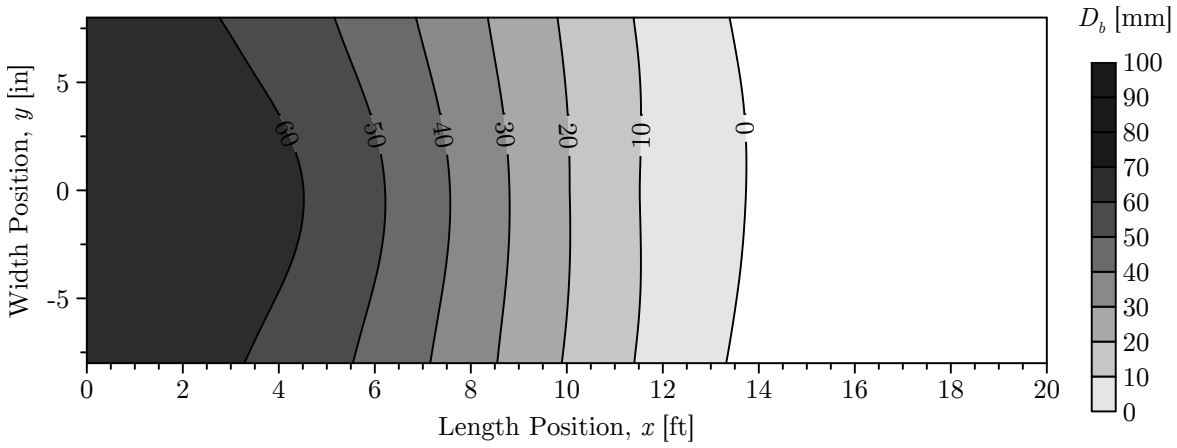

(a) Formulation F10.

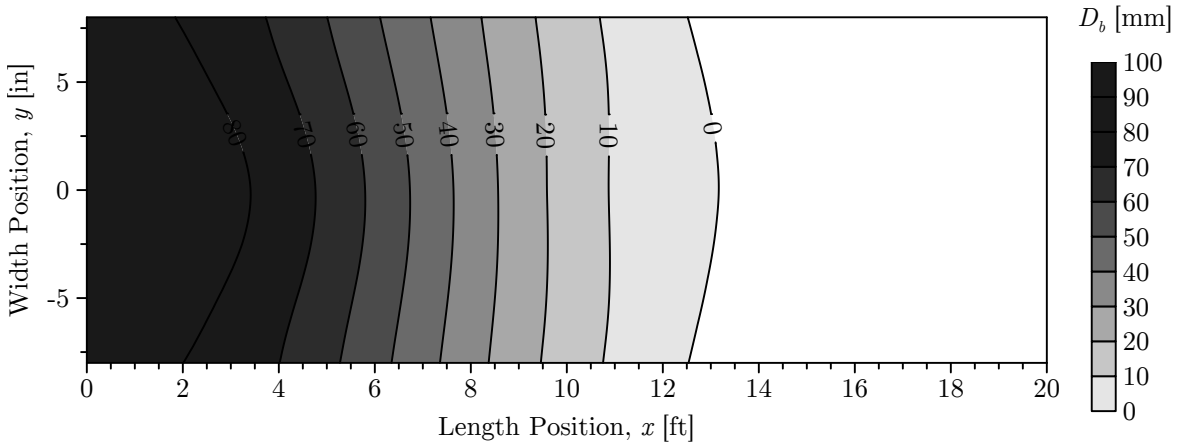

(b) Formulation F11-1.

Figure 3.1: Burned depth measurements for formulations F10 and F11-1.

Figure 3.2 shows side and end profiles of a Steiner tunnel specimen. In the figure, x represents position along the length of the specimen, y represents position along the width of the specimen, and z represents distance into the depth of the specimen.

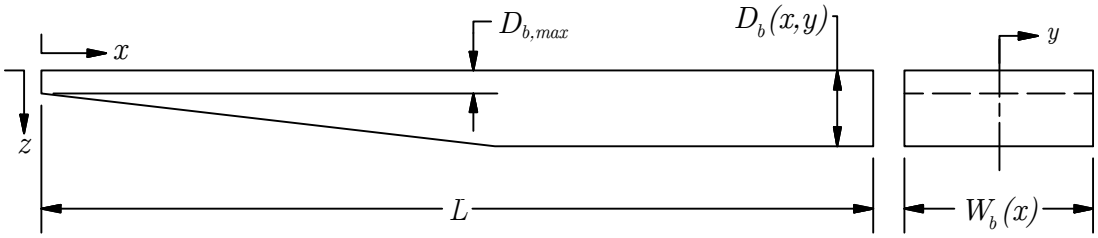

Figure 3.2: Side and end profiles of a Steiner tunnel specimen (not to scale).

As the specimen burns, $D_b(x, y)$ represents the depth of material burned along the length and width of the specimen, $W_b(x)$ represents the width of material burned along the length of the specimen, and $A_b(x)$ represents the area of a burned section along the length of the specimen. The burned section area is calculated by the double integral of depth and width functions, as in Equation 3.1.

$$A_b(x) = \int_{y=0}^{W_b(x)} \int_{z=0}^{D_b(x,y)} \mathrm{d}z \cdot \mathrm{d}y = \int_{y=0}^{W_b(x)} D_b(x, y) \cdot \mathrm{d}y \tag{3.1}$$

$W_b(x)$ is assumed to be constant along the length of the burned specimen. The specimens are prepared by spraying the liquid foam into a mould of fixed-width, so the width does not change along the length of the specimen. The manner in which the specimen is mounted in the apparatus restricts the available width for flame exposure to the interior width of the tunnel, which is given in the ASTM E84 standard to be 17.625 ± 0.375 inches (447.7 ± 9.5 millimetres).

$$W(x) = W_b$$

In order to simplify the burned section area expression to a one-dimensional problem, the burned section area is assumed to be rectangular. Figure 3.1 shows that the burned section profiles tend to be almost rectangular, with slight concavity at the centreline width. The depth measurement is taken at the centreline of the specimen width, representing the maximum burned depth in the y direction.

$$D_b(x, y) = D_b(x)$$

Since it is assumed that the burned depth does not change along the width of the specimen, the burned section area function is simplified to the product of burned width

and depth along the length of the specimen, as in Equation 3.2.

$$A_b(x) = \int_{y=0}^{W_b} D_b(x) \cdot \mathrm{d}y = W_b \cdot D_b(x) \tag{3.2}$$

The burned volume is calculated by integrating the burned section area along the length of the specimen, as in Equation 3.3.

$$V_b = \int_{x=0}^{L} A_b(x) \cdot \mathrm{d}x = W_b \int_{x=0}^{L} D_b(x) \cdot \mathrm{d}x \tag{3.3}$$

In order to evaluate this expression, instead of developing an analytical expression for burned depth, a discretized expression for the depth is developed based on depth measurements taken at regular intervals along the length of the specimen. It is assumed that depth measurements are taken at increments (Δx) of 0.5 feet (0.1524 metres) along the 24 foot (7.315 metre) length of the specimen. This spacing is selected to coincide with the flame spread increments. The numerical approximation of the integral expression in Equation 3.3 is developed using the composite trapezoid rule [42], and is simplified to Equation 3.4.

$$\int_{x=0}^{L} D_b(x) \cdot \mathrm{d}x \approx \Delta x \left(\frac{D_b(x_0)}{2} + \sum_{i=1}^{L/\Delta x - 1} D_b(x_i) + \frac{D_b\left(x_{L/\Delta x - 1}\right)}{2} \right)$$

$$V_b \approx W_b \cdot \Delta x \left(\frac{D_{b,0}}{2} + \sum_{i=1}^{47} D_{b,i} + \frac{D_{b,48}}{2} \right) \tag{3.4}$$

where

$$D_{b,i} = D_b(\Delta x \cdot i)$$

$$i = 1, 2, 3 \cdots 47$$

The $D_{b,48}$ term in Equation 3.4 represents the burned depth at the exhaust end of the tunnel. The expression may be further simplified by assuming that the flame does not propagate fully to the end of the tunnel (so, $D_{b,48} = 0$). This is the case for all materials in this study, and is the case for all materials meant to achieve a class A flame spread rating in the Steiner tunnel test. The expression for discretized burned volume is simplified to Equation 3.5.

$$V_{b,disc} = W_b \cdot \Delta x \left(\frac{D_{b,0}}{2} + \sum_{i=1}^{47} D_{b,i} \right) \tag{3.5}$$

From Equation 3.5, the burned volume may be approximated by measuring the burned depth at 0.5 foot increments along the specimen length following each Steiner tunnel test.

While this may be useful in theory, taking as many as 48 depth measurements after each test would be impractical. Therefore, a method is proposed by which to approximate the incremental burned depth based on flame spread during the test, as described below.

Incremental Burned Depth

To develop the expression for burned depth of a sample, a parallel is first drawn between the depth burning rate in the Steiner tunnel test (mm/s) and the charring rate of wood. It is demonstrated in various char depth models that the rate of charring (mm/s) on a specimen is influenced by the radiant heat flux or, alternatively, the fire severity [58, 59, 60]. As explained by Drysdale, there is a linear correlation between rate of charring and incident flux on a wood specimen [61, pp. 219]. Based on this parallel, it is proposed that the depth burning rate, β, is related to the intensity of the burning environment (temperature, heat flux) and the time of exposure at a particular position along the length of the specimen, $t_b\,(x)$.

Unfortunately the Steiner tunnel apparatus is not instrumented to monitor temperature or heat flux along the length of the tunnel*. Without means to extract heat or temperature information on a per-test basis, the intensity of the fire test environment and its impact on the depth burning rate is assumed to be constant while in the presence of flames. This is to say that whenever flames have propagated over an increment along the length of the tunnel, a contribution to burning depth will occur. It is proposed that the rate of burning into the depth of the sample in the presence of flames is constant, where the burned depth at each increment is dependent upon the incremental time of exposure to flames, $t_{b,i}$.

$$\frac{\mathrm{d}}{\mathrm{d}t_b} D_b\,(t_b) = \beta$$

$$D_{b,i} = \beta \cdot t_{b,i} + C \tag{3.6}$$

Where the specimen has not been exposed to flames ($t_{b,i} = 0$), the burned depth is zero ($D_{b,i} = 0$). Applying this initial condition to Equation 3.6 yields a constant of integration $C = 0$.

As demonstrated in Figure 3.1, the burned depth is at a maximum in the first four feet of the specimen, where the specimen is directly exposed to burner flames for the duration of the test ($t_{b,i} = \tau_2$). Let $D_{b,max}$ represent the maximum burned depth measured in the

*The stack temperature is monitored during the test, but it is not standard practise for the testing laboratory to provide the stack temperature data with test results, and consequentially the data was not available for this study

first four feet of the specimen. Applying this initial condition to Equation 3.6 results in a simplified expression for the incremental burned depth, Equation 3.7.

$$D_{b,i} = \left(\frac{D_{b,max}}{\tau_2} \right) \cdot t_{b,i} \tag{3.7}$$

The time of exposure to flames at each increment, $t_{b,i}$, is calculated using Visual Basic for Applications (VBA) in Excel. Listing 3.1 shows the VBA function used to calculate the incremental time of exposure to flames.

```
Function Calculate_tb(FS As Range) As Double
'This function takes a range input of FS (flame spread measured in 15 second increments)
'and outputs an array containing the burning time at each flame spread increment (of 0.5
'feet). The array may then be transposed and output into a range variable.
  Dim i As Integer, tb(48) As Double
  For i = 0 to 48
    If (0.5 * i) < 8
      'Burning time is 600 in the first four feet (burner region).
      tb(i) = 600
    ElseIf (0.5 * i - 4) > Application.Max(FS)
      'Burning time is 0 past the max flame propagation (no burning).
      tb(i) = 0
    Else
      'Burning time is accumulated in increments of 15 seconds.
      tb(i) = 15*(Application.Countif(CStr(FS) & """,>=""" & CStr(0.5 * i - 4))-1)
    End If
  Next i
  Calculate_tb = tb
End Function
```

Listing 3.1: Calculation of the incremental burning time.

Assembled Model for Burned Specimen Volume

Since $D_{b,0}$ is located in the region of maximum burned depth, it is understood that $D_{b,0} = D_{b,max}$. Equations 3.5 and 3.7 are assembled into a single expression for the approximated burned specimen volume, as in Equation 3.8.

$$V_{b,A} = \Delta x \cdot W_b \cdot D_{b,max} \left(\frac{1}{2} + \frac{1}{\tau_2} \sum_{i=1}^{47} t_{b,i} \right) \tag{3.8}$$

Equation 3.8 is further simplified for the case where the burned section width is taken to be the maximum value of 18 inches (457.2 millimetres). Equation 3.9 shows the simplified expression, where $D_{b,max}$ is measured in millimetres, $t_{b,i}$ is measured in seconds, and the

approximated burned volume is calculated in cubic metres.

$$V_{b,A} = D_{b,max} \left(3.484 \cdot 10^{-5} + 1.161 \cdot 10^{-7} \sum_{i=1}^{47} t_{b,i} \right) \tag{3.9}$$

Equation 3.9 may be used to approximate the volume of specimen burned using the reported flame spread results and a singular depth measurement. While the approximation is certainly limited by the assumptions outlined throughout Section 3.1.1, the model has great practical value as only a single depth measurement need be taken after each test. This raises the question of how the model compares to the recorded depth results for formulations F10 and F11-1.

Evaluation of the Burned Volume Model

Based on the measured maximum burned depth and the total test times, the burning rates into the depth of the specimens are calculated for formulations F10 and F11-1 to be 0.11 mm/s and 0.14 mm/s respectively. From Equation 3.7 and Listing 3.1, the incremental burned depth is then calculated for each formulation. All calculations are summarized in Appendix A.

Figure 3.3 contains a plot of the measured burned depth along with the approximated burned depth for formulations F10 and F11-1. Side profiles of the burned specimens are included to assist in visualization of the burned depth.

Finally, the burned volume is approximated using Equation 3.9 using both the burned depth model and the measured burned depth. Table 3.2 demonstrates that the model has predicted the burned volume to within 10% error for the two specimens used for validation.

Table 3.2: Results of the burned volume approximation for formulations F10 and F11-1.

Formulation	V_b [m^3]	$V_{b,A}$ [m^3]	$\%\epsilon$
F10	0.07378	0.07002	5.213%
F11-1	0.07947	0.08487	6.785%

The model appears to yield a reasonable approximation of burned specimen volume for the two validation specimens. Since these foam materials are characteristic of all materials used in this research, the same method is applied for determination of burned volume of all other specimens. These approximated values are considered in the development of cross-test correlations.

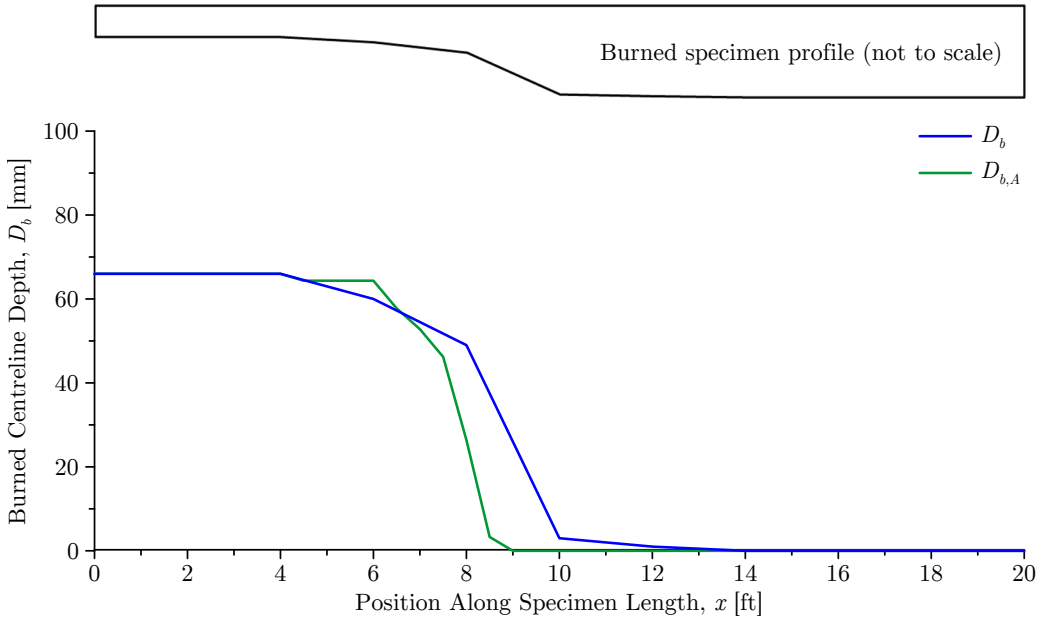

(a) Formulation F10.

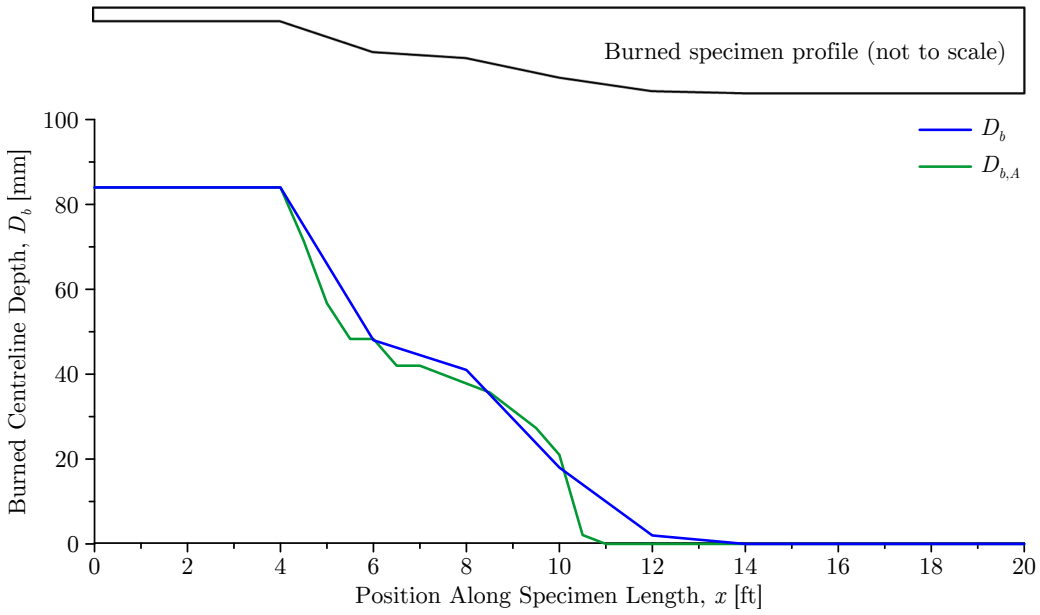

(b) Formulation F11-1.

Figure 3.3: Comparison of the measured burned depth and modelled burned depth along the length of a specimen.

3.2 Cone Calorimeter Tests

Cone calorimeter testing is conducted according to the ASTM E1354 standard using the FTT cone calorimeter described in Section 2.4. Test reports are created using the Conecalc software, although the entire data set is available for analysis. A sample test report may be found in Appendix C.

The following conditions on the ASTM E1354 standard are stipulated:

- specimens are cut to 100 mm $\pm$ 5 mm each in length and width, and 25 mm $\pm$ 2 mm in thickness;
- specimens are conditioned to moisture equilibrium at 21°C $\pm$ 2°C and 50% $\pm$ 5% relative humidity in a conditioning chamber;
- the testing environment is draft-free, at an ambient temperature of 21°C $\pm$ 2°C and relative humidity between 20% and 80% depending on the time of year;
- specimens are mounted in the horizontal configuration, with 25 mm spacing between the top surface of the specimen and the bottom edge of the cone heater; and
- the cone heater is set to radiate a uniform flux of 50 kW/m^2 incident on the surface of the specimen.

Materials for cone calorimeter tests are supplied directly by the manufacturer. Of the 20 formulations tested in the Steiner tunnel, 13 formulations are selected for cone calorimeter testing. Note that several formulations are unavailable for cone calorimeter testing as they were mixed early in the R&D phase of the project.

Cone calorimeter testing is conducted in sets of 3–5 samples per formulation, with reported results averaged for all tests. Figures 3.4, 3.5, and 3.6 show representative test results (averaged heat release rate, total heat release, and specimen mass respectively) for formulation F7.

For all samples, therefore, the results are obtained as follows:

- the heat release rate reported for a given formulation is the average of the time-indexed heat release rate for the 3–5 tests conducted on the same foam formulation;
- the total heat release reported for a given formulation is the average of the time-indexed total heat release for the 3–5 tests conducted on the same foam formulation; and
- the specimen mass reported for a given formulation is the average of the time-indexed specimen mass for the 3–5 tests conducted on the same foam formulation.

Cone calorimeter test results are considered in the development of cross-test correlations for Steiner tunnel flame spread in Chapter 4.

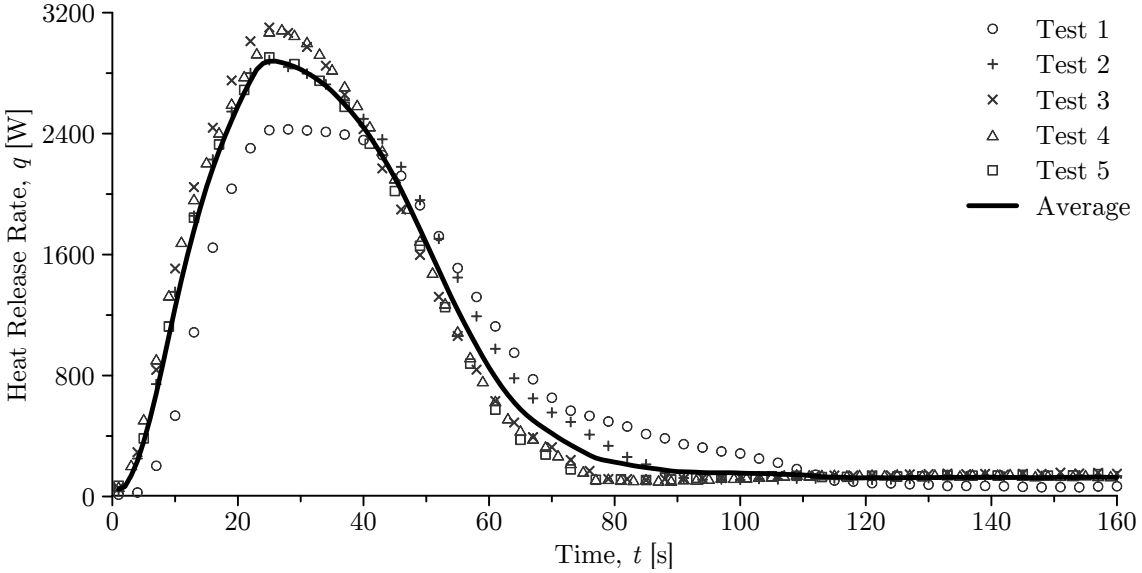

Figure 3.4: Averaged heat release rate curve for formulation F7.

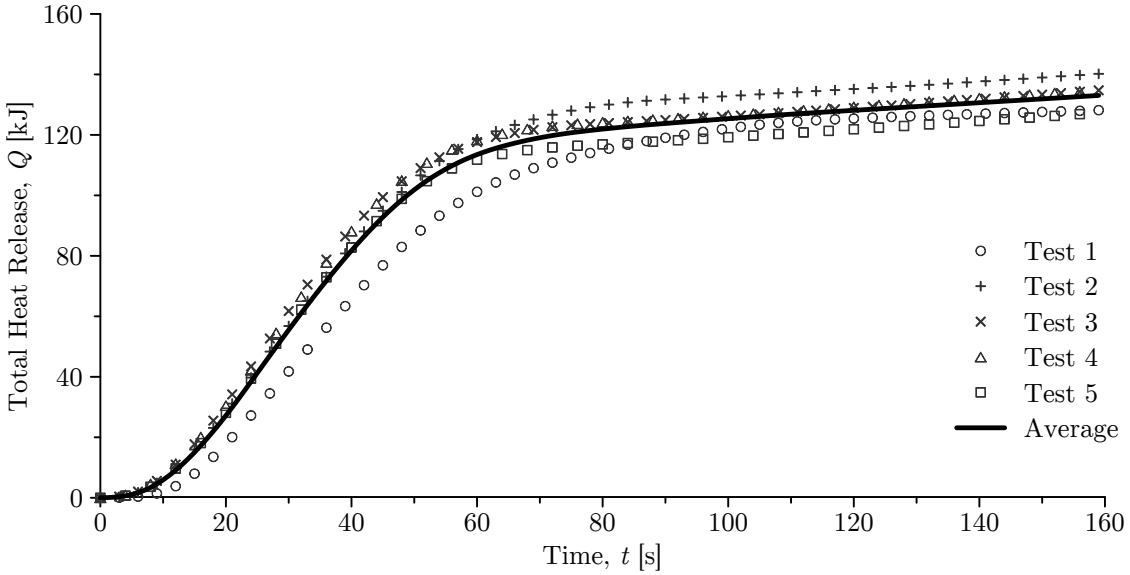

Figure 3.5: Averaged total heat release curve for formulation F7.

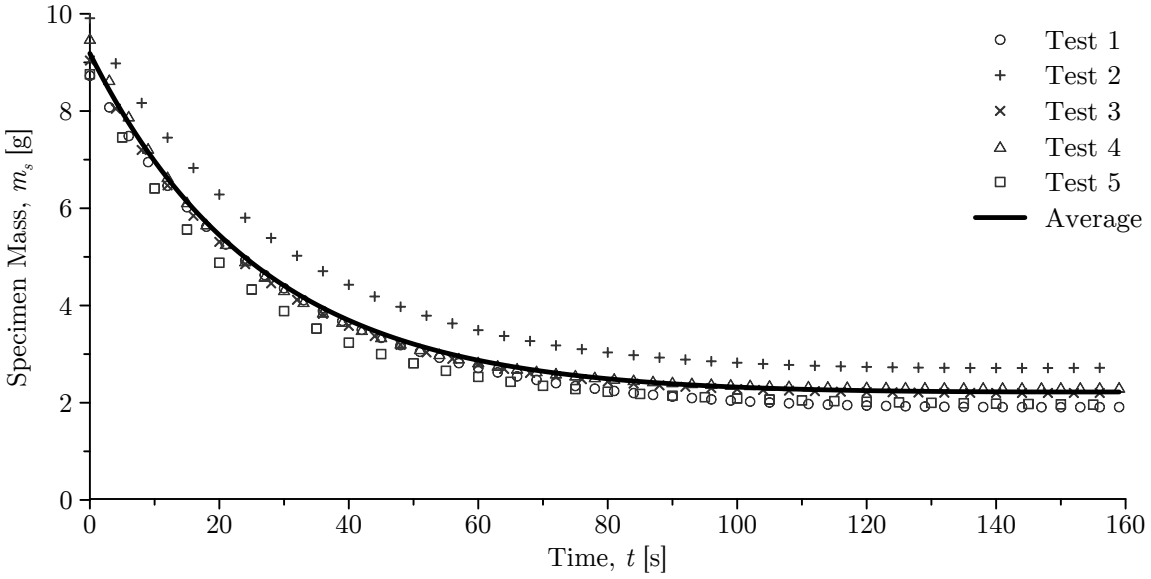

Figure 3.6: Averaged specimen mass curve for formulation F7.

3.3 Smoke Density Chamber Tests

Smoke density chamber testing is conducted according to the ISO 5659-2 standard using the FTT smoke density chamber described in Section 2.5. Test reports are created using the Smokebox software, and as with the cone calorimeter, the entire data set is available for analysis. A sample test report may be found in Appendix D.

The following conditions on the ISO 5659-2 standard are stipulated:

- specimens are cut to 75 mm $\pm$ 2 mm each in length and width, and 25 mm $\pm$ 2 mm in thickness;
- specimens are conditioned to moisture equilibrium at 21°C $\pm$ 2°C and 50% $\pm$ 5% relative humidity;
- the testing environment is draft-free, at an ambient temperature of 21°C $\pm$ 2°C and relative humidity between 20% and 80% depending on the time of year;
- the test is operated in Mode #2, which stipulates an incident heat flux of 25 kW/m^2 on the surface of the specimen, and using the pilot flame; and
- the test duration is extended to 2 minutes beyond the minimum optical transmission to observe any additional degradation of the specimen after that point.

Materials for the smoke density chamber tests are supplied directly by the manufacturer. Of the 20 formulations tested on the Steiner tunnel, 8 formulations are selected for smoke density chamber testing. Again, several formulations are unavailable for smoke density

chamber testing as they were mixed early in the R&D phase of the project. Furthermore, the smoke density chamber was not available for the first testing cycle, leaving some formulations unavailable for study.

Smoke density chamber testing is conducted in sets of 3–5 specimens per formulation, depending on the number of samples available for testing, with reported results averaged across the test data. Figures 3.7, 3.8 and 3.9 are representative results and show the averaged optical transmission, specific optical density, and specimen mass loss curves respectively for formulation F7.

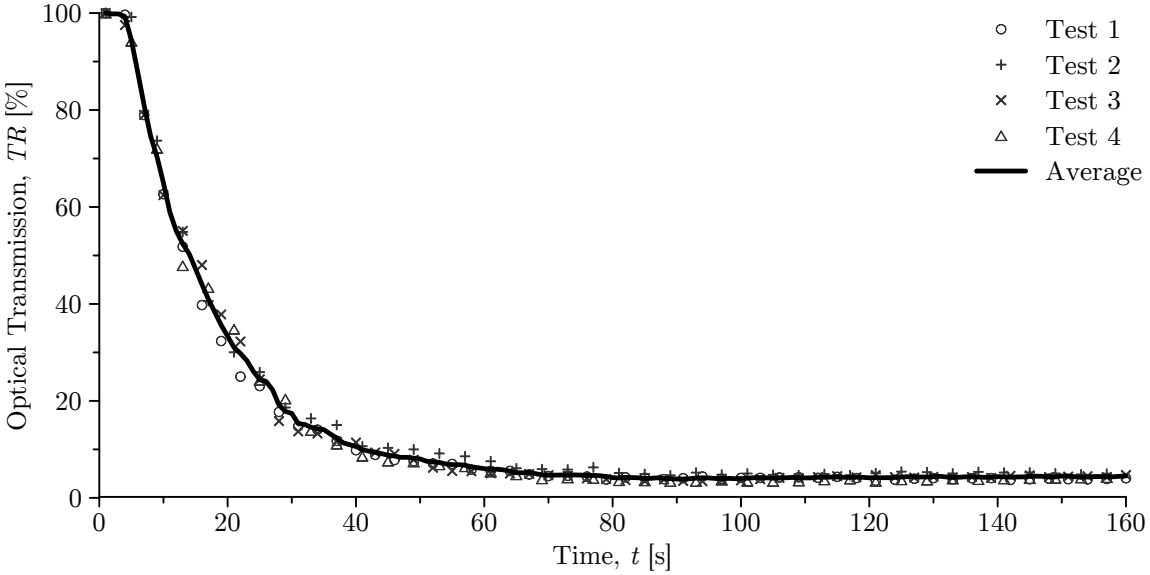

Figure 3.7: Averaged optical transmission curve for formulation F7.

For all samples, therefore, the results are obtained as follows:

- the optical transmission reported for a given formulation is the average of the time-indexed optical transmission for 3–5 tests of the same formulation;
- the specific optical density reported for a given formulation is the average of the time-indexed total heat release for 3–5 tests of the same formulation; and
- the specimen mass reported for a given formulation is the average of the time-indexed specimen mass for 3–5 tests of the same formulation.

Smoke density chamber test results are considered in the development of cross-test correlations for Steiner tunnel smoke development in Chapter 5.

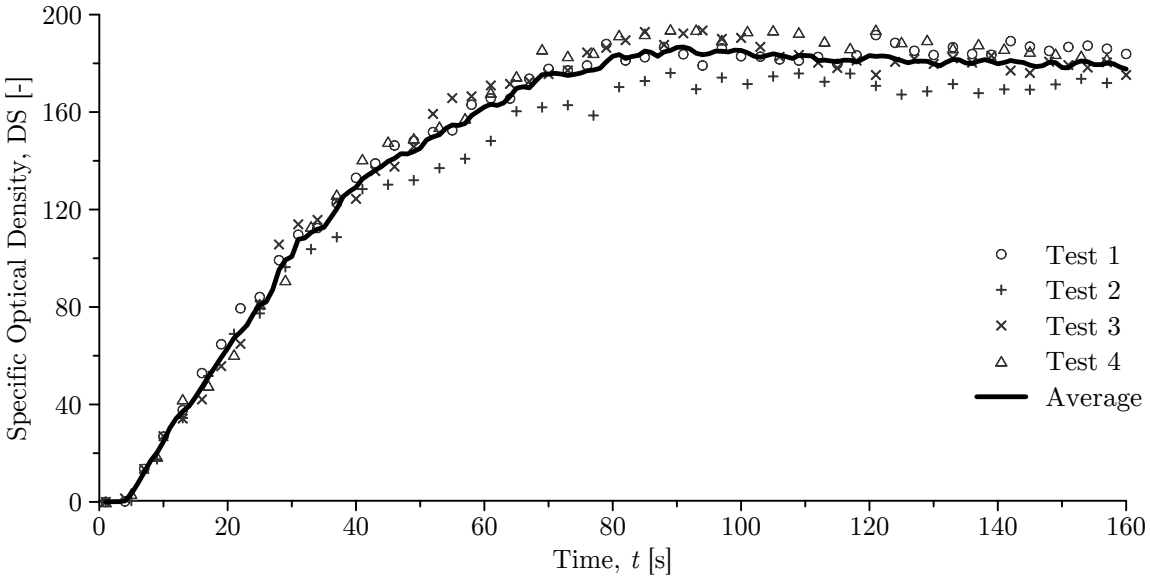

Figure 3.8: Averaged specific optical density curve for formulation F7.

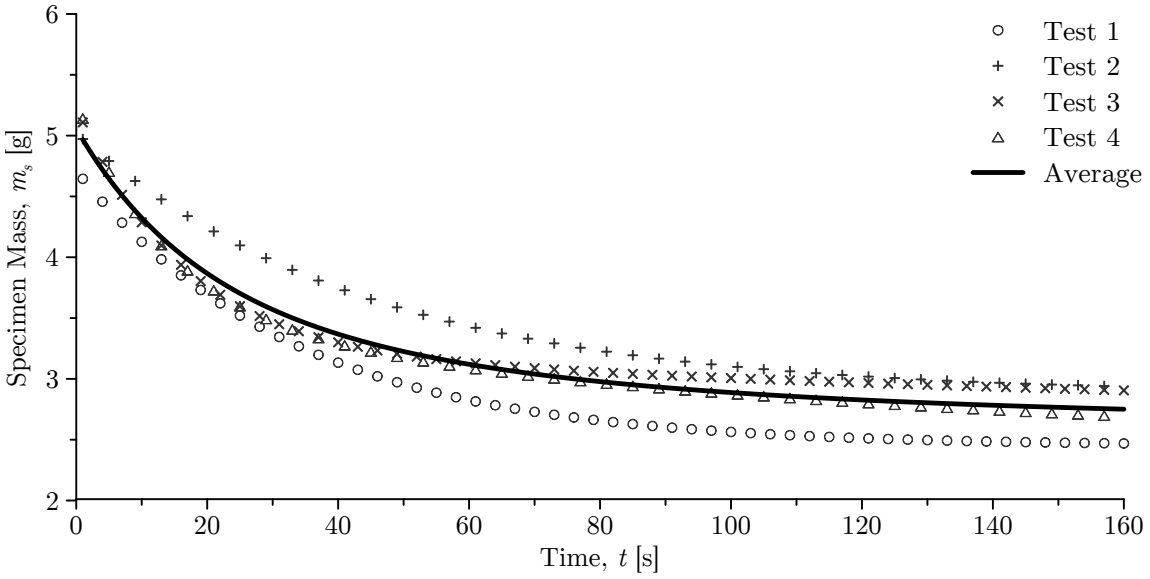

Figure 3.9: Averaged specimen mass curve for formulation F7.

3.4 Error Quantification

In order to use the data from the cone calorimeter and smoke density tests to accurately screen formulations using a cross-test model, it is extremely important to quantify error and confidence in various aspects of the model. A model may suggest that formulation A will achieve better classification than formulation B based on cone calorimeter and smoke density chamber results, but in order to confidently recommend formulation A over formulation B, the error in each individual result must first be quantified.

In Chapters 4 and 5 to follow, a general method for calculation and presentation of error is used. The method is outlined in this section, using the general term "X" to denote a given experimental result, the term "X_A" to denote an approximation of X using results from the same test, and "X_M" to denote a modelled result using cross-test correlations. The subscript "i" is used to denote the test number, and "n" represents the number of tests in the sample group.

Error can be defined as the difference between the experimental result and the modelled (or approximated) result, as in Equation 3.10. Note that modelled and approximated results can be used interchangeably in Equation 3.10, affecting only the context of the error.

$$\epsilon_i = X_i - X_{M,i} \tag{3.10}$$

Mean error and sample standard deviation error are calculated by Equations 3.11 and 3.12 respectively. These are used in the calculation of confidence intervals for each result.

$$\overline{\epsilon} = \frac{1}{n}\sum_{i=1}^{n}\epsilon_i \tag{3.11}$$

$$\hat{\epsilon} = \sqrt{\frac{1}{n-1}\sum_{i=1}^{n}(\epsilon_i - \overline{\epsilon})} \tag{3.12}$$

All modelled and approximated values are plotted with upper and lower error bars which indicate the upper and lower confidence limits, C_U and C_L. These limits represent the range of values within which, for a certain percentage of samples, the true average is likely to be contained [62]. 95% confidence limits are established for the mean error according to 3.13, where t_{95} represents the upper critical value of the Student's t-distribution with $n-1$ degrees of freedom and a 0.05 significance level.

$$C = \overline{\epsilon} \pm \frac{t_{95}\cdot\hat{\epsilon}}{\sqrt{n}} \tag{3.13}$$

When comparing the modelled result for two different formulations, if the lower error bar of formulation A is above the upper error bar of formulation B, then it can be said with good confidence that the result for formulation A will be greater than that for formulation B in the actual test.

Mean percent error, or percent difference, is used to assess the overall accuracy of a modelled result. Percent error is calculated for each test according to Equation 3.14, while mean percent error is calculated according to Equation 3.15. Mean percent error approaching zero indicates that, on average, the experimental data is centred on the modelled results. One of the goals of this study is to be able to predict the values of FSI and SDI for a given formulation to within 20%.

$$\%\epsilon_i = \frac{|X_i - X_{M,i}|}{X_i} = \frac{|\overline{\epsilon}|}{X_i} \tag{3.14}$$

$$\overline{\%\epsilon} = \frac{1}{n}\sum_{i=1}^{n} \%\epsilon_i \tag{3.15}$$

The coefficient of determination, R^2, is used to assess the fit of a model to experimental data. R^2 close to 1.0 indicates that a model is a good fit to the experimental data, while R^2 close to 0 indicates that a model is not a good fit to the experimental data. R^2 describes the proportion of variability in a data set that is accounted for by the model. Additionally, R^2 indicates how well future outcomes are likely to be predicted by the model [63]. The coefficient of determination is calculated according to Equation 3.16.

$$SS_{err} = \sum_{i=1}^{n} (X_i - X_{M,i})^2 = \sum_{i=1}^{n} {\epsilon_i}^2$$

$$SS_{tot} = \sum_{i=1}^{n} \left(X_i - \overline{X}\right)^2$$

$$\overline{X} = \frac{1}{n}\sum_{i=1}^{n} X_i$$

$$R^2 = 1 - \frac{SS_{err}}{SS_{tot}} \tag{3.16}$$

Equation 3.16 demonstrates that the coefficient of determination is maximized by minimizing the mean error. Thus, to determine a best-fit model for a given set of data, the coefficients in the model are selected so as to minimize the mean error.

The conventions outlined in this section are used in the following chapters to present results with limits of confidence, as well as to gain insight on the fit of proposed models to test results.

Chapter 4

Flame Spread Model

In this chapter, relationships are examined between fire performance results from the Steiner tunnel test and results from the cone calorimeter test. Key performance indicators are identified, and correlations are developed between the tests. Three models are proposed by which to predict the flame spread index of a material, and each is evaluated according to their ability to effectively screen materials for their expected classification in the Steiner tunnel test.

4.1 Flame Spread Area Approximation

During testing prior to this study, it had been observed that formulations which exhibited greater peak flame spread, even when only for a short time, tended also to have greater values of flame spread index. As demonstrated in Section 2.3.1, flame spread index is calculated directly from total flame spread area, F_T. Based on these observations, it would appear that peak flame spread, f_1, and time to reach peak flame spread, τ_1, as determined in the Steiner tunnel test have a significant influence on the calculated flame spread area. Therefore, in this stage of the research, a method is proposed by which to approximate the flame spread area using only those two Steiner tunnel results.

4.1.1 Peak Flame Spread and Time Model

Figure 4.1 shows the same illustrative flame spread curve as Figure 2.3, with the recorded values of flame spread indicated by dots. Peak flame spread is identified as f_1, final flame spread is identified as f_2, and τ_1 and τ_2 are the times corresponding to peak and final flame

spread. A line of approximation is drawn from the initial value of 0 flame spread at $\tau = 0$ to $f_1(\tau_1)$, and from $f_1(\tau_1)$ to $f_2(\tau_2)$.

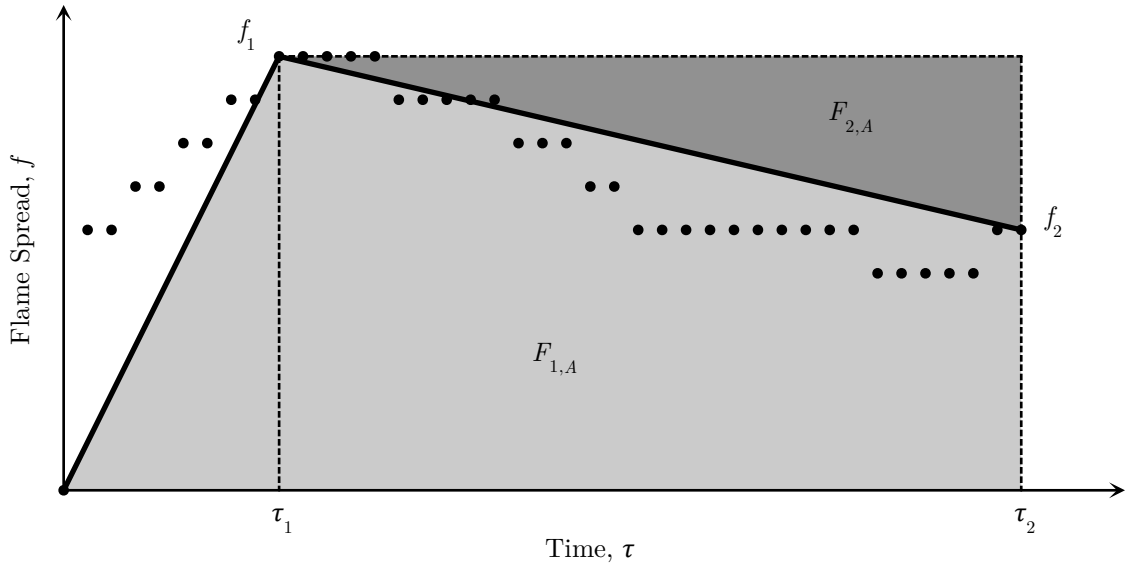

Figure 4.1: Approximate flame spread areas for an illustrative flame spread curve.

The line of approximation in Figure 4.1 represents a simplified flame spread curve, as if only two values of flame spread had been recorded in the test. From this simplified flame spread curve the approximated flame spread areas, $F_{1,A}$ and $F_{2,A}$, are calculated as in Equations 4.1 and 4.2.

$$F_{1,A} = \frac{f_1 \cdot \tau_1}{2} + (\tau_2 - \tau_1)\left(\frac{f_2 + f_1}{2}\right) = f_1\left(\frac{\tau_2}{2}\right) + f_2\left(\frac{\tau_2 - \tau_1}{2}\right) \tag{4.1}$$

$$F_{2,A} = \frac{(\tau_2 - \tau_1)(f_1 - f_2)}{2} = f_1\left(\frac{\tau_2 - \tau_1}{2}\right) - f_2\left(\frac{\tau_2 - \tau_1}{2}\right) \tag{4.2}$$

The total approximated flame spread area, $F_{T,A}$, is calculated by adding Equations 4.1 and 4.2, as in Equation 4.3.

$$F_{T,A} = F_{1,A} + F_{2,A} = f_1\left(\tau_2 - \frac{\tau_1}{2}\right) \tag{4.3}$$

Finally, a linear function is proposed by which to relate the actual flame spread area, F_T, to the approximated flame spread area, $F_{T,A}$, as indicated by Equation 4.4. This is a two-variable approximation function with dependent variables of peak flame spread and time to peak flame spread.

$$F_{T,A1} = A \cdot f_1\left(\tau_2 - \frac{\tau_1}{2}\right) + B \tag{4.4}$$

Equation 4.4 is applied to each of the thirty Steiner tunnel tests in this study to determine approximated flame spread areas. By minimizing the mean error between actual and approximated results, A and B are determined to be 0.9901 and 106.0 [m · s] respectively. The coefficient of determination of the model, R^2, is found to be 0.9498, indicating that the model provides an excellent fit to the data.

Figure 4.2 shows the values of $F_{T,A1}$ plotted as a contour plot for differing values of peak flame spread and time to peak flame spread. The figure demonstrates that at low and moderate values of f_1, the dependence of F_T on τ_1 is low. Since the FR-SPFs in this study tend to have low-to-moderate peak flame spreads, there is evidence that a one-variable model may be appropriate for approximating the total flame spread area. This possibility is examined in Section 4.1.2.

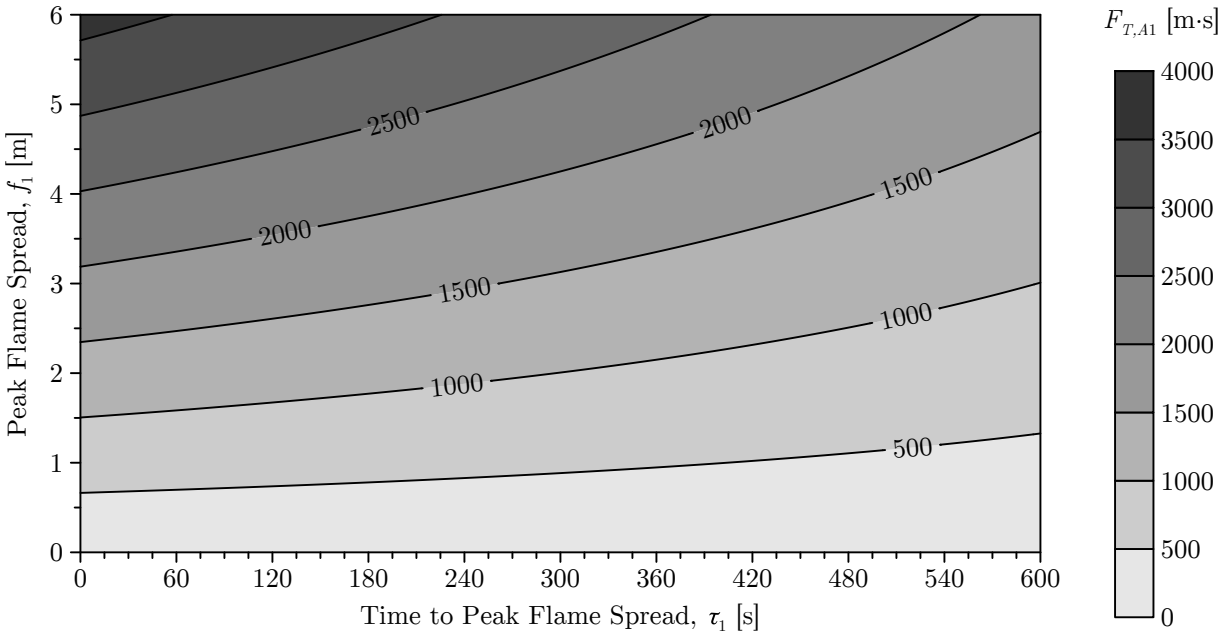

Figure 4.2: Two-variable flame spread area approximation function, 3D contour plot.

The model can be visualized in two dimensions by holding the time to peak flame spread constant at specific values. Three values of τ_1 are selected: the minimum possible value (15 seconds), the maximum possible value (600 seconds), and the average value for the 30 tests in this study (172 seconds). These values for all thirty tests are plotted in Figure 4.3, which demonstrates that as the peak flame spread increases, so too does the dependence of the model on τ_1.

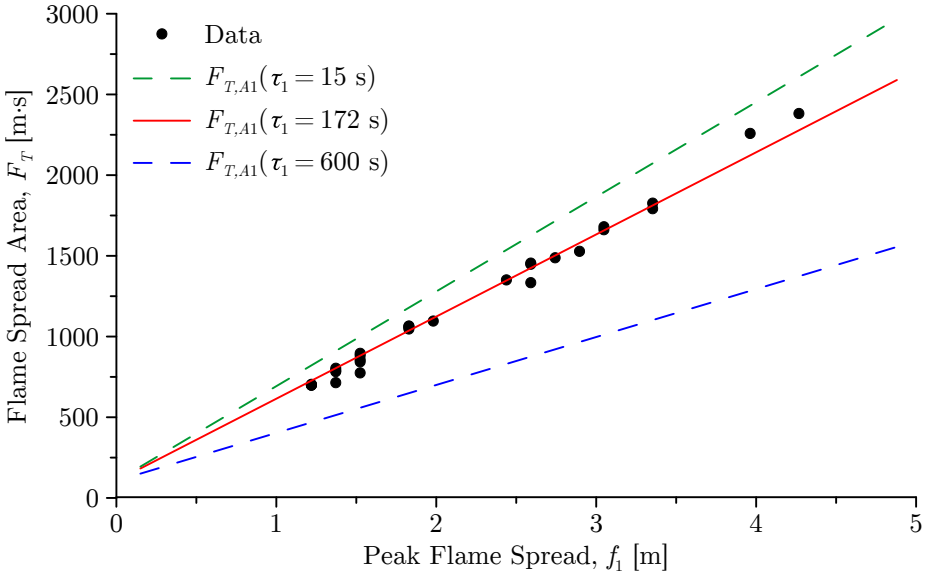

Figure 4.3: Two-variable flame spread area approximation function, 2D scatter plot.

Figure 4.4 shows the approximated flame spread area plotted along with the experimental flame spread area for all 30 Steiner tunnel tests in this study. The mean percent error between the experimental results and modelled results is 8.11%.

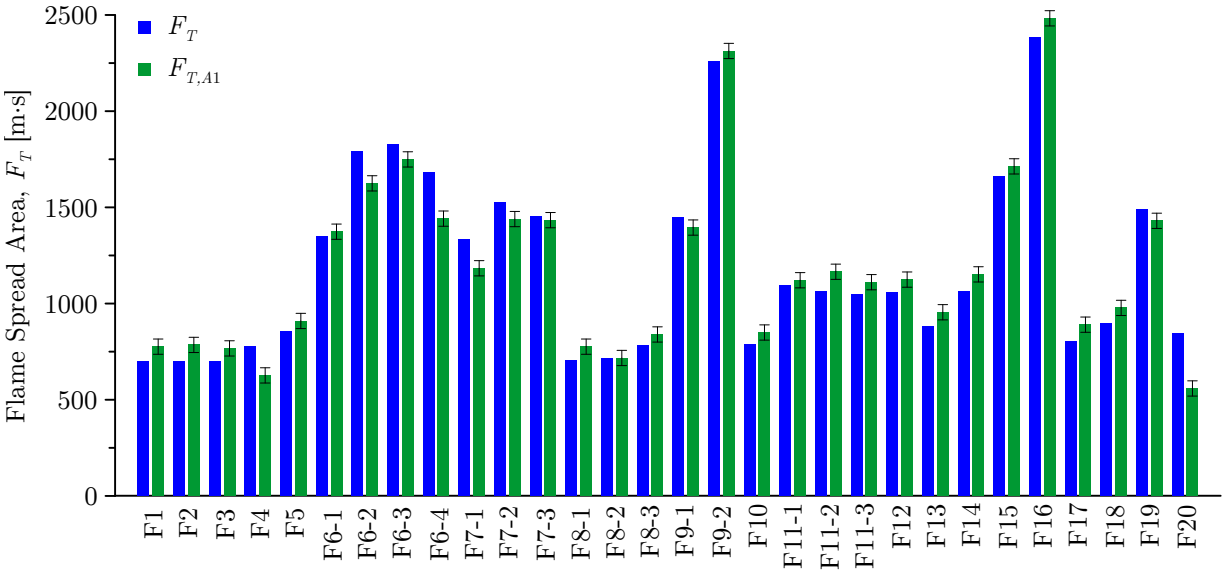

Figure 4.4: Comparison of the experimental flame spread area, F_T, and the two-variable approximated flame spread area, $F_{T,A1}$, for 30 Steiner tunnel tests.

4.1.2 Peak Flame Spread Model

With the observation from Section 4.1.1 that the dependence of F_T on τ_1 appears to be minimal for the set of tests in this study, a one-variable linear model is proposed for approximating flame spread area, as indicated by Equation 4.5. This one-variable model has a single dependent variable: peak flame spread.

$$F_{T,A2} = A \cdot f_1 + B \tag{4.5}$$

Equation 4.5 is applied to each of the thirty Steiner tunnel tests in this study to determine new values of approximated flame spread areas. By minimizing the mean error between actual and approximated results, A and B are determined to be 540.0 [s] and 34.47 [m · s] respectively. The coefficient of determination of the model, R^2, is found to be 0.9926, indicating that the model provides an excellent fit to the data.

Figure 4.5 shows the 1-variable approximation function for $F_{T,A2}$.

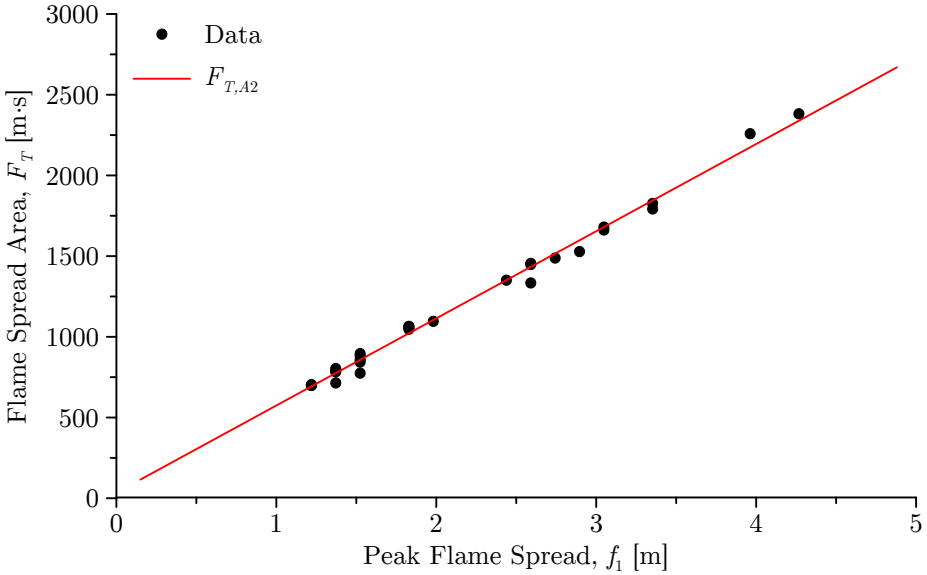

Figure 4.5: One-variable flame spread area approximation function.

Figure 4.6 shows the approximated flame spread area plotted along with the experimental flame spread area for all 30 Steiner tunnel tests in this study. The mean percent error between the experimental results and modelled results is 2.67%.

Accuracy, limitations, and appropriateness of the one-variable and two-variable models for approximated flame spread area are compared in the following section.

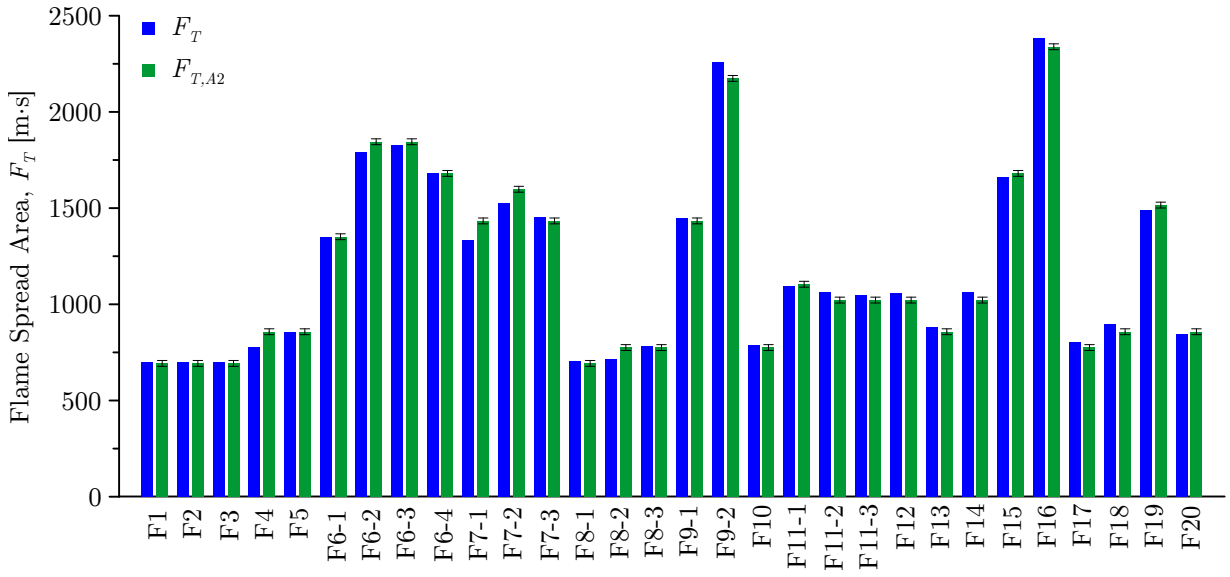

Figure 4.6: Comparison of the experimental flame spread area and the one-variable approximated flame spread area for 30 Steiner tunnel tests.

4.1.3 Evaluation of Flame Spread Area Models

Two models for approximating flame spread area have been proposed in Section 4.1 above. The average percent error between approximated and actual values for both models and the relative goodness of fit of the models are summarized in Table 4.1. Confidence limits on the results are summarized in Table 4.2.

Table 4.1: Results of the flame spread area approximation functions.

Model	Dependent Variables	$\overline{\%\epsilon}$	R^2
$F_{T,A1}$	f_1, τ_1	8.107%	0.9498
$F_{T,A2}$	f_1	2.671%	0.9926

In this section it is proposed that flame spread area may be approximated using only two results from the flame propagation curve: peak flame spread, f_1, and time to peak flame spread, τ_1. It was found that the calculated flame spread area for the materials in this study is highly dependent on the peak flame spread, regardless of the time it takes to reach that peak. From the perspective of improving flame spread performance in the Steiner tunel test then, it is clear that minimizing the peak flame spread should be a primary goal in the FR optimization phase of mixture design.

Table 4.2: Error and confidence limits for the flame spread area approximation functions.

Model	$\overline{\epsilon}$	$\hat{\epsilon}$	C_U	C_L
$F_{T,A1}$	0	106.1	39.63	-39.63
$F_{T,A2}$	0	40.80	15.23	-15.23

It is concluded that peak flame spread is the primary performance indicator for the Steiner tunnel test for the types of materials in this research. The main implication of this conclusion is that predictive models for flame spread index should strive to predict the peak flame spread based on the expected behaviour of a given material in the test. Looking back to Janssens Steiner tunnel model discussed in Section 2.1.2 [11], it is apparent that it failed in predicting flame spread index for polymeric insulation because it was not able to predict a realistic peak flame spread.

Comparing Figures 4.4 and 4.6, it appears that both the one-variable model (R^2 = 0.9926) and the two-variable model (R^2 = 0.9498) both provide reasonably accurate approximations of F_T for the thirty tests included in this study. Furthermore, the results demonstrate that the one-variable model for approximating flame spread area, $F_{T,A2}$, is the best fit to the experimental data. Moving forward, the one-variable model is used in conjunction with cross-test correlations for peak flame spread to develop generalized predictive models for flame spread index.

4.2 Cross-Test Correlations

Relationships are examined between results from cone calorimeter tests and Steiner tunnel tests for corresponding formulations. Of the group of Steiner tunnel tests conducted in this study, a subset of 20 tests (of 13 formulations) have corresponding cone calorimeter results. Several formulations were tested in duplicate or triplicate in the Steiner tunnel in order to examine variability. In such cases, the average Steiner tunnel result is used in the correlation. The original results are included in plots for reference, and are indicated using unfilled symbols.

A number of relationships are examined, and are summarized in Table 4.3.

Table 4.3: Cross-test relationships examined for the flame spread model.

Steiner Tunnel Test Result	Cone Calorimeter Test Result	Evaluation of Potential for Correlation
F_1 [m · s]	Q_b [MJ]	Some indication of correlation, $R^2 < 0.5$
F_1 [m · s]	q_p [kW]	Some indication of correlation, $R^2 < 0.5$
F_1 [m · s]	q_p/ρ [kW · m^3/kg]	No indication of correlation
F_1 [m · s]	q_p/ML_b [kW/g]	No indication of correlation
F_1 [m · s]	$\Delta H_{c,eff}$ [MJ/kg]	Some indication of correlation, $R^2 < 0.5$
F_1 [m · s]	q_b [kW]	Some indication of correlation, $R^2 < 0.5$
F_1 [m · s]	q_b/ρ [kW · m^3/kg]	No indication of correlation
F_1 [m · s]	q_b/ML_b [kW/g]	No indication of correlation
F_2 [m · s]	Q_b [MJ]	Some indication of correlation, $R^2 < 0.5$
F_2 [m · s]	q_p [kW]	No indication of correlation
F_2 [m · s]	q_p/ρ [kW · m^3/kg]	No indication of correlation
F_2 [m · s]	q_p/ML_b [kW/g]	No indication of correlation
F_2 [m · s]	$\Delta H_{c,eff}$ [MJ/kg]	Some indication of correlation, $R^2 < 0.5$
F_2 [m · s]	q_b [kW]	No indication of correlation
F_2 [m · s]	q_b/ρ [kW · m^3/kg]	No indication of correlation
F_2 [m · s]	q_b/ML_b [kW/g]	No indication of correlation
τ_1 [s]	t_{ign} [s]	No indication of correlation
τ_1 [s]	t_p [s]	No indication of correlation
τ_1 [s]	t_{fo} [s]	No indication of correlation
τ_1 [s]	t_b [s]	No indication of correlation
f_1 [m]	Q_b [MJ]	Some indication of correlation, $R^2 < 0.5$
f_1 [m]	q_p [kW]	Good indication of correlation, $R^2 < 0.8$
f_1 [m]	q_p/ρ [kW · m^3/kg]	Some indication of correlation, $R^2 < 0.5$
f_1 [m]	q_p/ML_b [kW/g]	Some indication of correlation, $R^2 < 0.5$
f_1 [m]	$\Delta H_{c,eff}$ [MJ/kg]	No indication of correlation
f_1 [m]	q_b [kW]	Excellent indication of correlation, $R^2 > 0.8$
f_1 [m]	q_b/ρ [kW · m^3/kg]	Some indication of correlation, $R^2 < 0.5$
f_1 [m]	q_b/ML_b [kW/g]	Excellent indication of correlation, $R^2 > 0.8$

continued on next page...

continued from previous page...

Steiner Tunnel Test Result	Cone Calorimeter Test Result	Evaluation of Potential for Correlation
f_2 [m]	Q_b [MJ]	Some indication of correlation, $R^2 < 0.5$
f_2 [m]	q_p [kW]	Some indication of correlation, $R^2 < 0.5$
f_2 [m]	q_p/ρ [kW $\cdot$ m^3/kg]	No indication of correlation
f_2 [m]	q_p/ML_b [kW/g]	No indication of correlation
f_2 [m]	$\Delta H_{c,eff}$ [MJ/kg]	No indication of correlation
f_2 [m]	q_b [kW]	Some indication of correlation, $R^2 < 0.5$
f_2 [m]	q_b/ρ [kW $\cdot$ m^3/kg]	No indication of correlation
f_2 [m]	q_b/ML_b [kW/g]	No indication of correlation
V_b [m^3]	ML_b [g]	Good indication of correlation, $R^2 < 0.8$
V_b [m^3]	ρ [kg/m^3]	No indication of correlation
V_b [m^3]	ML_b/ρ [m^3]	Some indication of correlation, $R^2 < 0.5$
f_1/V_b [m/m^3]	Q_b [MJ]	No indication of correlation
f_1/V_b [m/m^3]	q_p [kW]	No indication of correlation
f_1/V_b [m/m^3]	q_p/ρ [kW $\cdot$ m^3/kg]	Some indication of correlation, $R^2 < 0.5$
f_1/V_b [m/m^3]	q_p/ML_b [kW/g]	Good indication of correlation, $R^2 < 0.8$
f_1/V_b [m/m^3]	$\Delta H_{c,eff}$ [MJ/kg]	No indication of correlation
f_1/V_b [m/m^3]	q_b [kW]	No indication of correlation
f_1/V_b [m/m^3]	q_b/ρ [kW $\cdot$ m^3/kg]	Some indication of correlation, $R^2 < 0.5$
f_1/V_b [m/m^3]	q_b/ML_b [kW/g]	Excellent indication of correlation, $R^2 > 0.8$
f_2/V_b [m/m^3]	Q_b [MJ]	No indication of correlation
f_2/V_b [m/m^3]	q_p [kW]	No indication of correlation
f_2/V_b [m/m^3]	q_p/ρ [kW $\cdot$ m^3/kg]	No indication of correlation
f_2/V_b [m/m^3]	q_p/ML_b [kW/g]	No indication of correlation
f_2/V_b [m/m^3]	$\Delta H_{c,eff}$ [MJ/kg]	No indication of correlation
f_2/V_b [m/m^3]	q_b [kW]	No indication of correlation
f_2/V_b [m/m^3]	q_b/ρ [kW $\cdot$ m^3/kg]	No indication of correlation
f_2/V_b [m/m^3]	q_b/ML_b [kW/g]	No indication of correlation

Three relationships are identified in Table 4.3 that are worth pursuing, as indicated by an "Excellent" evaluation. These correlations are examined in detail in Sections 4.2.1 through 4.2.2.

4.2.1 Peak Flame Spread

First, the relationship between peak flame spread in the Steiner tunnel, f_1, and the average heat release rate of a sample in the cone calorimeter, q_b, is examined. As outlined in Section 2.4, q_b is the average rate of heat release during flaming combustion of a specimen in the cone calorimeter test. While not the sole performance indicator in the cone calorimeter test, it does describe the potential for rapid heat contribution of one material relative to another during a fire. It is understood that a formulation with a lower q_b would perform better than a formulation with a greater q_b regardless of the pass/fail criteria of a particular set of performance standards. Similarly, as identified in Section 4.1.3, f_1 is the primary performance indicator for flame in the Steiner tunnel; a formulation with lower f_1 performs better than a formulation with a greater f_1, resulting in a lower value of FSI.

Figure 4.7 shows two attempts at developing correlation plots between f_1 and q_b for the set of 20 tests. Note that unfilled symbols refer to repeated Steiner tunnel results for a given formulation, as indicated by multiple f_1 values for a given q_b.

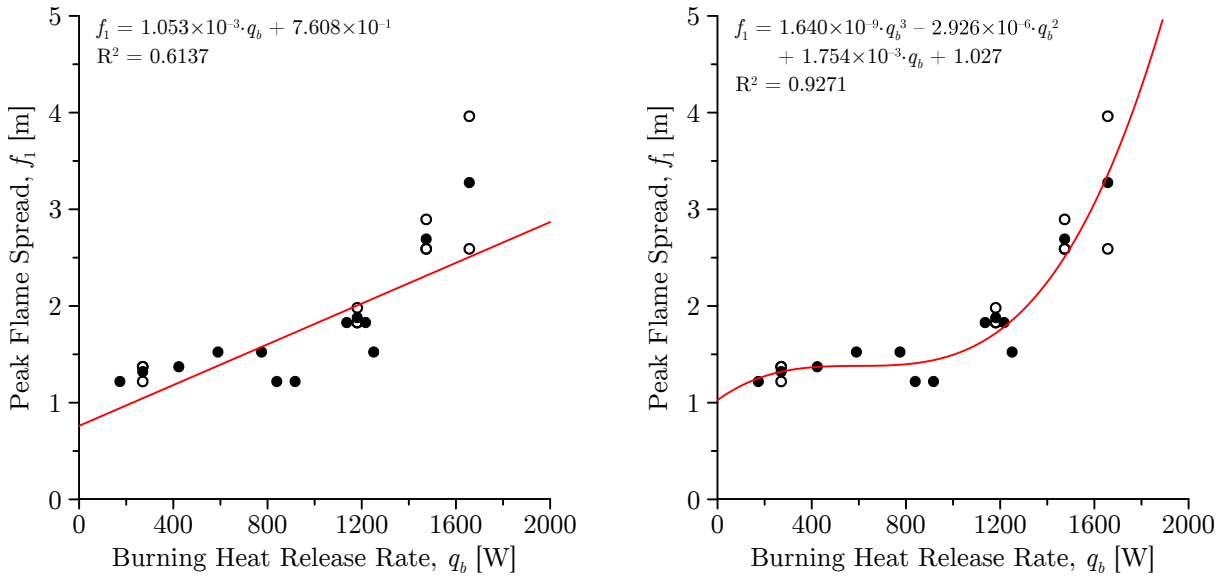

(a) Linear least-squares fit.

(b) Polynomial least-squares fit.

Figure 4.7: Peak flame spread correlations: average burning heat release rate.

Figure 4.7a would appear to indicate a positive linear correlation between the peak flame spread in the Steiner tunnel and the average heat release rate in the cone calorimeter. The two performance indicators for fire growth correlate positively, which serves as the rationale for development of a predictive model for flame spread.

Three distinct regions are identified in Figure 4.7b: an initial region of weak positive slope, a second region of zero slope, and a third region of strong positive slope. A third-order polynomial model can be used to describe this behaviour, with an inflection point located in the transition between the first and third regions. Such a model would imply that specimens with very low average heat release rates in the cone calorimeter would perform progressively better in the Steiner tunnel. Conversely, specimens with very high average heat release rates in the cone calorimeter would perform progressively worse in the Steiner Tunnel. It is reasoned that a polynomial relationship may be better suited to the data; Figure 4.7b shows f_1 plotted against q_b and fit with a third-order polynomial function.

Figure 4.7b demonstrates a strong positive cubic correlation between q_b and f_1. The correlation is stated in Equation 4.6 as the first proposed predictive model for f_1 based on results from cone calorimeter testing of the material of interest.

$$f_{1,M1} = A \cdot {q_b}^3 + B \cdot {q_b}^2 + C \cdot q_b + D \tag{4.6}$$

The next relationship identified in Table 4.3 involves the correlation between f_1 and q_b/ML_b. q_b is the average rate of heat release during flaming combustion, from the time of ignition to the time of flame extinction. Similarly, ML_b is the total amount of mass burned during flaming combustion, from the time of ignition to the time of flame extinction. The division of q_b by ML_b represents the effective potential heat release rate per unit mass of a substance. A parallel is drawn between the effective heat release rate (W/g) and the effective heat of combustion (J/g), which measures the effective potential heat energy per unit mass of a substance.

For a given formulation and set of apparatus conditions, q_b/ML_b is expected to remain fairly constant. For example, if one test resulted in greater average heat release in the same time than another test of the same formulation, it is expected that the first formulation underwent greater burning mass loss. Fluctuations in burning mass loss can be expected even between samples of the same formulation, due to variations in specimen conditioning, sample preparation, mixture discrepancies, and potentially even non-uniform dispersal of FRs in the foam mixture. For these reasons, the inclusion of ML_b into the correlation is expected to improve the fit by reducing scatter amongst results measured using similar formulations.

Figure 4.8 shows two attempts at developing correlation plots between f_1 and q_b/ML_b for the set of 20 tests. Note that unfilled symbols refer to repeated Steiner tunnel results for a given formulation, as indicated by multiple f_1 values for a given q_b/ML_b.

A good positive linear correlation is observed in Figure 4.8a between peak flame spread in the Steiner tunnel and effective heat release rate in the cone calorimeter. Compared to

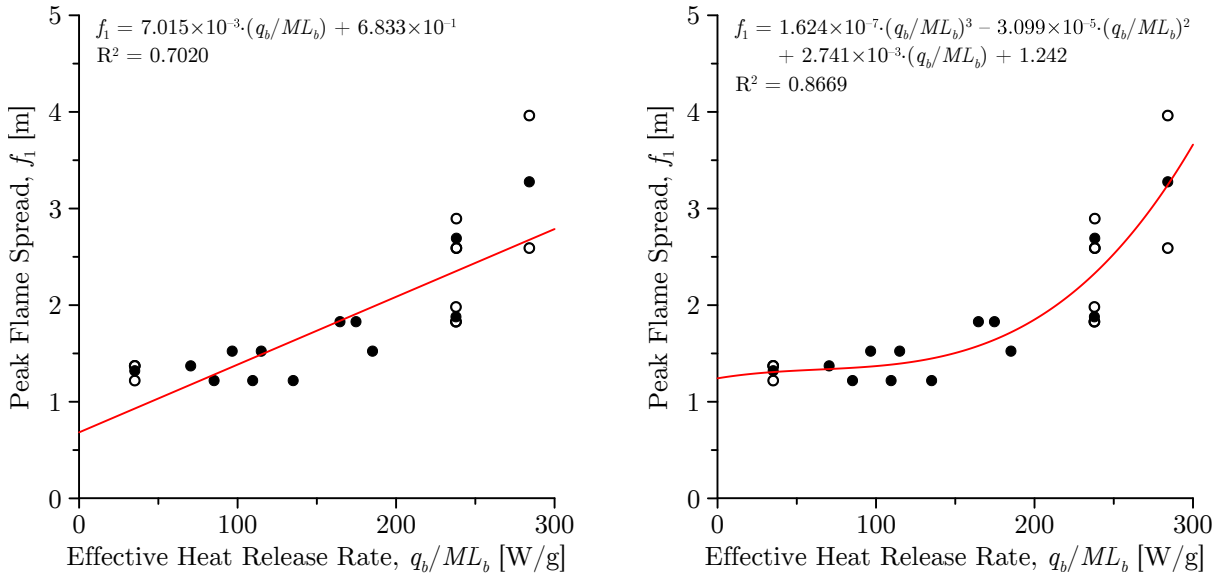

(a) Linear least-squares fit.

(b) Polynomial least-squares fit.

Figure 4.8: Peak flame spread correlations: effective heat release rate.

the first model, a linear correlation appears to be a better fit to this model. Still, distinct regions of weak positive slope, zero slope, and strong positive slope are identified. As such, Figure 4.8b shows f_1 plotted against q_b/ML_b with a third-order polynomial fit.

Figure 4.8b demonstrates a strong positive cubic correlation between peak flame spread in the Steiner tunnel and effective heat release rate in the cone calorimeter. The correlation is stated in Equation 4.7 as the second proposed predictive model for f_1.

$$f_{1,M2} = A \cdot \left(\frac{q_b}{ML_b}\right)^3 + B \cdot \left(\frac{q_b}{ML_b}\right)^2 + C \cdot \left(\frac{q_b}{ML_b}\right) + D \tag{4.7}$$

The next relationship identified in Table 4.3 involves the volume normalized peak flame spread. This relationship is examined in Section 4.2.2.

4.2.2 Normalized Peak Flame Spread

One caveat in assessing the strength of the correlations developed in Section 4.2.1 is in the appropriateness of using averaged Steiner tunnel results without accounting for variability. As discussed in Section 2.3, variability in repeated Steiner tunnel tests can be significant. For example, when a formulation is tested in triplicate, the flame spread may propagate notably further in the first test than in the following two. It is tempting to disregard such

a result on the grounds that it is not representative of the material's typical response in the test, and may perhaps be attributed to test-to-test inconsistencies. Statistically, however, three tests may not be enough to confidently distinguish any single test as an outlier. It could be argued that repeated testing might find the two tests with lower flame spreads to be non-representative.

First, variability in the Steiner tunnel test is examined for a subset of formulations. Of the set of 20 tests included in the flame spread model, four formulations are subjected to repeated testing; variability is quantified for those four formulations in Table 4.4.

Table 4.4: Variability in peak flame spread for three formulations.

Formulation	n	$\overline{f_1}$ [m]	$\hat{f}_1$ [m]	C_U [m]	C_L [m]	CV
F7	3	2.692	0.1760	3.130	2.255	0.06536
F8	3	1.321	0.08799	1.539	1.102	0.06662
F9	2	3.277	0.9699	–	–	0.2960
F11	3	1.880	0.08799	2.098	1.661	0.04681

In Table 4.4, CV represents the sample estimate of the coefficient of variation, which is a normalized measure of dispersion of a probability distribution [63]. CV expresses variability in relation to the mean, and being a unitless parameter, may be used to compare variability for different results. While the specific value of CV may not be relevant without context, a parameter with a lower value of CV is interpreted to have less variability than another parameter with a greater value of CV. The results may be interpreted as follows, using formulation F11 as an example:

- the sample mean of peak flame spread for formulation F11 with a sample size of 3 was determined to be approximately 1.9 metres;
- there is 95% confidence that the true mean peak flame spread lies approximately between 1.7 and 2.1 metres; and
- the ratio of the sample standard deviation to the sample mean for peak flame spread is calculated to be approximately 0.047.

Notably absent from Table 4.4 are confidence bounds on the result for formulation F9. Since only two tests were conducted for this formulation, it is not possible to calculate confidence bounds.

The confidence bounds on f_1 for a given formulation might be narrowed by increasing the number of tests conducted for each formulation. However, due to the high cost and time required for Steiner tunnel testing, repeated testing for the sole purpose of

establishing reasonable confidence limits on the result is not economically viable. As an alternative, the Steiner tunnel results are normalized in an attempt to improve variability. It is proposed that the approximated burned volume, V_b, may effectively normalize the primary performance indicator for flame spread, f_1. Table 4.5 quantifies variability in the normalized results for formulations F7, F8, F9, and F11.

Table 4.5: Variability in normalized peak flame spread for three formulations.

Formulation	n	$\overline{f_1/V_b}$ [m/m^3]	$\hat{f_1/V_b}$ [m/m^3]	C_U [m/m^3]	C_L [m/m^3]	CV
F7	3	25.62	1.518	29.39	21.85	0.05925
F8	3	14.57	0.2144	15.10	14.04	0.01471
F9	2	35.09	14.23	–	–	0.4055
F11	3	23.56	0.5153	24.84	22.28	0.02187

Table 4.5 demonstrates that normalizing f_1 by V_b has significantly reduced variability in the result for formulation F8, with CV reduced to 0.015 from 0.067. Variability is also greatly reduced for formulation F11, and slightly reduced for formulation F7. Unfortunately, variability is greatly increased for formulation F9. Therefore, the possibility of the F9 sub-group containing an outlying result is discussed below.

With the effect of normalization on Steiner tunnel variability assessed, the next step is to examine the relationship between normalized peak flame spread in the Steiner tunnel, f_1/V_b, and the effective heat release rate of a sample in the cone calorimeter, q_b/ML_b. The relationship between the two parameters is examined in Figure 4.9.

Figure 4.9 shows plots of the linear correlation between f_1/V_b and q_b/ML_b for the set of 20 tests. Note that unfilled symbols refer to repeated Steiner tunnel results for a given formulation, as indicated by multiple f_1/V_b values for a given q_b/ML_b.

Comparing Figures 4.8a and 4.9a, it is seen that normalizing f_1 by V_b produces the desired effect of reducing the spread in observed values on repeated tests of the same formulation, with one notable exception: formulation F9 yielded two Steiner tunnel results that differ by greater than 150%. The spread is also apparent in Figure 4.7a, although to a lesser degree. The previous two correlations have accommodated this spread in values by fitting a curve between the two points, implying that the true peak flame spread for F9 lies between the two extremes. It is tempting to exclude test F9-2 under the presumption that it is an erroneous result; however, F9-2 cannot be labelled an "outlier" according to the definition applicable to the ASTM E84 test without conducting a minimum of three

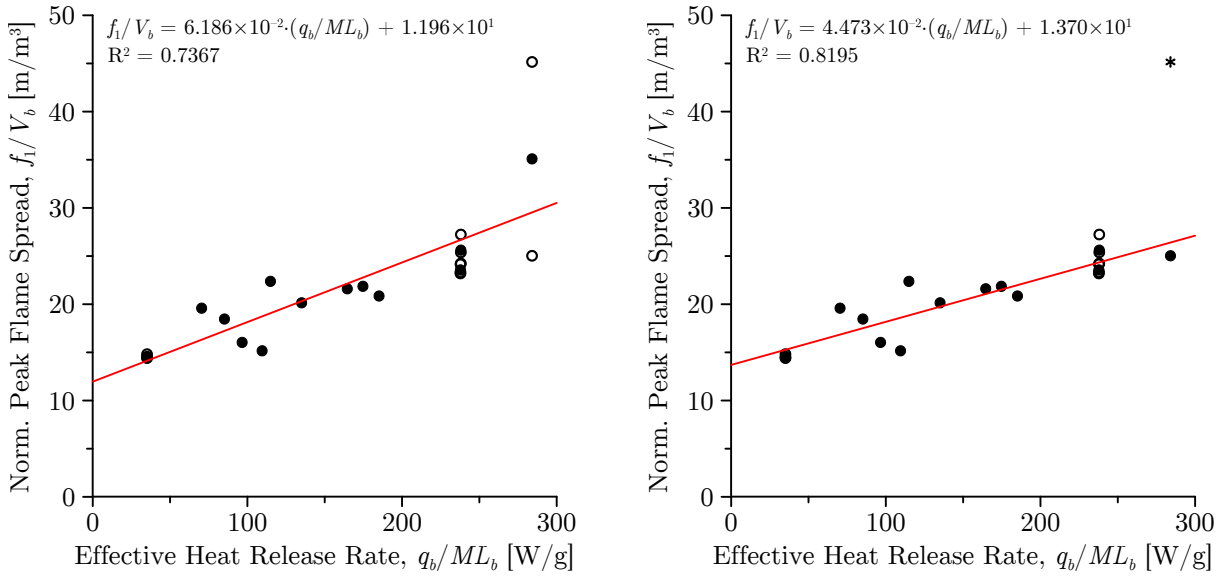

(a) Linear least-squares fit, all tests.

(b) Linear least-squares fit, F9-2 excluded.

Figure 4.9: Normalized peak flame spread correlations: effective heat release rate.

tests for a given material [64]. Even if retention of the result appears questionable, F9-2 cannot be excluded on statistical grounds.

Figure 4.9a suggests a positive linear correlation between f_1/V_b and q_b/ML_b, with coefficient of determination of 0.737. For comparison, Figure 4.9b shows the same results as Figure 4.9a, with the exception of formulation F9-2 being labelled as an outlier. The comparison strengthens the indication of positive linearity between the results with the coefficient of determination increasing to 0.820. The correlation is stated in Equation 4.8 as the third proposed predictive model for f_1.

$$\left.\frac{f_1}{V_b}\right|_{M3} = A \cdot \frac{q_b}{ML_b} + B \tag{4.8}$$

While this proposed model shows promise, it cannot be used in a predictive model for flame spread index, since V_b is derived from the Steiner tunnel flame spread curve. To distinguish Model 3 from Models 1 and 2, $f_{1,M3}$ is denoted with an asterisk superscript. Equation 4.8 is re-stated as Equation 4.9.

$${f_{1,M3}}^* = V_b \cdot \left(A \cdot \frac{q_b}{ML_b} + B\right) \tag{4.9}$$

With three correlations developed between Steiner tunnel and cone calorimeter test results, the next step is to develop predictive models for flame spread index in the Steiner tunnel based on these correlations.

4.3 Predictive Models for Flame Spread Index

Using each of the peak flame spread correlations developed in Section 4.2 in conjunction with the one-variable flame spread area approximation developed in Section 4.1, experimental flame spread indices are calculated. The following notation is used:

- FSI_{M1} refers to predicted flame spread index using $f_{1,M1}$ and $F_{T,A2}$;
- FSI_{M2} refers to predicted flame spread index using $f_{1,M2}$ and $F_{T,A2}$;
- FSI_{M3} refers to predicted flame spread index using ${f_{1,M3}}^*$ and $F_{T,A2}$.

Predicted flame spread index is calculated according to Equation 4.10. Note that although FSI is unitless, the equation changes depending on the units of FT; Equation 4.10 is derived from Equation 2.4 using metric units.

$$FSI_M = \begin{cases} \dfrac{4900}{195 - 0.05468 \cdot F_{T,M}} & F_{T,M} > 1783 \text{ m} \cdot \text{s} \\ 0.02816 \cdot F_{T,M} & F_{T,M} \leq 1783 \text{ m} \cdot \text{s} \end{cases} \tag{4.10}$$

Error is quantified for all experimental flame spread indices according to Section 3.4. Additionally, successful prediction of flame spread index for a given formulation is dictated by the percent error between the experimental FSI and the predicted FSI. It is deemed that a successful prediction is achieved when the percent error is less than or equal to 20%.

4.3.1 Model 1: Average Heat Release Rate

Summarizing the results from Sections 4.2 and 4.1, the assembled average heat release rate model for flame spread area is stated as Equation 4.11.

$$\begin{aligned} F_{T,M1} = {} & 8.856 \times 10^{-7} \cdot {q_b}^3 - 1.580 \times 10^{-3} \cdot {q_b}^2 \\ & + 9.474 \times 10^{-1} \cdot q_b + 5.890 \times 10^2 \end{aligned} \tag{4.11}$$

Using Equations 4.10 and 4.11, the predicted flame spread index is calculated for each of the 13 formulations. The results are plotted adjacent to the associated experimental results for all 20 tests in Figure 4.10. In the figure, blue bars represent experimental values of flame spread index, green bars represent predicted values of flame spread index less than 20% different than the associated experimental values, and red bars represent predicted values of flame spread index greater than 20% different than the associated experimental values.

Figure 4.10 shows that of the 20 Steiner tunnel tests conducted, the model is able to predict the flame spread index to within 20% difference for 18 tests, and 12 of the 13

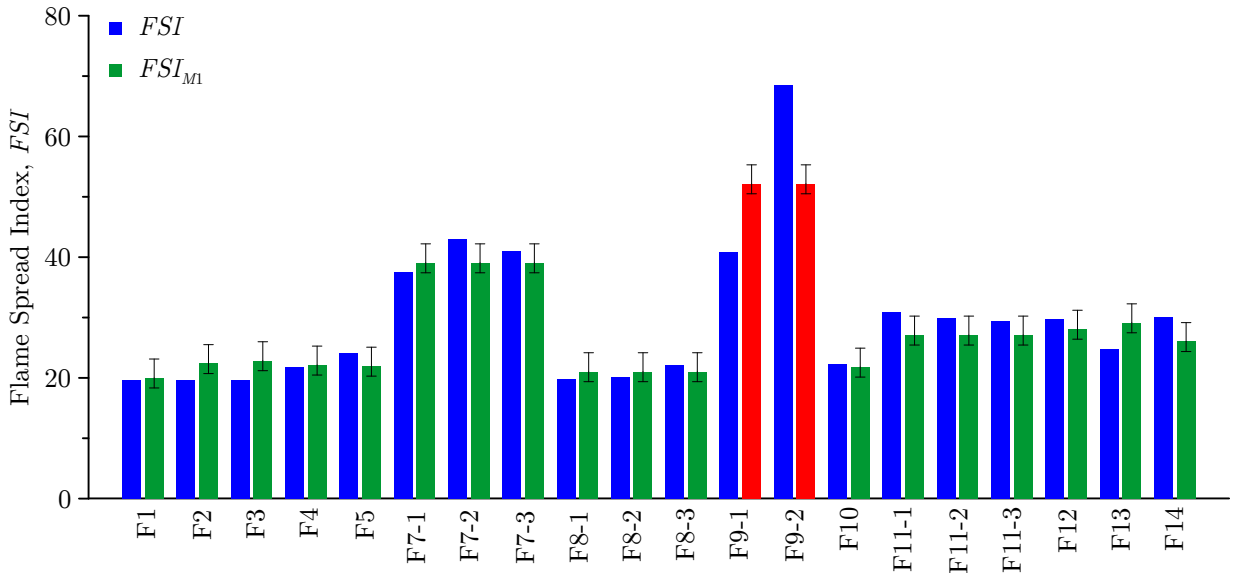

Figure 4.10: Experimental and predicted flame spread index for Model 1.

formulations. The one formulation that does not appear to fit the model is F9. There is no indication from the manufacturer that formulation F9 differed significantly from the other foam materials chemically or structurally. The result appears simply to be a case of significant variability in the Steiner tunnel, either in the apparatus, or in the cutting and mounting of specimens. Even so, the predicted flame spread index for F9 lies between the two recorded experimental results for F9, indicating that the true FSI may lie closer to the predicted result. If Model 1 is taken to be a representation of the expected behaviour of the material, it is supposed that were repeated testing conducted on formulation F9, the true FSI would lie somewhere between that of F9-1 and F9-2.

4.3.2 Model 2: Effective Heat Release Rate

Summarizing the results from Sections 4.2 and 4.1, the assembled effective heat release rate model for flame spread area is stated as Equation 4.12.

$$F_{T,M2} = 8.772 \times 10^{-5} \left(\frac{q_b}{ML_b}\right)^3 - 1.673 \times 10^{-2} \left(\frac{q_b}{ML_b}\right)^2 + 1.480 \left(\frac{q_b}{ML_b}\right) + 7.054 \times 10^2 \tag{4.12}$$

Using Equations 4.10 and 4.12, the predicted flame spread index is calculated for each of the 13 formulations. The results are plotted adjacent to the associated experimental

results for all 20 tests in Figure 4.11. In the figure, blue bars represent experimental values of flame spread index, green bars represent predicted values of flame spread index less than 20% different than the associated experimental values, and red bars represent predicted values of flame spread index greater than 20% different than the associated experimental values.

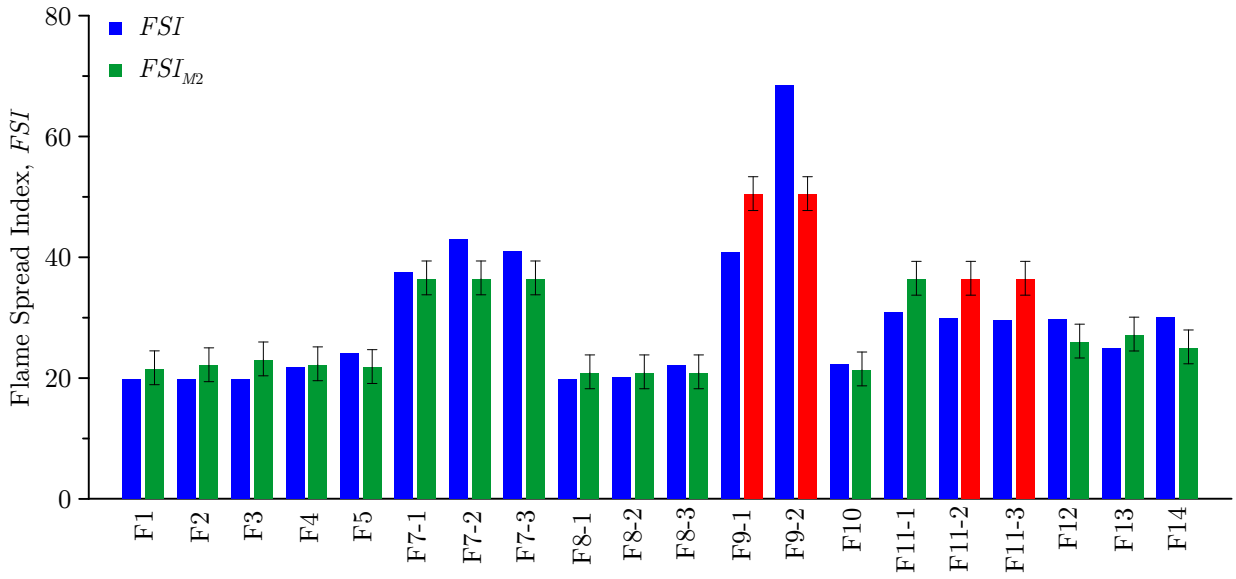

Figure 4.11: Experimental and predicted flame spread index for Model 2.

Figure 4.11 shows that of the 20 Steiner tunnel tests conducted, the model is able to predict the flame spread index to within 20% difference for 16 tests, and 11 of the 13 formulations. The two formulations that do not appear to fit the model are F9 and F11. The result for formulation F9 is expected, due to the large difference in tests F9-1 and F9-2. For formulation F11, only one of the three tests results is predicted to within 20% difference. Based on these observations, Model 2 does not appear to fit the sample data set as well as Model 1.

4.3.3 Model 3: Normalized Effective Heat Release Rate

Summarizing the results from Sections 4.2 and 4.1, the assembled effective heat release rate model for normalized flame spread area is stated as Equation 4.13.

$$F_{T,M3}{}^{*} = 3.341 \times 10^{1} \cdot V_b \cdot \frac{q_b}{ML_b} + 6.493 \times 10^{3} \cdot V_b \tag{4.13}$$

Using Equations 4.10 and 4.13, the predicted flame spread area is calculated for each of the 13 formulations. The results are plotted adjacent to the associated experimental

results for all 20 tests in Figure 4.11. In the figure, blue bars represent experimental values of flame spread index, green bars represent predicted values of flame spread index less than 20% different than the associated experimental values, and red bars represent predicted values of flame spread index greater than 20% different than the associated experimental values.

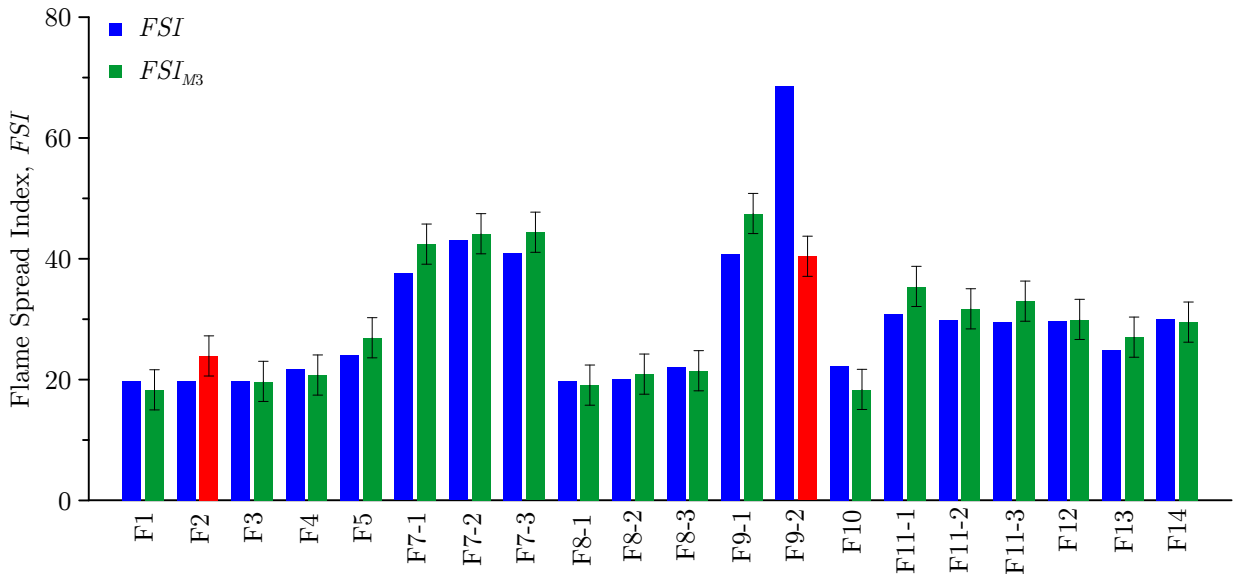

Figure 4.12: Experimental and predicted flame spread index for Model 3.

Figure 4.12 shows that of the 20 Steiner tunnel tests conducted, the model is able to predict the flame spread index to within 20% difference for 18 tests, and 12 of the 13 formulations. The two formulations that do not appear to fit the model are F2 and F9. Interestingly, the model was able to successfully predict the flame spread index for F9-1, and not F9-2. This result lends credence to the idea that the true flame spread index for formulation F9 is actually less than the average of F9-1 and F9-2, in fact lying closer to F9-1. In this regard, the model is able to identify a potential outlier in Steiner tunnel results based on the expected outcome from cone calorimeter results.

4.4 Screening Potential for Flame Spread Index

Three predictive models for flame spread index are proposed in Section 4.3. The results for all three models are summarized in Table 4.6, with error quantified in Table 4.7.

The tables show that Models 1 and 3 appear to be the best fit to the experimental data, with FSI predictions within 20% difference for 18 of the 20 Steiner tunnel tests. Model

Table 4.6: Results of the predictive models for flame spread index.

Model	Steiner Tunnel Prediction	Cone Calorimeter Results	Rate of Success	$\overline{\%\epsilon}$
Model 1	F_T	q_b	18/20	7.914%
Model 2	F_T	q_b, ML_b	16/20	9.602%
Model 3	${F_T}^*$	q_b, ML_b	18/20	7.507%

Table 4.7: Error and confidence limits for the predictive models for flame spread index.

Model	$\overline{\epsilon}$	$\hat{\epsilon}$	C_U	C_L
Model 1	0.7310	5.122	3.128	−1.666
Model 2	0.1895	5.981	2.989	−2.610
Model 3	0.0400	7.103	3.364	−3.284

2 also appears to be a good fit to the experimental data, with successful FSI predictions for 16 of the 20 Steiner tunnel tests. Since Model 3 is a non-predictive model, it cannot be used to screen for Steiner tunnel tests. Model 1 is recommended as a screening tool for flame spread index.

The final screened result for flame spread index, FSI_S, is calculated for 13 formulations in this study based on the average heat release rate model for flame spread index and the error listed in Table 4.7. Screened flame spread index is presented as a lower and upper range based on the 95% confidence limits of the mean error of the modelled flame spread index. The confidence limits on mean error indicate the range in which the mean error is likely to exist in 95% of the cases in a very large sample set. Error is applied to the modelled flame spread index for each formulation according to Equation 4.14; the results are tabulated in Table 4.8, along with the average experimental FSI.

$$FSI_S = \{FSI_M + C_L\} \; - \; \{FSI_M + C_U\} \tag{4.14}$$

Comparing the experimental results for all formulations, three performance tiers are identified:

- formulations F7 and F9 are found to have flame spread indices greater than 40;
- formulations F11, F12, F13, and F14 are found to have flame spread indices between 25 and 30; and
- formulations F1, F2, F3, F4, F5, F8, and F10 are found to have flame spread indices between 20 and 25.

Table 4.8: Screened flame spread index for 13 foam formulations.

Formulation	FSI_S	$\overline{FSI}$
F1	18.3 – 23.1	19.7
F2	20.7 – 25.5	19.7
F3	21.2 – 26.0	19.7
F4	20.5 – 25.3	21.8
F5	20.3 – 25.1	24.1
F7	37.4 – 42.2	40.5
F8	19.4 – 24.2	20.7
F9	50.5 – 55.3	54.7
F10	20.1 – 24.9	22.2
F11	25.4 – 30.2	30.1
F12	26.4 – 31.2	29.7
F13	27.5 – 32.3	24.9
F14	24.4 – 29.2	30.0

Comparing the screened results for all formulations, several suggestions can be made with regard to their expected relative performance in the Steiner tunnel test:

- formulations F7 and F9 are expected to have significantly greater flame spread index than all other formulations;
- formulations F11, F12, F13, and F14 are expected to have similar flame spread indices which are lesser than those of F7 and F9; and
- formulations F1, F2, F3, F4, F5, F8, and F10 are expected to have similar flame spread indices which are lesser than those of all other formulations.

The predictive model has screened all 13 formulations into the same set of performance tiers, in increments of 5 FSI, as in the experimental results. It is concluded that a predictive model based on cone calorimeter results can effectively screen the relative performance of FR-SPF materials in the Steiner tunnel test.

Comparing the screened results for the first three formulations, formulation F3 appears that it may have a greater FSI than F2, and similarly F2 appears that it may have a greater FSI than F1. Even though the ranges on the screened results differ slightly, it cannot be said with confidence that F1 is expected to have a lower flame spread index than F2 or F3. Neither can it be said with confidence that formulations F1, F2, and F3 are expected to have the same flame spread index. It can, however, be said with confidence that formulations F1, F2, and F3 are expected to have similar flame spread indices. In

general terms, it can only be said with confidence that some formulation "A" is expected to have a lower flame spread index than some other formulation "B" if the upper range of a A's screened result is less than the lower range of B's screened result.

Comparing the experimental results for the first three formulations, all three are found to have the same FSI. Notably, each of formulations F1, F2, and F3 had only a single experimental result. It is possible, and in fact probable, that triplicate testing of each formulation would produce slightly different average experimental flame spread indices. Interpretation of the screened results yields the same finding.

A flame spread index of 25, the threshold for Class A classification in flame spread, corresponds to a flame spread area of approximately 900 $\mathrm{m} \cdot \mathrm{s}$ (48.5 $\mathrm{ft} \cdot \mathrm{min}$). According to the 1-variable approximation model for flame spread area, this corresponds to a peak flame spread of approximately 1.6 metres (5.25 feet). From this, Model 1 indicates that an average heat release rate in the cone calorimeter greater than approximately 1.1 kW (or an average heat release rate density of 125 $\mathrm{kW/m^2}$) can be expected to approach the failure threshold for Class A classification in the the Steiner tunnel. Furthermore, Model 1 indicates that the peak flame spread does not increase significantly until the average heat release rate in the cone calorimeter is greater than approximately 1.1 kW. From these results, it is recommended that future screening studies strive to achieve an average heat release rate in the cone calorimeter less than 1.1 kW if the objective is to achieve a Class A classification in Steiner tunnel flame spread.

Comparisons between materials that perform in a similar fashion in the cone calorimeter cannot be made with any degree of certainty with regards to the expected performance of those materials in the Steiner tunnel. As demonstrated in Table 4.8, the range on the certainty of a given prediction is on the order of 5 FSI. Therefore, it is concluded that the predictive model cannot confidently predict small differences (approximately less than 5 FSI) in flame spread index. Interestingly, this difference coincides with the rounding scheme applied to reported flame spread indices per ASTM E84 [4].

Confidence limits for screening have been determined according to the set of materials in this project. Unfortunately, variability in the Steiner tunnel test cannot presently be quantified for different materials without prior knowledge of their behaviour in the test. As such, attempts to apply the present version of the model to as-yet untested materials cannot be not recommended. While screening is demonstrated to be an effective tool in the R&D phase of materials development, primary assessment of the behaviour of new materials in the Steiner tunnel is recommended in addition to screening.

Even though the normalized effective heat release rate model cannot be used in a predictive manner, the correlation between normalized parameters shows promise. It was demonstrated in Section 4.2.2 that normalization of flame spread results by a material loss

parameter reduced variability in most cases. With this said, a measured normalization parameter, as opposed to the approximated burned volume, would strengthen confidence in this result. Further research into the impact of normalization of flame spread results to reduce variability is recommended. Investigation into the use of total mass loss, measured via load cell post-test, is recommended as an alternative to an approximated normalization parameter.

Chapter 5

Smoke Developed Model

In this section, relationships between smoke performance results from the Steiner tunnel test and results from the smoke density chamber test are examined. Key performance indicators are identified, and correlations are developed between the test results. Three models are proposed by which to predict the smoke developed index of a material, and each is evaluated with respect to their use for effectively screening materials for their potential performance in the Steiner tunnel test.

5.1 Cross-Test Correlations

The smoke developed index in the Steiner tunnel test is generally greater when more dark smoke is visible in the observation windows, and when more of the material appears to have been burned. Based on these observations, it was thought that a combination of smoke obscuration data and mass loss data from smoke density chamber tests might correlate the expected smoke performance of a given formulation in the Steiner tunnel. Correlations are therefore developed between smoke density chamber test results and the set of Steiner tunnel tests results.

Of the group of Steiner tunnel tests conducted in this study, a subset of 15 tests (of 8 formulations) have corresponding smoke density chamber results. Several formulations were tested in duplicate or triplicate in the Steiner tunnel in order to examine variability. In such cases, the average Steiner tunnel result is used in the correlation. The original results are included in plots for reference, and are indicated using unfilled symbols.

As discussed in Section 2.5, a limited set of variables is available from the smoke density chamber test, compared to that available from the cone calorimeter test, for use in the

development of an empirical correlation. From this limited set of results, three parameters are identified; they are:

- peak optical obscuration, TO_1;
- peak specific optical density, DS_1; and
- specimen mass loss at the time of peak optical obscuration, ML_1.

From these parameters, three correlations are developed. They are examined in Sections 5.1.1 through 5.1.2.

5.1.1 Total Smoke Obscuration

First, the relationships between the measured values of total smoke obscuration in the Steiner tunnel, TSO, peak specific optical density in the smoke density chamber, DS_1, and peak optical obscuration, TO_1, are examined. It is understood that a formulation with a lower TO_1 or DS_1 has performed better in the smoke density chamber test than a formulation with a higher TO_1 or DS_1. Therefore, both TO_1 and DS_1 are considered to be performance indicators for smoke in the smoke density chamber test. Similarly, as identified in Section 2.3.2, TSO is the primary performance indicator related to the development of smoke in the Steiner tunnel; a formulation with a lower TSO performs better than a formulation with a higher TSO, resulting in a lower value of SDI.

Figure 5.1a shows the correlation between TSO and DS_1 for the set of 15 tests, and Figure 5.1b shows the correlation between TSO and TO_1 for the set of 15 tests. Note that unfilled symbols refer to repeated Steiner tunnel results for a given formulation, as indicated by multiple TSO values for a given TO_1 or DS_1.

A good positive linear correlation is observed between the total smoke obscuration determined in the Steiner tunnel test and the peak optical obscuration measured in the smoke density chamber; an even better positive linear correlation is observed with the peak specific optical density. The performance indicators for smoke obscuration correlate positively, which serves as the rational for a predictive model. The correlation is stated in Equation 5.1 as the first proposed predictive model for TSO.

$$TSO_{M1} = A \cdot DS_1 + B \tag{5.1}$$

Next, the influence of specimen mass loss, ML_1, on the TSO correlation is examined. Total smoke production is determined from optical obscuration over the course of the test, which consequentially is dictated by the optical density of combustion products. Optical density, in turn, is dictated by the size and concentration of gaseous and particulate products of combustion, as well as the rate of generation of these products. A specimen

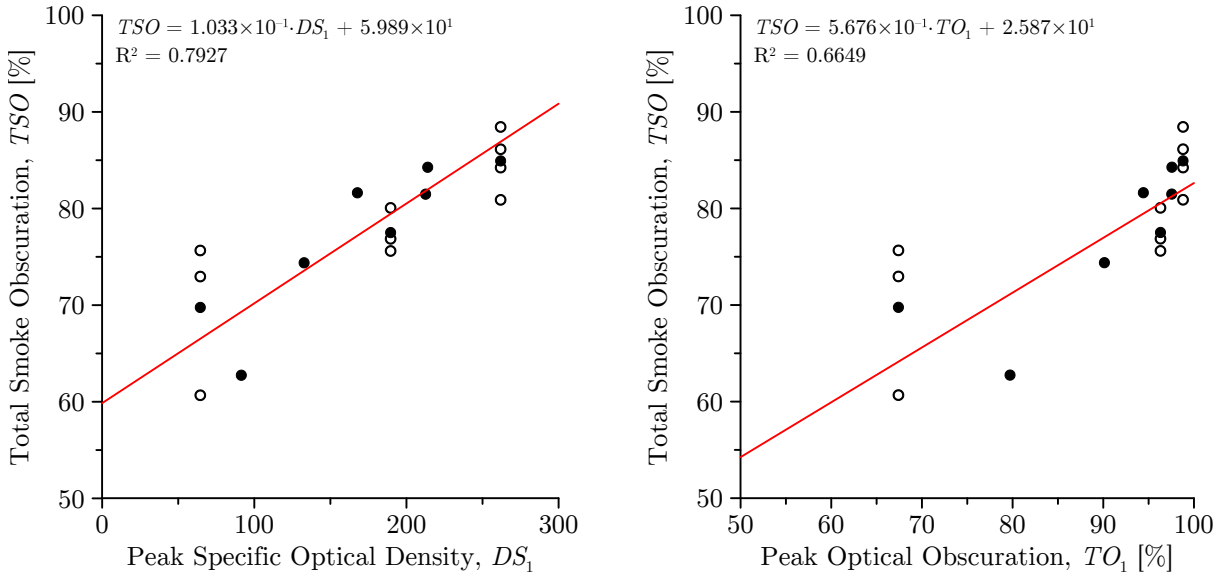

(a) Linear least-squares fit, DS_1.

(b) Linear least-squares fit, TO_1.

Figure 5.1: Total smoke obscuration correlations: peak specific optical density and peak optical obscuration.

which rapidly produces dark smoke containing high concentrations of light-absorbing particulate yields more net smoke than a specimen which produces the same density of particulate at a lesser rate, or less light-absorbing smoke at the same rate. This suggests that the total mass lost due to combustion during a certain period is related to the amount of particulate generated as a result of combustion; while direct proportionality is not suggested, positive correlation is presumed.

With the presumption of positive correlation between ML_1 and smoke production, relationships between total smoke obscuration in the Steiner tunnel and the linear products of DS_1 and ML_1, and TO_1 and ML_1, are examined. As in the first proposed predictive model for TSO, DS_1 is found to produce a better correlation than TO_1.

Figure 5.2 shows correlations between TSO and $DS_1 \cdot ML_1$ for the set of 15 tests. Note that unfilled symbols refer to repeated Steiner tunnel results for a given formulation, as indicated by multiple TSO values for a given $DS_1 \cdot ML_1$.

Comparing Figures 5.1a and 5.2a, the linear regression does not appear to be improved when DS_1 is replaced with $DS_1 \cdot ML_1$ in the correlation. Inspection of the trend in 5.2a, however, indicates that a logarithmic correlation may exist. A logarithmic model would imply that specimens which exhibit very low peak specific optical density and mass loss in the smoke density chamber will perform extremely well in smoke development in the

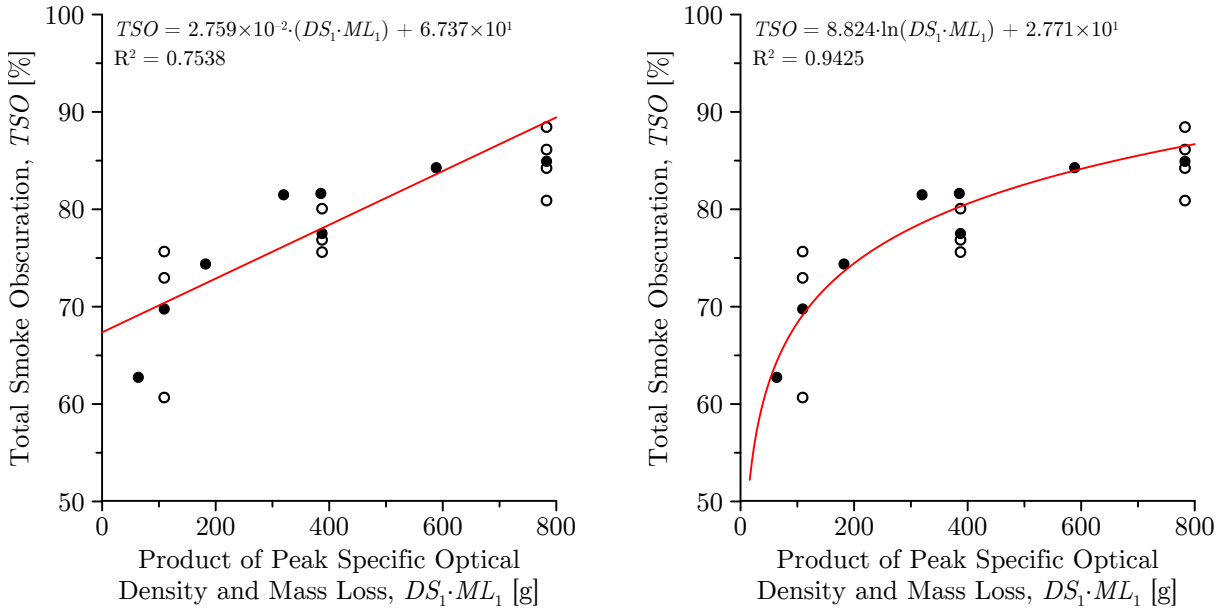

(a) Linear least-squares fit.

(b) Logarithmic least-squares fit.

Figure 5.2: Total smoke obscuration correlations: product of peak specific optical density and mass loss.

Steiner tunnel. Conversely, there will be a limit beyond which specimens with very high peak specific optical density and mass loss in the smoke density chamber will no longer perform significantly worse in smoke development in the Steiner tunnel.

Figure 5.2b shows total smoke obscuration plotted against the product of DS_1 and ML_1, with a logarithmic curve fit to the data. There is a strong positive logarithmic correlation between the data, with a coefficient of determination approaching 95%. The correlation is given in Equation 5.2 as the second proposed predictive model for TSO.

$$TSO_{M2} = A \cdot \ln(DS_1 \cdot ML_1) + B \tag{5.2}$$

Next, in Section 5.1.2, the relationship between volume normalized total smoke obscuration in the Steiner tunnel and smoke density chamber test results is examined.

5.1.2 Normalized Total Smoke Obscuration

As discussed in Section 4.2.2, assessing the strength of a correlation using averaged results without quantification of variability can lead to some uncertainty in the validity of the correlation. Of the set of 15 tests included in the smoke developed model, three

formulations are subjected to repeated testing; variability in total smoke obscuration is quantified for those three formulations in Table 5.1.

Table 5.1: Variability in total smoke obscuration for three formulations.

Formulation	n	$\overline{TSO}$ [%]	$T\hat{S}O$ [%]	C_U [%]	C_L [%]	CV
F6	4	84.93%	3.191%	90.01%	79.85%	0.03757
F7	3	77.51%	2.298%	83.22%	71.80%	0.02965
F8	3	69.76%	7.987%	89.60%	49.92%	0.1145

The results in Table 5.1 may be interpreted as follows, using formulation F8 as an example:

- the sample mean of total smoke obscuration for formulation F8 with a sample size of 3 was determined to be approximately 70%;
- there is 95% confidence that the true mean total smoke obscuration lies approximately between 50% and 90%; and
- the ratio of the sample mean to the sample standard deviation for total smoke obscuration is calculated to be approximately 0.1145.

The confidence bounds on TSO may be narrowed by increasing the number of tests conducted on each formulation, but as discussed in Section 4.2.2, repeated testing beyond $n = 3$ is not economically viable. Instead, an attempt is made to normalize the Steiner tunnel results to reduce variability. As in the case of the flame spread model, the volume of burned sample, V_b, is selected here as a normalization variable. Variability in the normalized results for formulations F6, F7, and F8 is summarized in Table 5.2.

Table 5.2: Variability in normalized total smoke obscuration for three formulations.

Formulation	n	$\overline{TSO/V_b}$ [%/m^3]	$T\hat{S}O/V_b$ [%/m^3]	C_U [%/m^3]	C_L [%/m^3]	CV
F6	4	8.469	0.3305	8.995	7.943	0.03902
F7	3	7.375	0.1317	7.702	7.048	0.01786
F8	3	7.680	0.4070	8.691	6.669	0.05299

Table 5.2 demonstrates that normalizing TSO by V_b has significantly improved variability in the result for formulation F8, with CV reduced to 0.053 from 0.11. Variability is also improved for formulation F7, and slightly worsened for formulation F6. A similar outcome was observed in the case of normalizing flame spread results.

Figure 5.3a shows the correlation between the normalized total smoke obscuration, TSO/V_B, and DS_1 for the set of 15 tests, and Figure 5.3b shows the correlation between TSO/V_B and TO_1 for the set of 15 tests. Unfilled symbols again refer to repeated Steiner tunnel results for a given formulation, as indicated by multiple TSO/V_B values for a given TO_1 or DS_1.

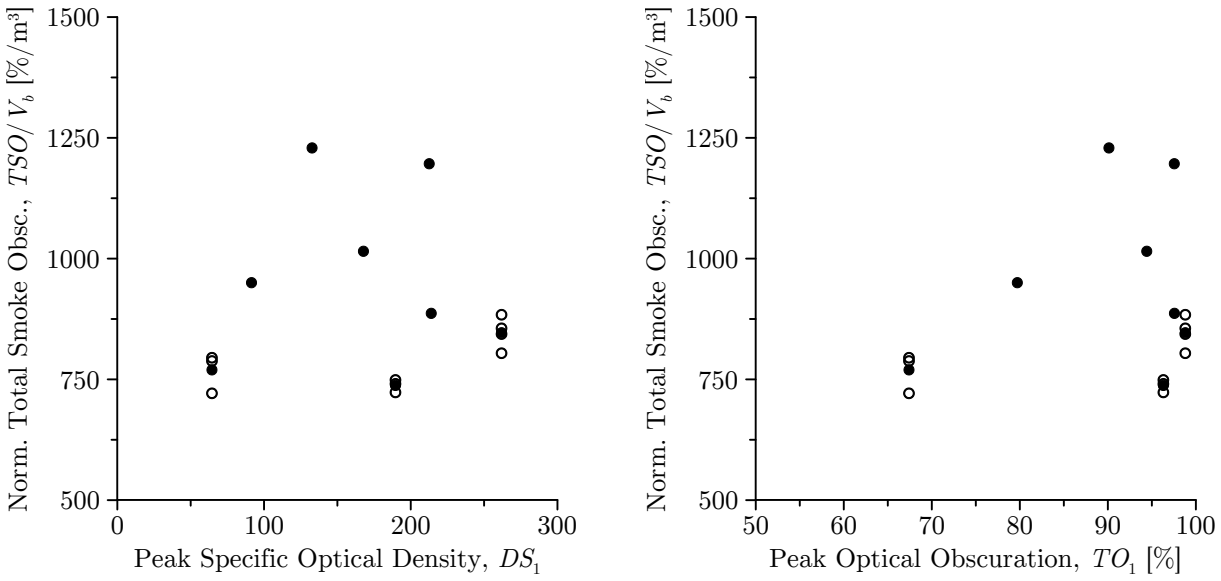

(a) Peak specific optical density.

(b) Peak optical obscuration.

Figure 5.3: Normalized total smoke obscuration – reduction in variability.

Comparing the spread in open-circle data points between Figures 5.1 and 5.3, it is apparent that normalizing TSO by V_b has produced the desired effect of reducing the spread in values of TSO between repeated tests of the same formulation. Unfortunately, normalization of the data appears to have significantly degraded the relationship between the selected performance indicators.

In a second attempt at correlating the normalized Steiner tunnel results, the smoke density chamber DS_1 measurement is normalized using a material loss parameter. Two parameters are identified for this purpose: ML_1 and ρ. Normalizing by ML_1/ρ produces interesting results. ML_1/ρ can be interpreted as an experimental approximation of the volume of material burned in the smoke density chamber test, with volumetric units (cubic metres).

Figure 5.4a shows the correlation between the normalized results TSO/V_B and $DS_1/(ML_1/\rho)$ for the set of 15 tests, and Figure 5.4b shows the correlation between the normalized results TSO/V_B and $TO_1/(ML_1/\rho)$ for the set of 15 tests. As previously,

unfilled symbols represent repeated Steiner tunnel results for a given formulation, as indicated by multiple TSO/V_B values for a given $TO_1/\left(ML_1/\rho\right)$ or $DS_1/\left(ML_1/\rho\right)$.

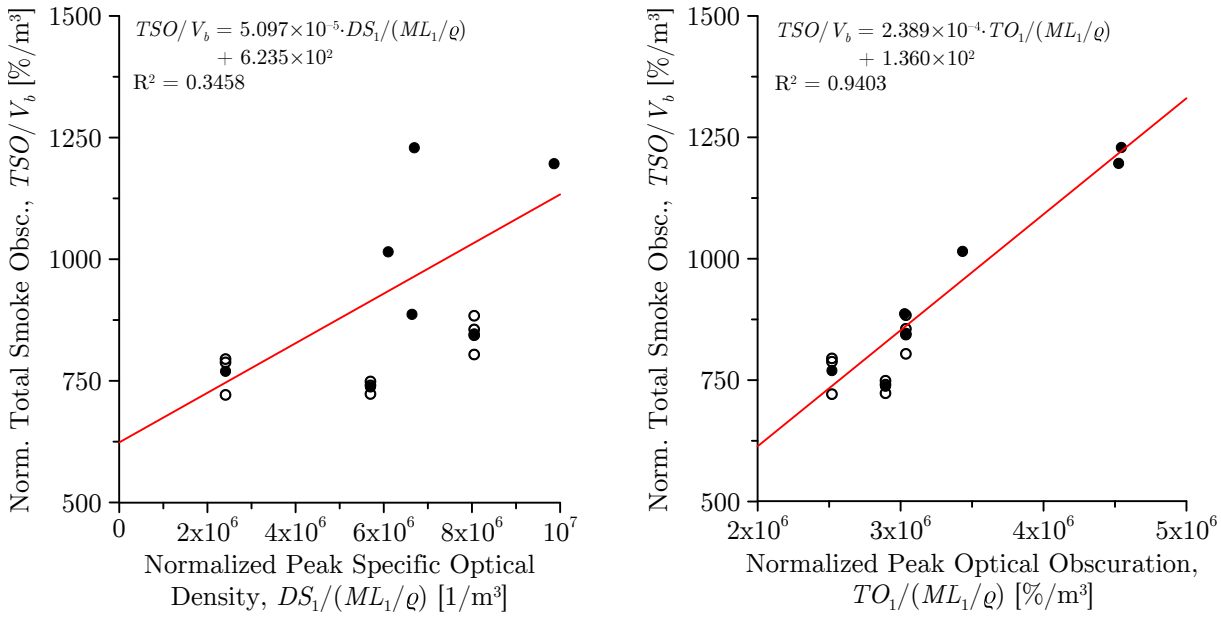

(a) Linear least-squares fit, DS_1.

(b) Linear least-squares fit, TO_1.

Figure 5.4: Normalized total smoke obscuration correlations: normalized peak specific optical density and normalized peak optical obscuration.

Figure 5.4 demonstrates the strong positive correlation that exists between the normalized values of TSO from Steiner tunnel tests and the normalized values of TO_1 from smoke density chamber tests. Interestingly, both parameters are representative of cumulative obscuration of a light path divided by an approximation of the volume of specimen burned in the test. This finding supports the fact that total smoke obscuration in the Steiner tunnel test may be predicted using a combination of smoke obscuration and mass loss results as measured in the smoke density chamber test. This correlation is presented as a linear relation via Equation 5.3 as the third proposed predictive model for TSO.

$$\left.\frac{TSO}{V_b}\right|_{M3} = A \cdot \frac{TO_1}{ML_1/\rho} + B \tag{5.3}$$

While the proposed relationship shows promise, it cannot be used in a predictive model for smoke developed index, since V_b must be derived from the experimental Steiner tunnel flame spread curve. To distinguish Model 3 from Models 1 and 2, TSO_{M3} is denoted with

an asterisk superscript. Equation 5.3 is re-stated as Equation 5.4.

$$TSO_{M3}{}^{*} = V_b \cdot \left(A \cdot \frac{TO_1}{ML_1/\rho} + B \right) \tag{5.4}$$

Based on the above three correlations developed between Steiner tunnel and smoke density chamber test results, the next step is to develop predictive models for smoke developed index in the Steiner tunnel based on these correlations.

5.2 Predictive Models for Smoke Developed Index

Using each of the total smoke obscuration correlations developed in Section 5.1, smoke developed indices are predicted for each of the 8 formulations. The following notation is used:

- SDI_{M1} refers to predicted smoke developed index using the TSO_{M1} correlation;
- SDI_{M2} refers to predicted smoke developed index using the TSO_{M2} correlation;
- SDI_{M3} refers to predicted smoke developed index using the $TSO_{M3}{}^{*}$ correlation.

Predicted smoke developed index is calculated according to Equation 5.5, where the reference smoke obscuration is taken to be 16.2% for the ST apparatus in this study, as outlined in Section 2.3.2.

$$SDI_M = 100 \cdot \frac{TSO_M}{TSO_R} = 617.3 \cdot TSO_M \tag{5.5}$$

The error for all predicted smoke developed indices is quantified according to Section 3.4. Additionally, successful prediction of smoke developed index for a given formulation is dictated by the percent error between the experimental SDI and the predicted SDI. A successful prediction is deemed to be achieved when the percent error is less than or equal to 20%.

5.2.1 Model 1: Peak Specific Optical Density

Summarizing the results from Section 5.1, the assembled model for total smoke obscuration as a function of peak specific optical density is stated as Equation 5.6.

$$TSO_{M1} = 0.1033 \cdot DS_1 + 59.89 \tag{5.6}$$

Using Equations 5.5 and 5.6, the smoke developed index is predicted for each of the 8 formulations. The results are plotted adjacent to the associated experimental results

for all 15 tests in Figure 5.5. In the figure, blue bars represent experimental values of smoke developed index, green bars represent predicted values of smoke developed index less than 20% different than the associated experimental values, and red bars represent predicted values of smoke developed index greater than 20% different than the associated experimental values.

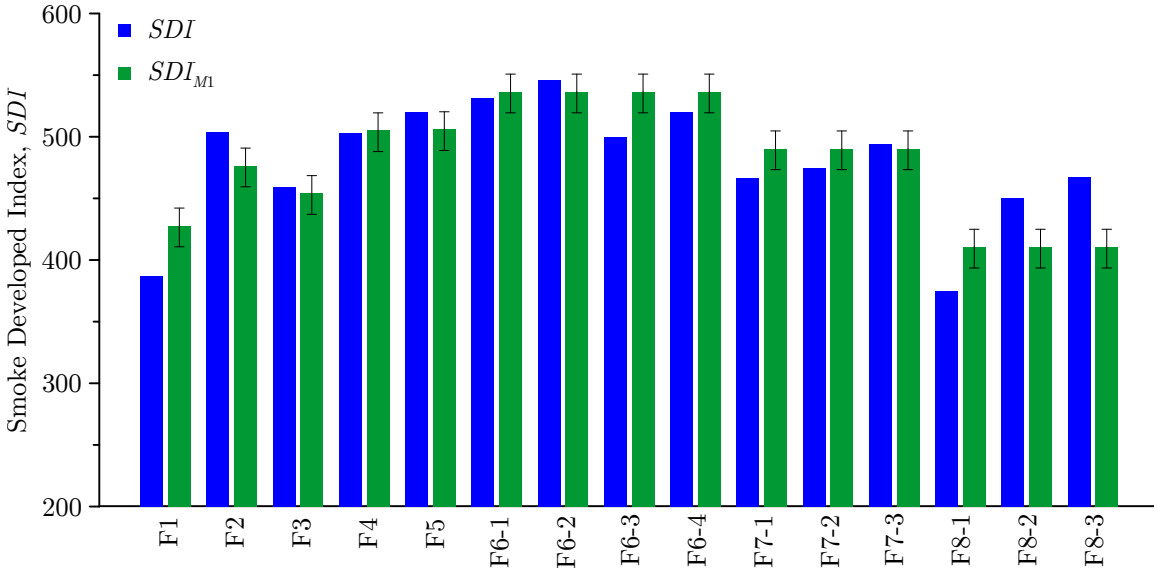

Figure 5.5: Experimental and predicted smoke developed index for Model 1.

Figure 5.5 shows that the model is able to predict the smoke developed index to within 20% for all 15 formulations tested in the Steiner tunnel. When repeated testing is conducted on formulations, the predicted smoke developed index is found to lie approximately in the centre of the experimental results. This is most clearly indicated by examination of the green bars (predicted values) relative to the blue bars (measured values) for formulation F8, in Figure 5.5. Model 1 appears to produce a reasonably accurate prediction of SDI.

5.2.2 Model 2: Peak Specific Optical Density and Mass Loss

Summarizing the results from Section 5.1, the model for total smoke obscuration as a function of peak specific optical density and mass loss is stated as Equation 5.7.

$$TSO_{M2} = 8.824 \cdot \ln\left(DS_1 \cdot ML_1\right) + 27.71 \tag{5.7}$$

Using Equations 5.5 and 5.7, the smoke developed index is predicted for each of the 8 formulations. The results are plotted adjacent to the associated experimental results

for all 15 tests in Figure 5.6. In the figure, blue bars represent experimental values of smoke developed index, green bars represent predicted values of smoke developed index less than 20% different than the associated experimental values, and red bars represent predicted values of smoke developed index greater than 20% different than the associated experimental values.

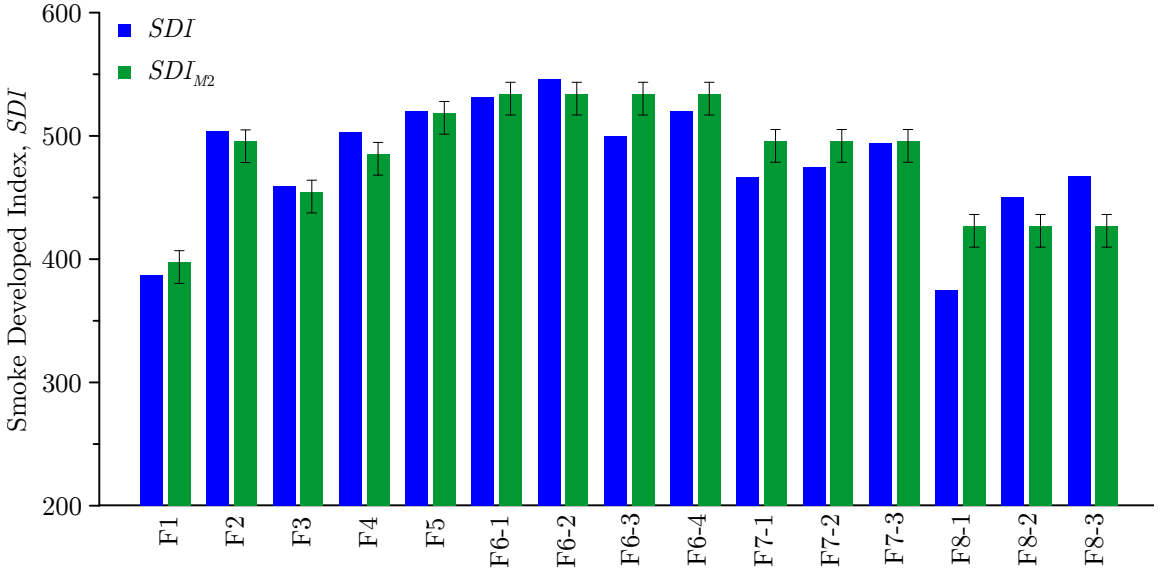

Figure 5.6: Experimental and predicted smoke developed index for Model 2.

Figure 5.6 shows that this model is able to predict the smoke developed index to within 20% for all of the 15 formulations tested in the Steiner tunnel. Comparing Figures 5.5 and 5.6, Model 2 appears to yield a more accurate prediction of SDI than Model 1 for the 8 formulations in this study.

5.2.3 Model 3: Normalized Peak Optical Obscuration

Summarizing the results from Section 5.1, the model for total smoke obscuration based on normalized values of peak optical obscuration is stated as Equation 5.8.

$$TSO_{M3}{}^{*} = 2.389 \times 10^{-4} \cdot V_b \cdot \frac{TO_1}{ML_1/\rho} + 136.0 \cdot V_b \tag{5.8}$$

Using Equations 5.5 and 5.8, the smoke developed index is predicted for each of the 8 formulations. The results are plotted adjacent to the associated experimental results in Figure 5.6. In the figure, blue bars represent experimental values of smoke developed index, green bars represent predicted values of smoke developed index less than 20% different

than the associated experimental values, and red bars represent predicted values of smoke developed index greater than 20% different than the associated experimental values.

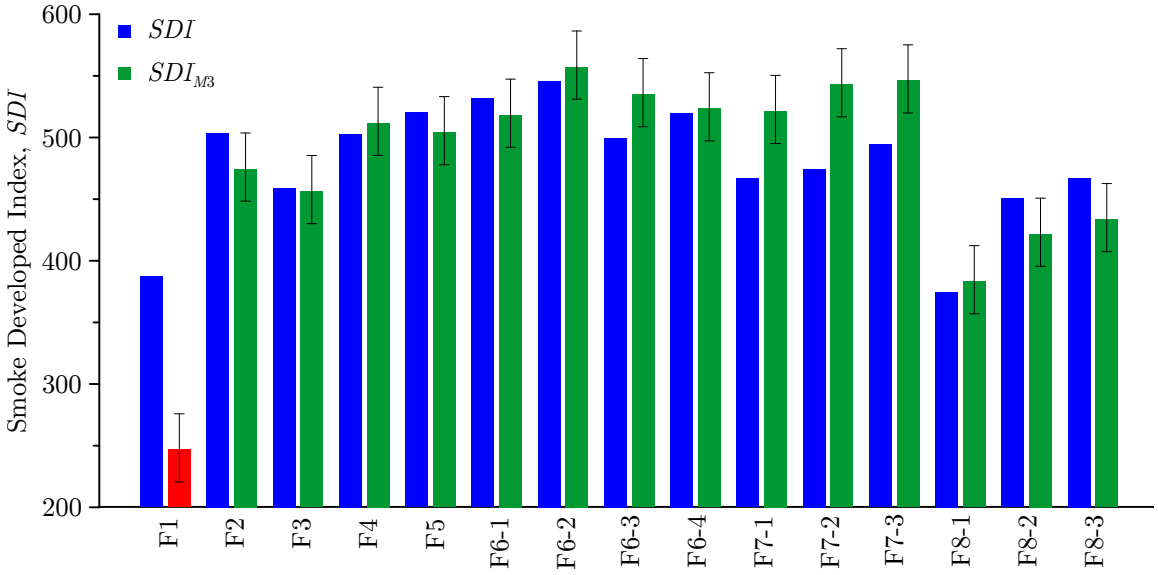

Figure 5.7: Experimental and predicted smoke developed index for Model 3.

Figure 5.7 shows that the model is able to predict the smoke developed index to within 20% for 14 of the 15 tests conducted, and 7 of the 8 formulations. Formulation F1 does not appear to fit the model. Notably, formulation F1 is categorized as a low density foam, and therefore the sample has a significantly lower mass than those of the other formulations. It is likely that the assumptions made during the approximation of the burned volume are not consistent across different classes of materials, resulting in an erroneous approximation in the uncharacteristically low-density material. The volume approximation model was not validated for low density materials, so this possibility cannot be confirmed.

5.3 Screening Potential for Smoke Developed Index

Three predictive models for smoke developed index are proposed in Section 5.2. The results for all three models are summarized in Table 5.3, and the error and confidence limits in the predicted values of TSO are summarized in Table 5.4.

The tables show that Model 2 appears to provide the best prediction of the experimental data, with SDI predictions within 20% difference for all 15 Steiner tunnel tests and the least mean percent error. Model 1 also appears to provide good predictions of the experimental data, with successful SDI predictions for all 15 Steiner tunnel tests, but does have a

Table 5.3: Results of the predictive models for smoke developed index.

Model	Steiner Tunnel Prediction	Smoke Density Chamber Results	Rate of Success	$\overline{\%\epsilon}$
Model 1	TSO	DS_1	15/15	4.875%
Model 2	TSO	DS_1, ML_1	15/15	4.011%
Model 3	TSO^*	DS_1, ML_1, ρ	14/15	5.440%

Table 5.4: Error and confidence limits for the predictive models for smoke developed index.

Model	$\overline{\epsilon}$	$\hat{\epsilon}$	C_U	C_L
Model 1	-1.372	28.35	14.33	-17.07
Model 2	-3.700	23.97	9.574	-16.97
Model 3	1.405	49.92	29.05	-26.24

higher mean percent error than for predictions made using Model 2. Model 3 provides reasonable predictions of the experimental results, excepting the case of the low density foam formulation. However, since Model 3 is not a full predictive model, it cannot be used to screen for Steiner tunnel tests. All the same, Model 3 provides meaningful insight on the relationship between volume and mass normalized obscuration results. For this research, Model 2 is recommended for use as a screening tool for the prediction of smoke developed index based on smoke density chamber test results.

The estimated values of smoke developed index, SDI_S, are calculated for the 8 formulations in this study based on the peak specific optical density and mass loss model (Model 2), and error bounds tabulated in Table 5.4. The 95% confidence limits of mean error on modelled smoke developed index are used to determine upper and lower bounds on predicted values of SDI according to Equation 5.9. The results are tabulated in Table 5.5, along with the average experimental values of SDI.

$$SDI_S = \{SDI_M + C_L\} \; - \; \{SDI_M + C_U\} \tag{5.9}$$

One method by which to compare the estimated and experimental results is by the relative rankings of the 8 formulations. The formulations are listed in order of ascending smoke developed index ("best" to "worst" smoke performance) in Table 5.6.

Table 5.5: Screened smoke developed index for 8 foam formulations.

Formulation	SDI_S	$\overline{SDI}$
F1	411 – 437	387
F2	459 – 486	504
F3	437 – 464	459
F4	488 – 515	503
F5	489 – 516	520
F6	520 – 546	524
F7	473 – 500	478
F8	394 – 420	431

Table 5.6: Ranking of formulations for screened and experimental smoke developed index.

Rank	1^{st}	2^{nd}	3^{rd}	4^{th}	5^{th}	6^{th}	7^{th}	8^{th}
$\overline{SDI}$	F1	F8	F7	F3	F2	F4	F5	F6
SDI_S	F8	F1	F3	F2	F7	F4	F5	F6

Table 5.6 demonstrates a relationship between the relative ranking of formulations by modelled and experimental smoke developed indices. Dividing the results into performance tiers:

- formulations F1 and F8 are ranked in the top-tier of smoke performance, achieving a passing classification in smoke performance in the Steiner tunnel test ($SDI < 450$);
- formulations F2, F3, and F7 are ranked in the middle-tier of smoke performance, just on the fringe of passing or failing in smoke performance in the Steiner tunnel test ($450 < SDI < 500$); and
- formulations F4, F5, and F6 are ranked in the lower-tier of smoke performance, clearly not achieving a passing classification in smoke performance in the Steiner tunnel test ($SDI > 500$).

The predictive model has ranked the 8 formulations similarly to the experimental results. It is concluded that a predictive model based on smoke density chamber results can effectively screen the relative performance of FR-SPF materials in the Steiner tunnel test.

In selecting two formulations with very similar predicted values of SDI, consider formulations F4 and F5. Even though the ranges on the screened results are almost identical, it cannot be said with confidence that F4 is expected to have the same smoke

developed index as F5. The screened results imply that there is sufficient confidence to indicate that formulations F4 and F5 are likely to have similar smoke developed indices. The range on the screened result is approximately 30; for the same two formulations, it is found that their experimental results differ by approximately 20. Since the difference in the experimental results is less than the range on the screened results, the screening is considered successful.

In comparison to the flame spread model, the confidence range on the screened smoke developed results is about the same as the confidence range on the screened flame spread results. This fact is demonstrated by dividing the respective confidence ranges of each parameter by the target values for pass/fail criteria for each parameter: $30/450 = 0.067$ for SDI, compared to $5/75 = 0.067$ for FSI). This tells us that, as in the case of the flame spread model, comparisons cannot be made with any certainty between materials which have very similar measured measured results in the smoke density chamber (DS_1, ML_1) with regards to their expected performance in the Steiner tunnel. It is concluded that a predictive model based on smoke density chamber results can confidently predict the relative ranking of materials with sufficiently large differences (approximately greater than 30) in their actual values of smoke developed index. Considering that reported values of smoke developed index are rounded to the nearest 50, the ability to use smoke density chamber tests to screen materials that might differ within a range of 30 SDI is very reasonable.

A smoke developed index of 450, the threshold for Class A classification in smoke development, corresponds to a total smoke obscuration of approximately 72.5%. From this, Model 1 indicates that a value of specific optical density in the smoke density chamber greater than approximately 120 can be expected to approach the failure threshold for Class A classification in the the Steiner tunnel. Furthermore, Model 2 indicates that a value of the product of specific optical density and mass loss greater than approximately 160 g can be expected to approach the failure threshold for Class A classification in the the Steiner tunnel. From these results, it is recommended that future screening studies strive to achieve these thresholds in smoke density chamber test results if the objective is to achieve a Class A classification in Steiner tunnel smoke development.

As in the case of the flame spread model, the range of error listed for the modelled smoke developed index has been determined according to the error bounds on measurement made using the set of materials in this research. As such, it is entirely possible that different types of FR-SPF may generate quite different and potentially more variable amounts of smoke. Therefore, it is recommended to apply this model only to the family of materials studied within the scope of this project. While screening is demonstrated to be an effective tool for reducing the number of formulations that might be envisioned during the R&D phase of materials development, primary assessment of the behaviour of any resulting materials

in the Steiner tunnel is still required.

The normalized peak optical obscuration model, even though it cannot be used in a predictive manner, warrants special mention. The correlations in Section 4.2.2 demonstrate that normalization of smoke developed results by a material loss parameter reduced variability in most cases. Furthermore, normalization was found to linearize the relationship between smoke performance indicators. Total smoke obscuration in the Steiner tunnel is an integrated value, encapsulating the total smoke generated by a specimen over the duration of burning. Similarly, peak optical transmission in the smoke density chamber is a cumulative measurement of total smoke generation, owing to the fixed-volume of the smoke density chamber. Both parameters measure cumulative smoke generation and both are normalized by an approximation of burned volume. It is recommended that the possibility of a physical relationship between results from the smoke density chamber and the Steiner tunnel be further studied.

That said, it is important to note that the burning environment is significantly different between the two tests. Scale aside, combustion in the Steiner tunnel takes place in an environment of constant pressure and excess air, while combustion in the smoke density chamber occurs in an environment of increasing pressure and deficient air. The propensity of a material to generate smoke is highly dependent on the environment and rate of combustion, particularly when fire retardants add complexity to the combustion dynamics. Such effects would add significant complexity to the prospect of developing a physical model for smoke generation. All the same, further research is recommended into the development of a dimensional, normalized model for smoke development. As in the case of the flame spread results, measurement of the actual total mass loss, measured via load cell post-test, is recommended as an alternative to the present approximated normalization parameter, V_b.

Chapter 6

Conclusions and Recommendations

The stated objective of this research is to develop a screening tool by which a recommendation can be made as to the probability of a material passing the Steiner tunnel test based on the performance of the material in small-scale cone calorimeter and smoke density chamber tests. The scope of the study is limited to development of a screening tool for the fire-retarded sprayed polyurethane foam materials produced specifically for this research.

A screening tool has been developed which is capable of predicting values of flame spread and smoke developed indices for the majority of formulations tested to within 20 percent of those that would be measured for the same materials in the Steiner tunnel test. While the models developed here are not based on a specific physical relationship between fire performance parameters, material composition, or the presence of particular fire retardant additives, they are able to provide a consistent method by which to assess the relative performance of a material in the Steiner tunnel based on cone calorimeter and smoke density chamber results.

It is concluded that for the materials tested in this study, there is sufficient evidence of consistency in cross-test performance ranking to recommend the adoption of the screening tool for future testing and R&D activities. This is expected to result in decreased R&D cycles in the formulation of new materials that are required to meet specific flammability criteria as well as reduced R&D costs, allowing the manufacturer to bring products to market in less time, and potentially gain market advantage.

Additionally, the following conclusions are made.

1. **A proportionality is demonstrated between horizontal flame propagation and burned depth along the length of a Steiner tunnel specimen.**

A model was developed to approximate the burned volume of a Steiner tunnel specimen based on measurement of the maximum burned depth into the sample. The basis of the model is a proportionality between the flame propagation and the burned depth along the length of the specimen, demonstrating that the through-depth burning rate is directly related to the horizontal flame propagation. The model has great practical benefit as only a single depth measurement need be taken to obtain a reasonable representation of the amount of material burned during a given Steiner tunnel test. However, it should be noted that measuring the remaining mass of the specimen after a test would provide a similar measure of burned material without the need to use the approximate methods developed here.

2. **Peak flame spread is of paramount importance in determining the flame spread index of a material.**

A two-variable model was developed for the approximation of flame spread area, and hence flame spread index, based on the peak flame spread and time to peak flame spread measured during a Steiner tunnel test. Furthermore, it was found that for the materials in this study, the flame spread area was highly dependent on the peak flame spread alone. This finding is of great importance in the context of future developments of both empirically- and mechanistically-based models for prediction of fire performance of materials in Steiner tunnel tests. Future models need only predict the peak flame spread to achieve a reasonably accurate approximation of the expected value of flame spread index that would be measured in the Steiner tunnel test.

Additional testing on a wide variety of building materials is recommended in order to test the versatility of this approximation, and to determine material constants for a range of building materials.

3. **Materials which burn with greater intensity in the cone calorimeter appear to burn to a greater extent in the Steiner tunnel.**

An empirical correlation was developed between the peak flame spread measured in the Steiner tunnel and the average heat release rate measured in the cone calorimeter. The correlation implies that materials which release more heat during flaming combustion, and therefore burn more intensely on average in the cone calorimeter, can be expected to exhibit a greater peak flame spread index in the Steiner tunnel.

It is found that peak flame spread does not tend to increase significantly until the average heat release rate density is greater than 125 kW/m^2. In future screening studies, when the objective is to predict whether a material will achieve a Class A classification in

Steiner tunnel flame spread, it is recommended that an average heat release rate density in the cone calorimeter less than 125 kW/m^2 be achieved.

4. **Materials which are characterized by higher values of specific optical density and mass loss in the smoke density chamber appear to exhibit higher values of smoke developed index in the Steiner tunnel.**

An empirical correlation was developed between measured values of total smoke obscuration in the Steiner tunnel and the product of peak specific optical density and mass loss as measured in the smoke density chamber. The correlation implies that materials which produce less dense smoke with less mass loss in the smoke density chamber can be expected to do the same in the Steiner tunnel. Notably, the combustion environments in the two test systems are drastically different, and it is possible that untested combinations of FRs may react differently in the air-starved environment of the smoke density chamber.

Total smoke obscuration in the Steiner tunnel is found to approach the critical values for Class A classification in Steiner tunnel smoke development at values of specific optical density greater than 120, and at values of the product of specific optical density and mass loss greater than 160 g in the smoke density chamber. It is recommended in future screening studies, when the objective is to predict whether a material will achieve a Class A classification in Steiner tunnel smoke development, to strive to meet these thresholds in the smoke density chamber test.

5. **Normalization of Steiner tunnel results by the amount of material burned shows promise in reducing test variability.**

Variability in Steiner tunnel results is identified as an issue inherent in the test methodology, and consequently affects the development of predictive models by which to make recommendations on the probability of a material passing the Steiner tunnel test based on the performance of that material in small-scale tests. Normalization of Steiner tunnel results for both flame spread and smoke developed index shows promise in terms of reducing variability amongst the normalized results. If measurement of the mass burned during the Steiner tunnel test were standardized, it is possible that flame spread and smoke developed indices normalized on the basis of mass of sample burned would improve the overall confidence in the results.

Additional testing of repeated formulations incorporating mass loss measurements is recommended in order to validate these findings and make potential improvements to the first generation of screening tools developed in the current research.

References

[1] Parker, W., 1983. Assessment of the correlations between laboratory and full-scale experiments for the FAA aircraft fire safety program, Part 3: ASTM E84. NBSIR 82-2564, National Bureau of Standards, Gaithersburg, MD.

[2] ASTM Standard E119-12a, 2012. "Standard Test Methods for Fire Tests of Building Construction and Materials". ASTM International, West Conshohocken, PA.

[3] ASTM Standard D2863-12e1, 2012. "Standard Test Method for Measuring the Minimum Oxygen Concentration to Support Candle-Like Combustion of Plastics (Oxygen Index)". ASTM International, West Conshohocken, PA.

[4] ASTM Standard E84-12c, 2012. "Standard Test Method for Surface Burning Characteristics of Building Materials". ASTM International, West Conshohocken, PA.

[5] ASTM Standard E1354-11b, 2011. "Standard Test Method for Heat and Visible Smoke Release Rates for Materials and Products Using an Oxygen Consumption Calorimeter". ASTM International, West Conshohocken, PA.

[6] Babrauskas, V., and Peacock, R. D., 1992. "Heat release rate — the single most important variable in fire hazard". *Fire Safety Journal,* ***18***(3), pp. 255–272.

[7] ISO Standard 5659-2:2006, 2006. "Plastics – Smoke Generation – Part 2: Determination of Optical Density by a Single-Chamber Test". International Organization for Standardization, Geneva, Switzerland.

[8] Flisi, U., 1989. "Large-scale fire reaction tests". *Polymer Degradation and Stability,* ***23***(4), pp. 385–396.

[9] Schartel, B., and Hull, T. R., 2007. "Development of fire retarded materials – Interpretation of cone calorimeter data". *Fire and Materials,* ***31***(5), pp. 327–354.

[10] Christopoulos, A., and Lew, M. J., 2000. "Beyond eyeballing: Fitting models to experimental data". *Critical Reviews in Biochemistry and Molecular Biology,* ***35***(5), pp. 359–391.

[11] Janssens, M. L., Huczek, J., and Sauceda, A., 2008. "Development of a model of the ASTM E84 Steiner tunnel test". In Proceedings of the Ninth International Symposium, Fire Safety Science, International Association for Fire Safety Science, pp. 279–289.

[12] Wu, P. K., and Bill, R. G., 2008. "Comparison of simulated wet bench fires with small- and intermediate-scale fire tests". *Fire and Materials,* ***32***(8), pp. 445–456.

[13] Babrauskas, V., 1984.. Bench-scale methods for prediction of full-scale fire behavior of furnishings and wall linings. SPFE Tech. Rep. 84-10, Society of Fire Protection Engineers, Boston, MA.

[14] Wickström, U., and Göransson, U., 1987. "Prediction of heat release rates of surface materials in large-scale fire tests based on cone calorimeter results". *Journal of Testing and Evaluation,* ***15***(6), pp. 364–370.

[15] Wickström, U., and Göransson, U., 1992. "Full-scale/bench-scale correlations of wall and ceiling linings". *Fire and Materials,* ***16***(1), pp. 15–22.

[16] Östman, B. A.-L., and Tsantaridis, L. D., 1994. "Correlation between cone calorimeter data and time to flashover in the room fire test". *Fire and Materials,* ***18***(4), pp. 205–209.

[17] Östman, B. A.-L., and Tsantaridis, L. D., 1995. "Heat release and classification of fire retardant wood products". *Fire and Materials,* ***19***(6), pp. 253–258.

[18] Hansen, A. S., and Hovde, P. J., 2002. "Prediction of time to flashover in the iso 9705 room corner test based on cone calorimeter test results". *Fire and Materials,* ***26***(2), pp. 77–86.

[19] Petrella, R. V., 1994. "The assessment of full-scale fire hazards from cone calorimeter data". *Journal of Fire Sciences,* ***12***, pp. 14–43.

[20] Wang, Z., Hu, X., Jia, F., and Galea, E. R., 2012. "A two-step method for predicting time to flashover in room corner test fires using cone calorimeter data". *Fire and Materials*, Published online in Wiley Online Library, DOI: 10.1002/fam.2139.

[21] Heskestad, A. W., and Hovde, P. J., 1999. "Empirical prediction of smoke production in the iso room corner fire test by use of iso cone calorimeter fire test data". *Fire and Materials,* ***23***(4), pp. 193–199.

[22] Dietenberger, M. A., and Grexa, O., 2000. "Correlation of smoke development in room tests with cone calorimeter data for wood products". In The proceedings of Wood & Fire Safety 2000 (part one), Technical University of Zvolen, pp. 45–55.

[23] Cleary, T. G., 1992. "Flammability characterization with the LIFT apparatus and the cone calorimeter". In Technical and Marketing Issues Impacting the Fire Safety of Building and Construction and Home Furnishings Applications, Spring Conference, 1992, Fire Retardant Chemicals Association, Technomic Publishing Co., pp. 99–115.

[24] Quintiere, J., 2006. "A theoretical basis for flammability properties". *Fire and Materials,* ***30***(3), pp. 175–214.

[25] Quintiere, J., and Lian, D., 2009. "Inherent flammability parameters – Room corner test application". *Fire and Materials,* ***33***(8), pp. 377–393.

[26] Grayson, S., 2013. Fire Properties for Fire Safety Engineering Calculations. Personal communication, ASTM Sub-Committee E5.33.

[27] Welch, S., and Marshall, N. R., 2003. "Development and validation of a comprehensive model for flame spread and toxic products in full-scale scenarios". In 4th International Seminar on Fire and Explosion Hazards, International Association for Fire Safety Science, Londonderry, UK.

[28] Timm, W., and Smith, P. M., 1982. "Effect of the adverse press on the insulation industry". *Journal of Building Physics,* ***5***(3), pp. 115–139.

[29] Moriya, K., et al., 2009. Q & A on fire and fire prevention of rigid polyurethane foam. Tech. Rep., Japan Urethane Industry Institute, Nishi-Shinbashi, Minato, Tokyo, Japan.

[30] Kawaller, S. I., 1976. "Exposed plastic foam insulation requires thermal barrier protection". *Fire Journal,* ***70***(6), pp. 66–68.

[31] Mehaffey, J. R., 1987. "Fire performance of combustible insulation in buildings". *Journal of Thermal Insulation,* ***10***(4), pp. 256–269.

[32] Hirschler, M. M., 2008. "Polyurethane foam and fire safety". *Polymers for Advanced Technologies,* ***19***(4), pp. 521–529.

[33] Jurs, J. L., 2007. Development and testing of flame retardant additives and polymers. Tech. Rep. DOT/FAA/AR-07/25, Department of Transportation, Federal Aviation Administration, Washington, DC.

[34] Hirschler, M. M., 2004. Fire Testing of Interior Finish. Published online by Fire Protection Engineering Magazine. Article retrieved March, 2013, from <http://magazine.sfpe.org/special-hazards/fire-testing-interior-finish>.

[35] Laymon, R. K., 2004. Assessing the Burning Characteristics of Interior Finish Materials – Standard Test Method for Surface Burning of Building Materials. Fire Protection Engineering, <http://magazine.sfpe.org/special-hazards/assessing-burning-characteristics-interior-finish-material>.

[36] Resing, J. V., Gandhi, P. D., Sloan, D. E., and Laymon, R. K., 2011. "Measurement uncertainty and statistical process control for the steiner tunnel (UL 723, ASTM E84)". *Journal of Testing and Evaluation,* ***39***(6), pp. 1–6.

[37] UL Standard 723, 2008. "Standard for Test for Surface Burning Characteristics of Building Materials". Underwriters Laboratories, Chicago, IL.

[38] CAN/ULC Standard S102, 2010. "Standard Method of Test for Surface Burning Characteristics of Building Materials and Assemblies". Underwriters Laboratories of Canada, Toronto, ON.

[39] CAN/ULC Standard S102.2, 2010. "Method of Test for Surface Burning Characteristics of Flooring, Floor Coverings, and Miscellaneous Materials and Assemblies". Underwriters Laboratories of Canada, Toronto, ON.

[40] CAN/ULC Standard S127, 2007. "Standard Corner Wall Method of Test for Flammability Characteristics of Non-Melting Foam Plastic Building Materials". Underwriters Laboratories of Canada, Toronto, ON.

[41] Laymon, R. K., 2004. Surface Burning Characteristics for Materials Used in Plenums - ASTM E84 (UL 723) vs. ULC S102.2: What's the difference? Underwriter's Laboratories Inc., <http://www.ul.com/global/documents/offerings/perspectives/regulators/electrical/technicaltopics/ASTME84_ULCS102.2.pdf>.

[42] Nagle, K. R., Saff, E. B., and Snider, D. A., 2003. *Fundamentals of Differential Equations and Boundary Value Problems*, 4 ed. Addison Wesley.

[43] Babrauskas, V., 1984. "Development of the cone calorimeter – A bench-scale heat release rate apparatus based on oxygen consumption". *Fire and Materials,* ***8***(2), pp. 81–95.

[44] Babrauskas, V., 1993. "Ten years of heat release research with the cone calorimeter". In Japan Syposium on Heat Release and Fire Hazard, First (1st) Proceedings, Session 3, Tsukuba, Japan, pp. III/1–8.

[45] ISO Standard 5660-1:2002, 2002. "Reaction-to-Fire Tests – Heat Release, Smoke Production and Mass Loss Rate – Part 1: Heat Release Rate (Cone Calorimeter Method)". International Organization for Standardization, Geneva, Switzerland.

[46] NFPA Standard 264, 1992. "Standard Method of Test for Heat and Visible Smoke Release Rates for Materials and Products Using an Oxygen Consumption Calorimeter". National Fire Protection Association, Quincy, MA.

[47] ULC Standard S135, 2004. "Standard Test Method for the Determination of Combustibility Parameters of Building Materials Using an Oxygen Consumption Calorimeter (Cone Calorimeter)". Underwriters Laboratories of Canada, Toronto, ON.

[48] CAN/ULC Standard S135, 1992. "Standard Method of Test for Determination of Degrees of Combustability of Building Materials Using an Oxygen Consumption Calorimeter". Underwriters Laboratories of Canada, Toronto, ON.

[49] Fire Testing Technology Limited, 2008. *CONECALC* [Computer Program]. Version 5.4b, Distributed by Fire Testing Technology Limited, East Grinstead, West Sussex, United Kingdom, <`http://www.fire-testing.com`>.

[50] Janssens, M., 2002. *SFPE Handbook of Fire Protection Engineering*, 3rd ed. Section 3: Hazard Calculations, Chapter 2: Calorimetry. National Fire Protection Association, Quincy, Massachusetts, pp. 38–62.

[51] Babrauskas, V., 2002. *SFPE Handbook of Fire Protection Engineering*, 3rd ed. Section 3: Hazard Calculations, Chapter 3: The Cone Calorimeter. National Fire Protection Association, Quincy, Massachusetts, pp. 63–81.

[52] Hirschler, M. M., 1992. "Smoke results from a set of over 100 carpets in the nbs smoke density chamber: Statistical analysis and investigation of affecting factors". *Fire and Materials,* ***16***(3), pp. 127–133.

[53] Lee, T. G., 1971. Interlaboratory evaluation of smoke density chamber. final report. NBS Technical Note No. 708, National Bureau of Standards, Washington, D.C.

[54] ASTM Standard E662-09, 2009. "Standard Test Method for Specific Optical Density of Smoke Generated by Solid Materials". ASTM International, West Conshohocken, PA.

[55] ASTM Standard E1995-12, 2012. "Standard Test Method for Measurement of Smoke Obscuration Using a Conical Radiant Source in a Single Closed Chamber, With the

Test Specimen Oriented Horizontally". ASTM International, West Conshohocken, PA.

[56] Fire Testing Technology Limited, 2008. *SMOKEBOX* [Computer Program]. Version 3.7i, Distributed by Fire Testing Technology Limited, East Grinstead, West Sussex, United Kingdom, <http://www.fire-testing.com>.

[57] Richter, T., et al., 2012. *ENGAUGE DIGITIZER* [Computer Program]. Version 5.1, Distributed as open-source software under the GNU GPLv2, <http://sourceforge.net/projects/digitizer/>.

[58] White, R. H., and Nordheim, E. V., 1992. "Charring rate of wood for ASTM E119 exposure". *Fire Technology,* ***28***(1), pp. 5–30.

[59] Kodur, V. K. R., and Harmathy, T. Z., 2002. *SFPE Handbook of Fire Protection Engineering*, 3rd ed. Section 1: Fundamentals, Chapter 10: Properties of Building Materials. National Fire Protection Association, Quincy, Massachusetts, pp. 155–181.

[60] Butler, C. P., 1971. Notes on charring rates in wood. Fire Research Note No. 896, Department of the Environment and Fire Offices Committee Joint Fire Research Organization.

[61] Drysdale, D., 2011. *An Introduction to Fire Dynamics*, 3 ed. Wiley, Chichester, United Kingdom.

[62] NIST/SEMATECH, 2003. Engineering Statistics Handbook. Published online by the National Institute of Standards and Technology, <http://www.itl.nist.gov/div898/handbook/index.htm>.

[63] Steel, R. G. D., and Torrie, J. H., 1980. *Principles and Procedures of Statistics: A Biometrical Approach*. McGraw-Hill, New York.

[64] ASTM Standard E178-08, 2008. "Standard Practise for Dealing With Outlying Observations". ASTM International, West Conshohocken, PA.

APPENDICES

Appendix A

Burned Depth Measurements

Depth measurements were taken to estimate the through-depth burning of the specimens for two of the Steiner tunnel tests in this study, F10 and F11-1. Results were used to validate the burned depth model based on two specimens with markedly different burned depth profiles. This appendix documents the measurement process.

Burned depth was measured along the length, x, and width, y, of a specimen over a grid. The grid measured 2 feet in the positive length direction starting from the burned end ($\Delta x = 2$ft), and 8 inches in both positive and negative directions starting from the centreline of the specimen ($\Delta y = 8$in).

The measurement-to-measurement distance, Δx, was selected to provide a reasonable number of measurements over the specimen length within the available time alloted for taking the measurements. The increment away from the centreline across the width of the specimen, Δy, was selected to ensure that depth measurements would be taken at the centreline, as well as close to both specimen edges, while remaining inside the burned region. Since the burned width of a specimen is approximately 18 inches ($\pm$9in from the width centreline), $\Delta y = 8$in lies within the burned region.

A thin rod depth gauge was use to measure the thickness of unburned material at each grid location. Burned depth was then calculated as the difference between the initial specimen thickness and the thickness of unburned material. As demonstrated in Figure A.1, for many materials, the unburned material was covered by a layer of burned material. In such cases, the char layer was scraped away to facilitate the measurement.

Figure A.2 shows a cut section across the width of the specimen for the F10 test at the burned end. A distinct difference in burned depth is observed between the specimen centreline and the edge of the burned section, indicating that more material is burned along the centreline.

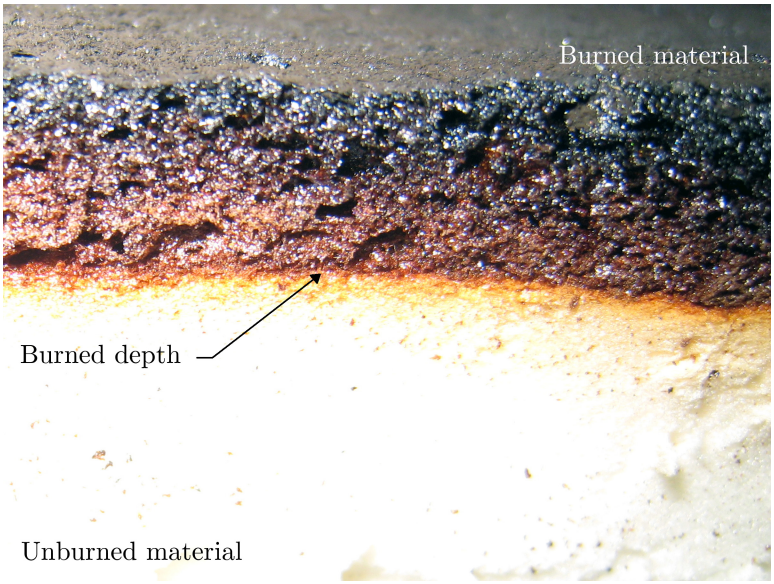

Figure A.1: Detailed view of the separation between burned and unburned material regions.

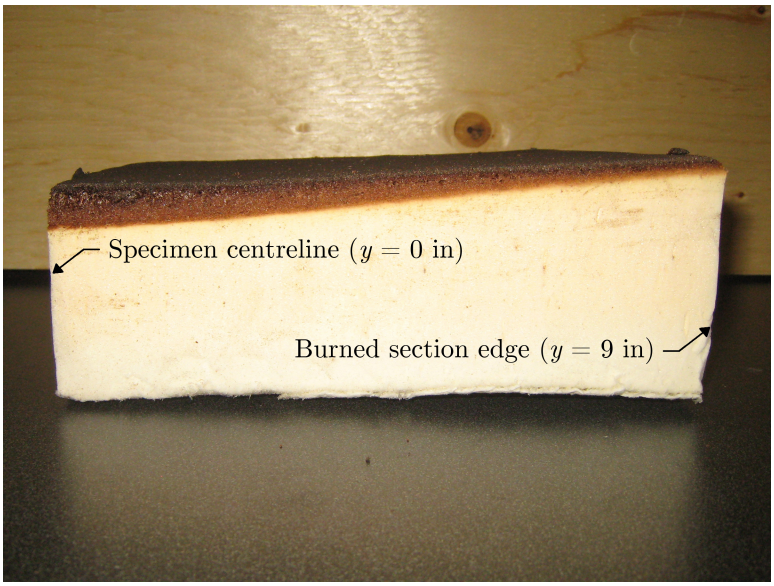

Figure A.2: Cut section of a burned specimen from the F10 test at the burned end.

Figure A.3 shows a cut section across the width of the specimen for the F11-1 test at the burned end. In comparison to Figure A.2, it is apparent that the F11-1 test had a greater burned depth at the burned end of the specimen.

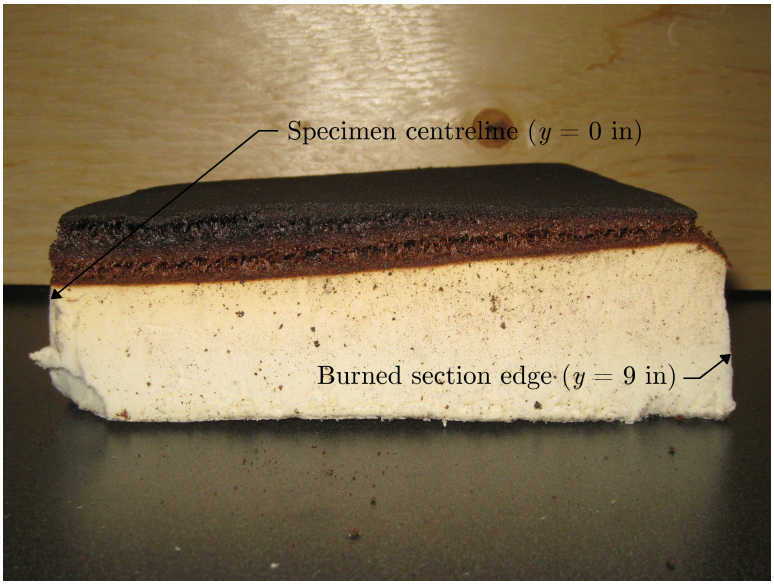

Figure A.3: Cut section of a burned specimen from the F11-1 test at the burned end.

Figure A.4 shows a cut section across the width of the specimen for the F10 test approaching the unburned end. The figure also shows the two inches at the specimen edge which were not burned, indicating the initial specimen thickness. The char layer is shown not to spread into the covered specimen edge, and the burned depth is shown to be lesser approaching the unburned specimen end.

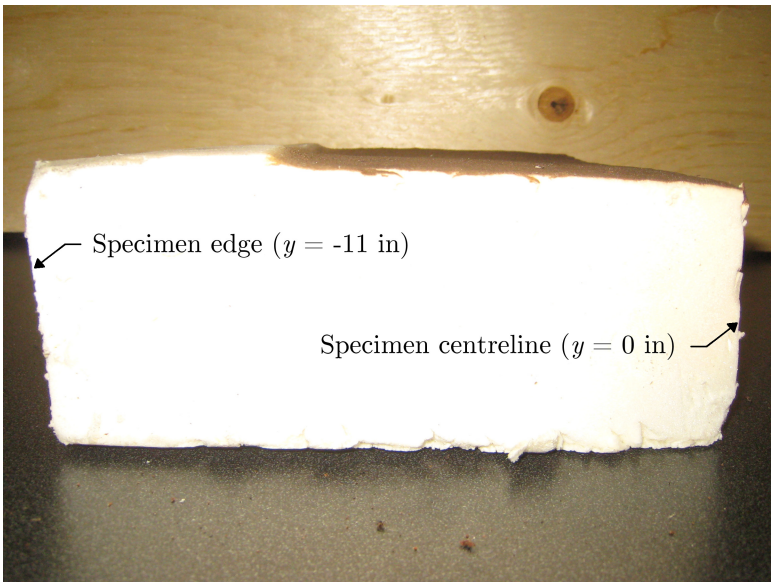

Figure A.4: Cut section of a burned specimen from the F10 test at the unburned end.

Burned depth measurements for both specimens are tabulated in Table A.1. This data is used in the surface plots in Figure 3.1.

Table A.1: Burned depth measurements for formulations F10 and F11-1.

x [ft]	y [in]	D_b [mm]	
		F10	F11-1
0	−8	60	72
0	0	66	84
0	8	58	77
2	−8	59	76
2	0	66	84
2	8	59	75
4	−8	59	75
4	0	65	82
4	8	57	75
6	−8	47	54
6	0	51	58
6	8	44	50
8	−8	36	33
8	0	38	38
8	8	33	33
10	−8	15	11
10	0	18	12
10	8	17	11
12	−8	4	3
12	0	4	3
12	8	4	3
14	−8	0	0
14	0	0	0
14	8	0	0
...	...	...	...
20	−8	0	0
20	0	0	0
20	8	0	0

Appendix B

Illustrative Test Report for the Steiner Tunnel Test

Steiner tunnel tests were conducted at the Exova testing laboratories in Mississauga, ON. Facility information is provided, for reference:

> Exova Testing Laboratories, Mississauga
> 2395 Speakman Drive
> Mississauga, ON
> L5K 1B3
> Tel: 905 822-4111
> Web: `http://www.exova.ca/index.php`

A sample test report is attached, with confidential information redacted. The four page test report includes a general description of the test method, the reported flame spread and smoke developed indices, and plots of the recorded flame spread and percent light absorption. Internal codes, which are used to identify materials, report numbers, and manufacturer information, are redacted in the sample test report.

Note that the test report has been scaled to 75% of the original size in order to adhere to University of Waterloo typographic conventions for theses.

Exova
2395 Speakman Dr.
Mississauga
Ontario
Canada
L5K 1B3

T: +1 (905) 822-4111
F: +1 (905) 823-1446
E: sales@exova.com
W: www.exova.com

Testing. Advising. Assuring.

ASTM E 84 Surface Burning Characteristics of [redacted] Insulation

A Report To: [redacted]

Phone: [redacted]
E-mail:

Attention: [redacted]

Submitted by: [redacted]

Report No. [redacted]
4 Pages

Date: [redacted]

ACCREDITATION To ISO/IEC 17025 for a defined Scope of Testing by the Standards Council of Canada

SPECIFICATIONS OF ORDER

Determine the Flame Spread and Smoke Developed Indices based upon a single test conducted in accordance with ASTM E 84-10, as per your open Purchase Order [redacted] and our Quotation [redacted]

SAMPLE IDENTIFICATION (Exova sample identification number [redacted])

Spray foam insulation material identified as [redacted].

TEST PROCEDURE

The method, designated as ASTM E 84-10, "Standard Method of Test for Surface Burning Characteristics of Building Materials", is designed to determine the relative surface burning characteristics of materials under specific test conditions. Results are expressed in terms of Flame Spread Index (FSI) and Smoke Developed (SD).

Although the procedure is applicable to materials, products and assemblies used in building construction for development of comparative surface spread of flame data, the test results may not reflect the relative surface burning characteristics of tested materials under all building fire conditions.

SAMPLE PREPARATION

The test sample consisted of 3 sections of material applied to a 6 mm thick, fiberglass reinforced cement board substrate (by client), each nominally 4.5 inches (114 mm) in thickness by 21 inches (533 mm) in width by 96 inches (2438 mm) in length. The sections were butted together to create the requisite specimen length. Prior to testing, the sample was conditioned at a temperature of 73 ± 5°F (23 ± 3°C) and a relative humidity of 50 ± 5%. During testing, by client request, the sample was supported over its entire length by 2 inch (50 mm) hexagonal wire mesh and was further supported across its width by 1/4 inch (6 mm) steel rods spaced nominally at 24 inch (610 mm) intervals.

The testing was performed on: [redacted]

SUMMARY OF TEST PROCEDURE

The tunnel is preheated to 150 ± 5°F (66 ± 2.8°C), as measured by the floor-embedded thermocouple located 23.25 feet (7087 mm) downstream of the burner ports, and allowed to cool to 105 ± 5°F (40.5 ± 2.8°C), as measured by the floor-embedded thermocouple located 13 feet (3962 mm) from the burners. At this time the tunnel lid is raised and the test sample is placed along the ledges of the tunnel so as to form a continuous ceiling 24 feet (7315 mm) long, 12 inches (305 mm) above the floor. Three 8 foot (2438 mm) sections of 0.25 inch (6 mm) cement board are then placed on the back side of the sample end-to-end, to protect the tunnel lid, and the lid is then lowered into place.

SUMMARY OF TEST PROCEDURE (continued)

Upon ignition of the gas burners, the flame spread distance is observed and recorded every 15 seconds. Flame spread distance versus time is plotted, ignoring any flame front recessions. Calculations are based on comparison with flame spread characteristics of select red oak, determined in calibration trials and arbitrarily established as 100. If the area under the curve (A) is less than or equal to 97.5 min·ft, FSI = 0.515·A; if greater, FSI = 4900/(195-A). Smoke Developed is determined by comparing the area under the obscuration curve for the test sample to that of inorganic reinforced cement board and red oak, arbitrarily established as 0 and 100, respectively.

TEST RESULTS

SAMPLE	FSI	SD
[redacted] Insulation	50	600

Observations of Burning Characteristics

- The sample ignited immediately after exposure to the test flame.
- The flame front propagated to a maximum distance of 11 feet (3.4 metres) at approximately 3.5 minutes.
- Smoke Developed was recorded during the test (see accompanying chart).

Authorities having jurisdiction usually refer to these categories:

	Flame-Spread Index	Smoke Development
Class 1 or A	0 - 25	450 Maximum
Class 2 or B	26 - 75	450 Maximum
Class 3 or C	76 - 200	450 Maximum

[redacted]

[redacted]

Note: This report and service are covered under Exova Canada Inc. Standard Terms and Conditions of Contract which may be found on the Exova website (www.exova.com), or by calling 1-866-263-9268.

FLAME SPREAD INDEX

[redacted] Insulation

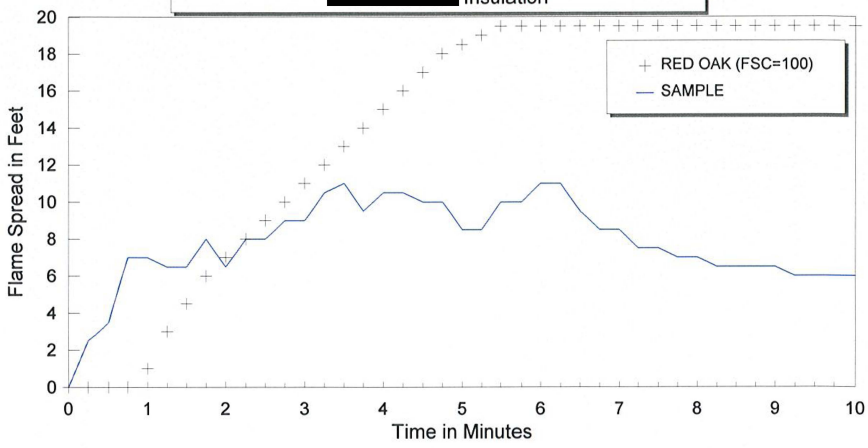

SMOKE DEVELOPED

[redacted] Insulation

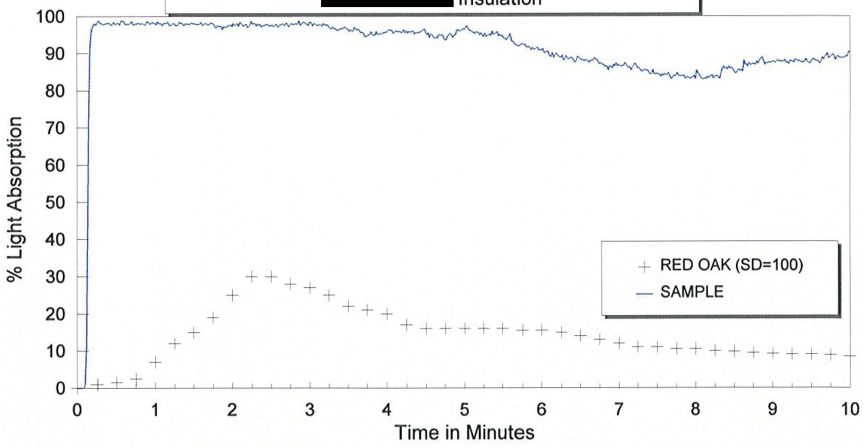

FSI	SD
50	600

Appendix C

Illustrative Test Report for the Cone Calorimeter Test

Cone calorimeter tests were conducted at the University of Waterloo Live Fire Research Facility in Waterloo, ON. All tests were conducted by the author. Facility information is provided, for reference:

University of Waterloo Live Fire Research Facility
1001 Erbs Road
Waterloo, ON
N2J 3Z4
Tel: 519-746-8561
Web: `http://mme.uwaterloo.ca/~firelab/index.html`

A sample test report is attached, with generalized specimen identification fields. The two page test report includes general information about the specimen, test conditions, apparatus specifications, and test results. Total, mean, and peak test results are reported over the burning interval. Furthermore, cumulative results are reported over 60 second intervals from the time of specimen ignition. Plots are provided for the heat release rate, total heat release, total smoke release, specimen mass, carbon monoxide production, and carbon dioxide production. In addition to the information provided in the test report, all data traces are recorded and are available for additional analysis.

Note that the test report has been scaled to 75% of the original size in order to adhere to University of Waterloo typographic conventions for theses.

Cone Calorimeter Test Report

Laboratory name	University of Waterloo Fire Research Lab
Operator	Matt DiDomizio
Filename	SAMPLE REPORT
Report name	SAMPLE REPORT
Sample description	Flame Retarded Sprayed Polyurethane Foam Insulation
Material name/ID	SAMPLE REPORT

Specimen information

E	13.1 MJ/kg	Specimen number	1	Conditioned?	Yes
Thickness	25.0 mm	Nominal duct flow rate	24 l/s	Temperature	21°C
Initial mass	12.866 g	Edge frame used?	Yes	RH	50%
Surface area	88.4 cm²	Grid used?	No		
Heat flux	50 kW/m²	Manufacturer	SAMPLE REPORT		
Separation	25 mm	Sponsor	SAMPLE REPORT		
Orientation	Horizontal				

Test

Standard used	ASTM E 1354
Date of test	DD/MM/YYYY
Time of test	HH:MM
Date of report	DD/MM/YYYY

Apparatus specifications

C-factor	0.04168
Duct diameter	0.114 m
O2 delay time	11 s
CO2 delay time	10 s
CO delay time	10 s
OD corr. factor	1.0000

Pre-test conditions

Ambient temperature	21°C
Ambient pressure	97.786 kPa
Relative humidity	30%

Initial conditions

Baseline ambient oxygen	20.793%
Baseline oxygen	20.953%
Baseline carbon dioxide	0.0403%
Mass at sustained flaming	12.8 g

Test times

Time to ignition	4 s
Time to flameout	370 s
End of test criterion	ASTM E 1354
End of test time (for calculations)	371 s

Heat Release Results

THR (0-300)	35.77 MJ/m²
THR (0-600)	-
THR (0-1200)	-
Fuel load	24.79 MJ/kg

Test results (between 4 and 371 s)

Total heat release	36.1 MJ/m²
Total oxygen consumed	23.9 g
Mass lost	12.7 g
Average specific MLR	7.24 g/(s·m²)
Total smoke release	527.7 m²/m²
Total smoke production	4.7 m²
MAHRE	261.8 kW/m²

	Mean	Peak	at time (s)
Heat release rate (kW/m²)	98.30	439.52	43
Effective heat of comb. (MJ/kg)	25.09	49.71	49
Mass loss rate (g/s)	0.035	0.291	17
Specific extinction area (m²/kg)	366.13	1214.17	8
Carbon monoxide yield (kg/kg)	0.0252	1.3248	62
Carbon dioxide yield (kg/kg)	2.17	87.51	60

Test averages

from ignition to ignition plus...	1 min	2 min	3 min	4 min	5 min	6 min	0 s - 463 s	4 s - 463 s
Heat release rate (kW/m²)	278.71	238.29	186.71	146.73	119.26	100.16	78.14	78.79
Effective heat of comb. (MJ/kg)	23.67	25.35	25.78	25.63	25.44	25.11	24.19	24.31
Mass loss rate (g/s)	0.104	0.083	0.064	0.051	0.041	0.035	0.029	0.029
Specific extinction area (m²/kg)	450.06	380.47	365.92	364.66	365.64	365.64	362.19	363.54
Carbon monoxide yield (kg/kg)	0.0134	0.0209	0.0218	0.0227	0.0240	0.0251	0.0259	0.0261
Carbon dioxide yield (kg/kg)	1.69	2.00	2.06	2.14	2.18	2.17	2.10	2.11

Smoke results

Total smoke release: non-flaming phase (0 s - 4 s)	1.2 m²/m²
Total smoke release: flaming phase (4 s - 371 s)	527.7 m²/m²
Total smoke release: whole test (0 s - 371 s)	528.9 m²/m²

The test results relate to the behaviour of the test specimens of a product under the particular conditions of the test; they are not intended to be the sole criterion for assessing the potential fire hazard of the product in use.

Cone Calorimeter Test Report

Laboratory name	University of Waterloo Fire Research Lab
Operator	Matt DiDomizio
Filename	SAMPLE REPORT
Report name	SAMPLE REPORT
Sample description	Fire Retarded Sprayed Polyurethane Foam Insulation
Material name/ID	SAMPLE REPORT

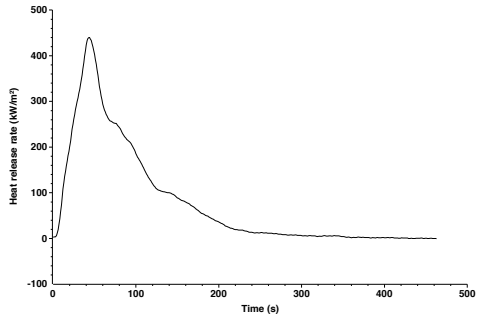

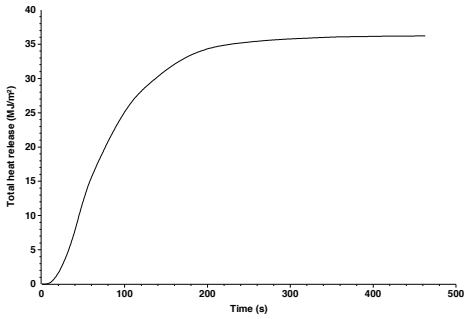

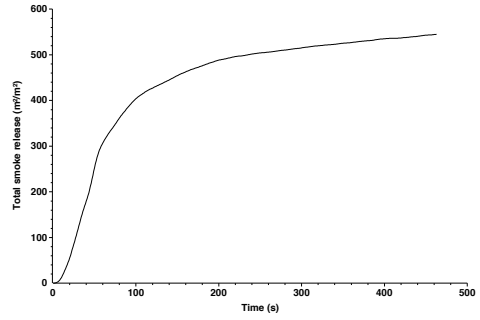

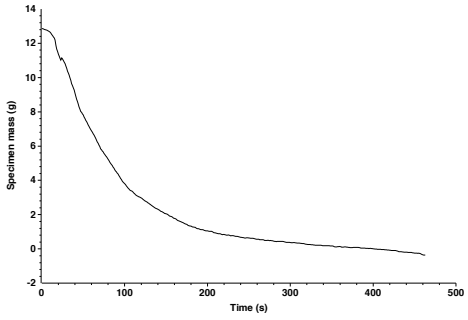

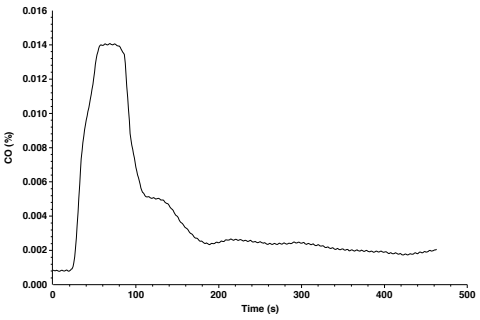

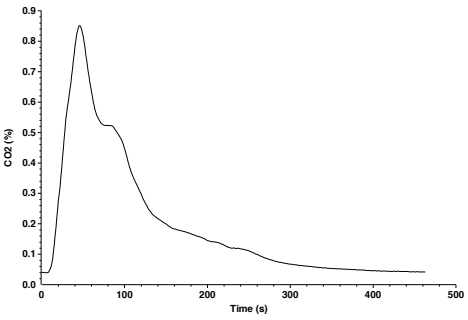

The test results relate to the behaviour of the test specimens of a product under the particular conditions of the test; they are not intended to be the sole criterion for assessing the potential fire hazard of the product in use.

Appendix D

Illustrative Test Report for the Smoke Density Chamber Test

Smoke density chamber tests were conducted at the University of Waterloo Live Fire Research Facility in Waterloo, ON. All tests were conducted by the author.

A sample test report is attached, with generalized specimen identification fields. The three page test report includes general information about the specimen, test mode, conditions, and test results. Maximum specific optical density is listed as the first and foremost result. Additional transmission and mass loss results are included, which may be used to further characterize smoke production. Two plots are provided; the first contains optical transmission over the test duration, while the second contains both specific optical density (plotted with a red trace) and specimen mass (plotted with a blue trace). Finally, optical transmission and specific optical density are tabulated in increments of 30 seconds. In addition to the information provided in the test report, all data traces are recorded and are available for additional analysis.

Note that the test report has been scaled to 75% of the original size in order to adhere to University of Waterloo typographic conventions for theses.

Smoke Density Chamber Single Specimen Report

Standard	: ISO 5659
Laboratory	: University of Waterloo Fire Research Lab
Date of test	: DD/MM/YYYY
Specimen description	: Flame Retarded Sprayed Polyurethane Foam Insulation
Test name	: SAMPLE REPORT
File name	: SAMPLE REPORT
Test number in series	: 1
Thickness (mm)	: 25.0
Initial mass (g)	: 13.0
Final mass (g)	: 10.6
Mass loss (g)	: 2.4
Mass loss (%)	: 18.5
Test mode	: 2: 25 kW/m² with pilot burner
Test duration	: 10 minutes 00 seconds (600 s)
Conditioned?	: Yes
Conditioning temp. (°C)	: 20
Conditioning RH (%)	: 50

Test Results

Maximum specific optical density	: 145.33
Time to maximum specific optical density	: 1 minutes 47 seconds (107 s)
Clear beam transmission (%)	: 74.31
Corrected maximum specific optical density	: 128.31
Mass optical density at end of test (m²/kg)	: 198.1
Mass optical density at 10 minutes (m²/kg)	: 196.4
Specific optical density at 1.5 minutes	: 140.57
Specific optical density at 4 minutes	: 132.7
Specific optical density at 10 minutes	: 113.54

Comments:

These results relate only to the behaviour of the specimens of the product under the particular conditions of the test; they are not intended to be the sole criterion for assessing the potential smoke obscuration hazard of the product in use.

Transmission Graph

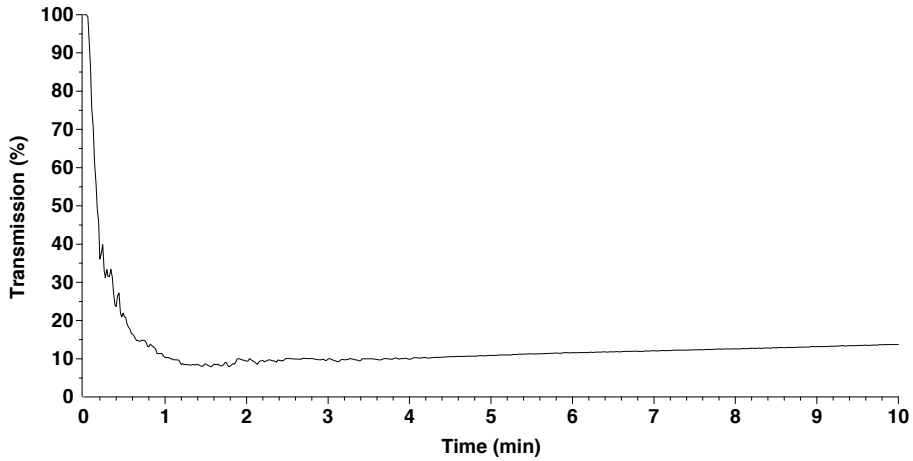

Test name : SAMPLE REPORT
File name : SAMPLE REPORT

Specific Optical Density and Mass Graph

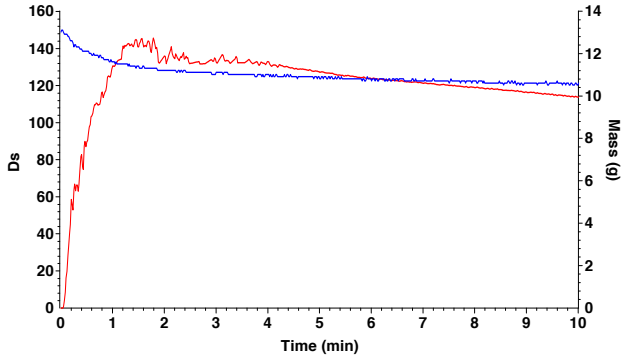

These results relate only to the behaviour of the specimens of the product under the particular conditions of the test; they are not intended to be the sole criterion for assessing the potential smoke obscuration hazard of the product in use.

Tabulated Results

Time (s)	T (%)	Ds
0	100.0	0.0
30	20.9	89.64
60	10.3	130.4
90	8.61	140.6
120	9.37	135.8
150	10.1	131.7
180	9.92	132.5
210	9.98	132.1
240	9.88	132.7
270	10.6	128.9
300	10.9	126.8
330	11.3	125.2
360	11.6	123.3
390	11.8	122.4
420	12.1	120.9
450	12.4	119.8
480	12.6	118.7
510	12.9	117.6
540	13.2	116.2
570	13.4	115.2
600	13.8	113.5

These results relate only to the behaviour of the specimens of the product under the particular conditions of the test; they are not intended to be the sole criterion for assessing the potential smoke obscuration hazard of the product in use.